An Investigation of Mechanisms Driving Prolonged Droughts in Southeast Australia

by

Blake Xu

Submitted in partial fulfilment of the requirements for the degree of
Master of Environment (Advanced)
of the Australian National University
October 2025


NATURAM PRIMUM COGNOSCERE RERUM
Australian
National
University

Candidate's Declaration

This thesis contains no material which has been accepted for the award of any other degree or diploma in any university. To the best of the author's knowledge, it contains no material previously published or written by another person, except where due reference is made in the text.

Blake Xu

Date: 23/10/2025

Acknowledgements

I would like to express my deepest gratitude to my supervisors, Dr. Chiara Holgate, Dr. Nicola Maher, Professor Sarah-Perkins Kirkpatrick and Professor Nerilie Abram.

To Chiara and Nicola - Thank you for your unwavering support and thoughtful guidance throughout my thesis journey. At times, especially in the beginning, I often felt overwhelmed and uncertain, but your mentorship and encouragement have helped me find my way. Looking back, I realize I asked many “silly” questions, and I’m truly grateful for your patience and advice on every occasion. You always took the time to support me whenever I felt stuck or lost, reminding me that moments of difficulty are just part of the process and that there’s always a way through them. Your warm support gave me confidence and inspired me to keep exploring and try different approaches throughout my work.

To Sarah - Thank you for your guidance and support throughout this journey. The opportunities to discuss ideas and share insights with your research group were invaluable and inspiring, and your encouragement and advice have helped me make steady progress throughout my research.

To Nerilie - Your passion for climate science inspired me and sparked my interest in the field. Thank you for introducing me to research, helping me discover my own enthusiasm, and providing guidance throughout the process. I probably would not have chosen climate science, nor developed such a strong interest in it, without you.

I would also like to thank Dr. Pele Cannon, for your general guidance on thesis writing and your warm feedback on my progress throughout the year.

This research was made possible thanks to computing resources from the National Computational Infrastructure (NCI), provided through ARC Centre of Excellence for 21st Century Weather, and I am grateful to have been part of this collaborative community.

Finally, I would like to thank my partner, Ava. You encouraged me to leave a field I didn’t enjoy and to take the leap into something new. The process was challenging, and there were many moments when I doubted my ability to complete the research. Your support during those times of frustration was invaluable, and I could not have completed this journey without you.

Abstract

This study investigates the mechanisms driving prolonged droughts in Southeast Australia (SEA), an important agricultural region that is highly vulnerable to water scarcity due to significant precipitation variability. Employing a three-stage analytical framework consisting of development (12-month pre-drought persistence period), persistence (sustained period with SPI-12 ⩽ -1.0 for at least 12 consecutive months), and termination (recovery period from when SPI-12 rises above -1.0 until reaching +1.0), this research uses 30-member GFDL_SPEAR_MED large ensemble climate model simulations (1921–2100) and 12-month Standardized Precipitation Index (SPI-12) to address five key questions examining: (1) the characteristics of prolonged SEA droughts across these temporal stages; (2-3) the behaviour of individual climate drivers including the El Niño–Southern Oscillation (ENSO), Indian Ocean Dipole (IOD), and Southern Annular Mode (SAM), and their combinations during drought temporal evolution; and (4-5) the frequency, intensity, and spatial patterns of synoptic-scale weather systems throughout the drought lifecycle.

SPI-12 analysis shows that droughts develop either directly, occurring in 40–60% of events with a rapid onset from normal or above-normal conditions, or gradually, emerging from below-normal conditions or from an incomplete recovery after prior droughts. Persistence phases substantially exceed termination phases in duration (approximately 30 vs. 10 months), with extreme events extending beyond 200 months, whereas drought termination proceeds rapidly and consistently once initiated.

Large-scale climate driver analysis shows ENSO as the dominant driver of droughts, remaining influential across all drought stages. The suppression of rainfall associated with La Niña events tends to be more critical than the drought enhancement linked to El Niño during dry periods. Notably, a return to neutral or weak La Niña conditions does not necessarily end droughts in SEA; relief occurs mainly during strong to extreme La Niña events, often alongside -IOD and +SAM phases. The IOD amplifies drought conditions during the mid-development and persistence stages, rather than serving as the initial trigger. SAM shows notable shift during development, ranking second to ENSO in overall changes in phase frequency. When considering the co-occurrence of different phases climate drivers: standalone climate driver events show the largest deviations overall, neutral-neutral combinations increase substantially during development, whereas more extreme phase pairings generally produced greater shifts.

At the synoptic scale, anticyclone frequency rises and cyclone frequency declines over SEA during drought development and persistence, with opposite trends during termination. Spatial analysis identifies the Tasman Sea as a hotspot for both cyclones and anticyclones, with their intensity anomalies increasing toward higher southern latitudes.

ENSO, IOD, and SAM collectively modulate prolonged droughts by altering large-scale circulation and moisture availability, creating conditions that either favour or suppress precipitation. Whilst synoptic-scale systems such as cyclones and anticyclones determine the immediate precipitation patterns at regional scales. By clarifying the roles of climate drivers and synoptic processes in prolonged drought stages, this research improves our understanding of prolonged drought mechanisms and offers insights to enhance prolonged drought prediction and support long-term water resource management under a changing climate.

Keywords: Prolonged Drought, Southeast Australia, ENSO, IOD, SAM, Extratropical Cyclone, Anticyclone, Large Ensemble Simulations, Drought stages

Table of Contents

List of Figures

List of Tables

List of acronyms and abbreviations

AAO: Antarctic Oscillation

DMI: Dipole Mode Index

EIO: Eastern Indian Ocean

ENSO: El Niño–Southern Oscillation

EOF: Empirical Orthogonal Function

GFDL: Geophysical Fluid Dynamics Laboratory

GFDL_SPEAR_MED: Seamless System for Prediction and Earth System Research (GFDL Medium-Resolution SPEAR Model)

IOD: Indian Ocean Dipole

ITCZ: Intertropical Convergence Zone

K-S: Kolmogorov-Smirnov

MSLP: Mean Sea-Level Pressure

NSW: New South Wales

PDFs: Probability Density Functions

PSL: Sea Level Pressure

SA: South Australia

SAM: Southern Annular Mode

SST: Sea Surface Temperature

TAV: Time-Averaged

VIC: Victoria

WIO: Western Indian Ocean

NOAA: National Oceanic and Atmospheric Administration

Chapter 1: Introduction

Droughts are among the least understood yet most consequential natural hazards, significantly impacting global water availability, agriculture, energy production, and ecosystems (UNDRR, 2021). Multi-year droughts impose cumulative and cascading impacts. Their extended timeframe creates substantial opportunities for compounding effects, feedback mechanisms, and intricate interactions with various external factors that fluctuate over time (van Dijk et al., 2013). Multi-year droughts (⩾2 years duration) have especially severe consequences for both natural environments and human societies, with previous Southeast Australia (SEA) droughts demonstrating major losses in agricultural production and devastating environmental degradation intensified by sustained groundwater and surface water extraction (Falster et al., 2024a).

Australia has experienced numerous severe and prolonged droughts with profound consequences for agriculture, water resources, and ecosystems. Major multi-year droughts since records began include the Federation Drought (1895–1902) and the World War II Drought (1937–1945) (BOM, 2020a). The SEA's Millennium Drought (2001–2009), locally termed the "Big Dry," brought serious impacts including reduced irrigation allocations that diminished agricultural production, prolonged habitat changes affecting biodiversity, altered bushfire regimes, and constrained industrial and consumptive water availability (BOM, 2011, 2020aa; Falster et al., 2024a; Ummenhofer et al., 2009; van Dijk et al., 2013; Verdon-Kidd and Kiem, 2009). More recently, the Tinderbox Drought (2017–2019) marked the driest three-year period in Australia since records began in 1911, severely stressing water resources in rural Southeast Australia and posing a significant risk to Sydney’s water supply (Abram et al., 2021; BOM, 2020a; NSW DPI, 2019). Such droughts have triggered cascading impacts across multiple sectors, most dramatically in agriculture, where rice production collapsed by over 90% and wheat and barley yields declined substantially during the 2018 and 2019 growing seasons, while also setting the stage for the catastrophic Black Summer fires that consumed more than 5.8 million hectares of forest (Devanand et al., 2024b). Most of these major droughts predominantly affected SEA, highlighting the region's inherent susceptibility to drought conditions (Devanand et al., 2024b). This susceptibility stems from the region's considerable precipitation variability (Murphy and Timbal, 2008; Nicholls et al., 1997), which is primarily modulated by remote oceanic and atmospheric circulation patterns (Risbey et al., 2009).

Drought conditions in SEA result from complex interactions between large-scale climate drivers and synoptic-scale weather systems. Key large-scale modes of climate variability such as

the El Niño-Southern Oscillation (ENSO), Indian Ocean Dipole (IOD), and Southern Annular Mode (SAM) significantly influence regional precipitation patterns (CoastAdapt, 2018; CSIRO, 2021; Falster et al., 2024b; Rudeva et al., 2021). These drivers modulate drought conditions through distinct physical mechanisms. While the El Niño phase of ENSO suppress precipitation by enhancing atmospheric subsidence and reducing moisture availability (Holgate et al., 2022a), the positive phase of IOD generates anomalous lower-level anticyclonic circulation and subsidence over Australia via cold sea surface temperature (SST) anomalies near Indonesia, suppressing precipitation (Ashok et al., 2003), and the negative phase of SAM phases shift storm tracks poleward while blocking easterly moisture inflows (Hendon et al., 2007). When these modes synchronize, their combined influence produces more severe precipitation shifts than any single driver alone, with prolonged droughts arising when multiple drivers persist simultaneously in drought-promoting phases (Agriculture Victoria, 2025; Cleverly et al., 2016; Risbey et al., 2009).

While large-scale climate modes establish background conditions modulating precipitation, synoptic-scale weather systems serve as the immediate mechanism translating large-scale climate conditions into actual precipitation (Pepler, 2020b), with variations in system frequency and intensity producing substantial impacts on total precipitation (Pook et al., 2012; Risbey et al., 2012). Extratropical cyclones deliver the largest proportion of both average and extreme precipitation across extratropical regions, including southern Australia (Pepler and Dowdy, 2022b). Anticyclone positioning further modulates these patterns, either suppressing precipitation over land or facilitating moisture transport from adjacent seas (Boschat et al., 2015; Holgate et al., 2023).

Climate change is anticipated to amplify both the frequency and intensity of drought events in some parts of southern Australia, with projections indicating drier conditions on average, presenting substantial risks to natural ecosystems and human societies (Falster et al., 12/2024b, 2024a; Stevenson et al., 2022; Ukkola et al., 2020). Future multi-year droughts in SEA are projected to last longer and be more intense than those observed during the 20th century, driven by a combination of natural climate variability and anthropogenic climate change (Falster et al., 2024a; Holgate et al., 2025; Ukkola et al., 2020). Furthermore, paleoclimate records show that Australia has experienced multi-year to decadal megadroughts far more severe and prolonged than those in the instrumental record (Freund et al., 2017; Ho et al., 2015). One notable example is a 39 year drought approximately eight centuries ago (Vance et al., 2015), demonstrating that natural droughts can substantially surpass the severity and duration observed in modern records even without human influence (Devanand et al., 2024b). These findings suggest that intrinsic drought risk may be underestimated in future planning (Leblanc et al., 2012). Multi-model

projections indicate significant increases in drought hazard metrics across Australia under climate change scenarios, with this intensified drought risk projected to affect a substantially larger geographic area than earlier studies suggested, particularly in SEA (Kirono et al., 2020). Given SEA's high vulnerability to water scarcity and its contribution of approximately 40% to Australia's total agricultural output (Murray-Darling Basin Authority, 2010), these climate change projections combined with paleoclimate evidence demonstrate the urgent need for improved understanding of prolonged drought mechanisms in SEA. Investigating how these prolonged multi-year droughts develop, persist and terminate is essential for enhancing prediction capabilities and informing water resource management under a changing climate.

However, investigation of long-term drought is constrained by the inherent limitations of observational precipitation records. With most records spanning only a century or less, they fail to capture the full spectrum of potential drought scenarios, especially those rare but severe prolonged droughts with devastating impacts (Devanand et al., 2024b; Falster et al., 2024a). A key aspect of understanding drought variability involves characterizing internal variability, the natural fluctuations arising from the chaotic and nonlinear characteristics of the climate system (Deser et al., 2012; Lafaysse et al., 2014). Climate model simulations relying on small ensembles of simulations or single-model outputs inadequately represent the full range of internal climate variability (Jain et al., 2023; Maher et al., 2018), and consequently incompletely represent drought events. These constraints limit the ability of observations and models to robustly characterize multi-year drought variability (Falster et al., 2024a). To address these challenges, this study utilizes single-model initial-condition large ensemble simulations from the GFDL SPEAR_MED climate model (Delworth et al., 2020; Lu et al., 2020). These single-model initial-condition ensembles produce multiple climate condition realizations within the same model framework, enabling a clearer distinction between forced climate responses and internal variability, while offering an extensive database for studying droughts that observational records or smaller ensembles cannot capture (Delworth et al., 2020; Lu et al., 2020; Maher et al., 2024, 2018). As it allows for extreme events such as drought to be captured, it enables a more comprehensive assessment of drought dynamics in relation to large-scale climate drivers and synoptic weather systems (Maher et al., 2024), which could help to strengthen our ability to understand the mechanisms and patterns of prolonged droughts in SEA.

This research aims to advance the understanding of prolonged drought mechanisms in SEA by investigating large-scale climate drivers (ENSO, IOD, SAM) and synoptic-scale weather systems (extratropical cyclones, anticyclones) that govern drought development, persistence, and

termination. Utilizing 30-member GFDL-SPEAR ensemble simulations (1921-2100), this study analyses rare, prolonged drought events to identify favourable and unfavourable conditions across different drought stages. The research scope is confined to meteorological drought processes, excluding hydrological, agricultural, and socioeconomic drought impacts, with spatial focus centred in SEA.

Research questions include:

1. What are the simulated characteristics of prolonged SPI-12 SEA droughts in their development, persistence, and termination stages?
2. What are the characteristics of individual climate driver phases (ENSO, SAM, IOD) during these drought stages?
3. How do climate driver phase combinations (ENSO-IOD, ENSO-SAM, SAM-IOD) vary during drought stages?
4. How do extratropical cyclone and anticyclone frequency and intensity anomalies evolve across drought stages in SEA and the Tasman Sea regions?
5. What are the spatial patterns of cyclone and anticyclone distribution during different drought stages?

To address these research questions, this thesis is structured as follows: Chapter 2 reviews the literature on drought processes, climate variability, and synoptic weather systems, identifying critical knowledge gaps in understanding prolonged drought evolution. Chapter 3 outlines the study's quantitative methodology, including drought identification procedures, climate driver analysis techniques, and cyclone detection algorithms applied to large-ensemble climate model simulations. Chapter 4 presents the findings across three analytical components: drought stage characteristics, climate driver behaviours during drought evolution, and shift in synoptic weather systems throughout drought lifecycles. Chapter 5 interprets the results, explains underlying mechanisms, compares them with existing research, and outlines limitations and future research directions. Chapter 6 summarises the key insights into prolonged drought mechanisms, highlights their scientific contributions, and discusses their relevance for drought prediction, water management, and climate resilience in SEA.

Chapter 2: Literature Review

2.1 Type of droughts

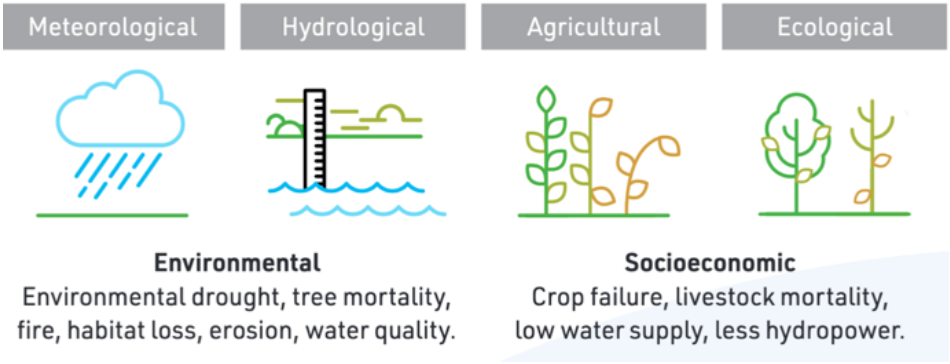

Figure 1. Classification of drought types and their environmental and socioeconomic impacts. (Derived from Devanand et al. (2022))

Droughts can be classified into four interconnected types: meteorological, hydrological, agricultural, and ecological, each of which operates at different scales and affects different aspects of environmental and socioeconomic systems (Figure 1) (Devanand et al., 2022). Van Loon (2015)'s process framework (Figure 2) demonstrates how precipitation deficiencies and temperature variations sequentially propagate through the hydrological cycle. The drought cascade begins with meteorological drought, defined as "the result of a prolonged reduction in precipitation" (Devanand et al., 2022), often exacerbated by high temperatures and increased evaporation rates (van Dijk et al., 2013). As moisture deficits propagate through the hydrological cycle, they trigger a cascade of drought types with escalating impacts. Soil moisture drought develops first when insufficient moisture becomes available for plant growth (Van Loon, 2015), directly compromising vegetation health and crop yields (Zargar et al., 2011). Subsequently, hydrological drought emerges as water reserves in streams, rivers, reservoirs, and groundwater systems become depleted, a process influenced by both climatic factors and anthropogenic water management practices (Van Lanen et al., 2013). This sequential propagation demonstrates the interconnected nature of drought processes: initial precipitation deficits systematically cascade through environmental systems, generating progressively broader impacts whose timing varies according to regional characteristics and antecedent conditions (Van Loon, 2013).

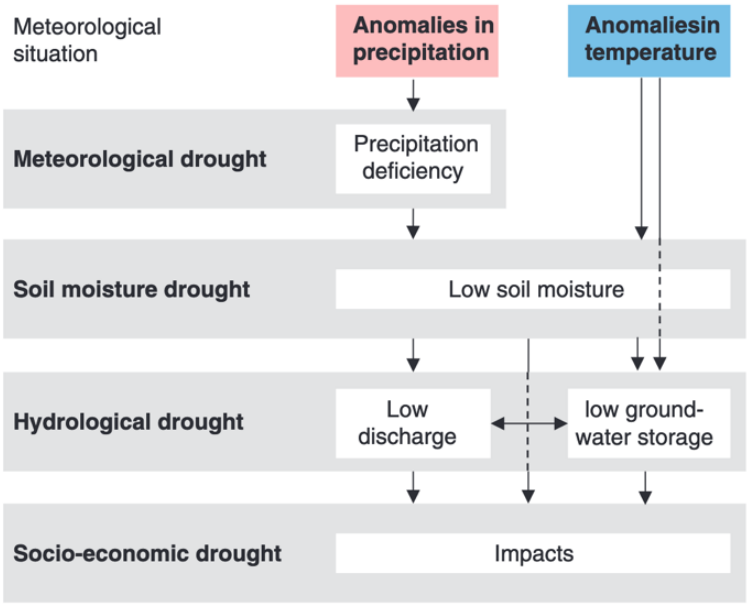

Figure 2. Conceptual framework illustrating drought type classification and sequential development. (Derived from Van Loon (2015))

Meteorological drought, as the initial trigger in the drought sequence, is the focus of this study, as it represents the primary and fundamental cause of drought propagation. This focus is further justified by the fact that climate models demonstrate superior predictive accuracy for precipitation relative to other hydrologically-relevant drought variables (Falster et al., 2024a; Ukkola et al., 2018).

2.2 Mechanisms of Drought

Drought cycles are commonly classified into three stages: development, persistence (also often called intensification), and termination. Understanding the stages of drought requires attention to the complex mechanisms that operate across multiple scales. On a larger spatial scale, climate modes of variability such as ENSO, IOD, and SAM create teleconnections that influence regional drought patterns, accounting for the majority of precipitation deficits during past Australian droughts (e.g. van Dijk et al. (2013)). On smaller spatial scales, the emergence and intensification of meteorological drought largely reflect the lack of weather systems that drive substantial moisture transport and precipitation (Holgate et al., 2020a; Pepler, 2020b). Land-atmosphere feedback amplifies drought severity by reinforcing precipitation deficits through soil moisture–atmosphere interactions (Holgate et al., 2025). Nevertheless, while these feedbacks

influence drought intensification once a drought is established, large-scale oceanic and atmospheric drivers remain the dominant controls on drought initiation and termination, which is the primary focus of this study (Holgate et al., 2020a).

Climate model simulations of drought are crucial for uncovering the links between processes and for providing a foundation for reliable drought prediction and projection. Holgate et al. (2025)'s review paper introduced a comprehensive framework for systematic evaluation of the key physical processes crucial to drought progression from climate models (Table 1). The framework encompasses four primary components: precipitation characteristics (including statistical distribution and persistence of anomalies), large-scale oceanic and atmospheric processes (Pacific and Indian Ocean SSTs, tropical climate variability modes, and relationships with Australian precipitation), weather systems (frequency and characteristics of cyclones, anticyclones, jet streams, and Rossby wave-breaking), and land surface processes (evapotranspiration and soil moisture evolution). Following this framework, the present research focuses primarily on the large-scale oceanic and atmospheric drivers, which govern the drought cycle in Australia, as well as weather systems including extratropical cyclones and anticyclones (Holgate et al., 2025, 2020a).

Table 1. Key climate system characteristics for assessing drought using models in Australia (Derived from Holgate et al. (2025).

Theme	Feature
Precipitation	Statistical distribution of precipitation: Models need to simulate the observed mean and variance to correctly simulate drought intensity. Models need to accurately simulate the tails of the distribution (e.g. 10th and 90th percentiles) to get the correct frequency of low or no rain sufficient to establish a drought and allow it to persist and the correct frequency of heavy rain to terminate a drought.
	Persistence of precipitation anomalies: Models need to be able to simulate clusters of mostly dry periods that lack very wet periods, in order to correctly simulate drought frequency and duration.
Large-scale processes	Pacific and Indian Ocean SSTs and interactions between these ocean basins
	Seasonality and interannual variability in tropical Pacific and Indian Ocean SSTs
	Relationships between modes of climate variability and Australian precipitation
	Frequency of co-occurring phases of different modes
	Location and intensity of subtropical jet and eddy-driven jet
	Rossby wave-breaking characteristics and processes
Weather systems	Frequency, precipitation intensity and stationarity of co-occurring deep cyclones and adjacent anticyclones; may be part of a blocking system
	Frequency, precipitation intensity and stationarity of WCBs and PV streamers
	Interactions between weather systems and the broader conditions in which they sit, such as the strength and locations of the jets and Rossby wave-breaking; interactions with larger-scale, lower-frequency ocean-atmosphere modes of variability; and interaction with smaller-scale land surface processes
Land processes	Evapotranspiration before and during droughts
	Evolution of soil moisture state during the various drought stages

Additionally, while models can reasonably capture the duration of seasonal meteorological droughts in Australia, they consistently struggle to reproduce observed drought intensity (Devanand et al., 2022; Ukkola et al., 2020). These limitations, evident across most regions, in

part stem from difficulties in representing land surface processes (Devanand et al., 2022; Ukkola et al., 2016). Consequently, this study focuses this study focuses on drought's duration rather than its severity.

2.3 Large-Scale climate drivers

This study focuses on three large-scale climate drivers, including ENSO (Wang et al., 2017; McPhaden et al., 2006), IOD (Saji et al., 1999) and SAM (Thompson et al., 2000), due to their established dominance in controlling precipitation variability in SEA (Cai et al., 2011a; Hendon et al., 2007; McKay et al., 2023; Risbey et al., 2009). Unlike most Australian regions where precipitation variability is dominated by one or two large-scale climate modes, precipitation in SEA is uniquely influenced across most seasons by the combined effects of ENSO, IOD, and SAM (Ashcroft et al., 2014; Risbey et al., 2009). Together, these three drivers provide the most robust basis for drought prediction (Dikshit et al., 2022; Hobeichi et al., 2024).

2.3.1 ENSO

ENSO represents Earth's most prominent interannual mode of variability, marked by irregular oscillations between warm (El Niño) and cold (La Niña) phases in the tropical Pacific Ocean (Bjerknes, 1966; McPhaden et al., 2006; Wyrtki, 1975). This coupled ocean-atmosphere phenomenon typically recurs every 2-7 years (BOM, 2025c), and lasts from about 9 months to several years (NOAA, 2024), contributing approximately 25%-50% of precipitation variance across different seasons in Australia (Risbey et al., 2009).

The physical mechanism driving ENSO centres on the Bjerknes feedback, a positive feedback mechanism involving ocean-atmosphere interaction that determines the strength of Pacific trade winds and zonal SST gradients (Bjerknes, 1966; Cane, 2005). Under neutral ENSO conditions (Figure 3b.), trade winds push warm surface water westward, accumulating warm waters in the western Pacific while drawing cooler, deeper water to the surface in the eastern Pacific through upwelling (BOM, 2025c).

El Niño

During El Niño (Figure 3a), trade winds weaken across the equatorial Pacific, resulting in higher atmospheric pressure in the western Pacific and decreased pressure in the eastern Pacific. This weakening allows the warm water in the western Pacific to migrate eastward while reducing upwelling in the east, creating anomalous warming in the central and eastern Pacific (McPhaden et al., 2006). The Bjerknes feedback then operates in reverse, weakening trade winds and warming SSTs reinforce each other, intensifying El Niño development (Wang, 2001; Wang and Picaut, 2004).

El Niño phases typically begin forming during autumn or winter and usually weaken quickly after maturing in austral summer (BOM, 2025c; Okumura and Deser, 2010). These events tend to occur as singular episodes with lower temporal persistence compared to La Niña and are most frequently followed by neutral ENSO conditions (Freund et al., 2024). During El Niño events, SEA often experiences warmer and drier conditions (BOM, 2025a), with precipitation deficits being most pronounced between June and February, with winter often showing the strongest impacts (Risbey et al., 2009).

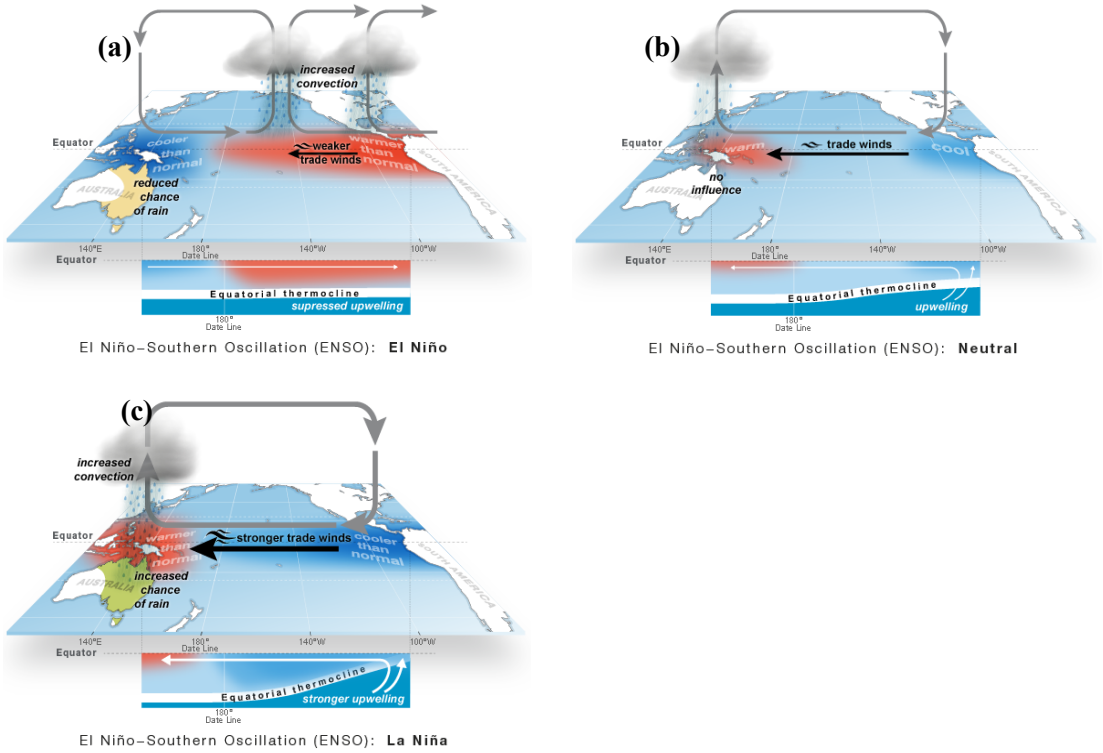

Figure 3. Ocean-atmosphere interactions during El Niño (a), neutral conditions (b), and La Niña (c). (Derived from (BOM 2013))

La Niña

Conversely, La Niña (Figure 3c) is characterized by cooling of tropical Pacific waters, significantly strengthened trade winds, and opposite pressure patterns with higher pressure in the east and lower pressure in the west, leading to enhanced upwelling in the eastern Pacific and a westward shift of warmer waters that concentrate in the western Pacific (BOM, 2025d; Gillett et al., 2023).

La Niña events usually develop during winter and dissipate in the following autumn (BOM, 2025e), demonstrating greater temporal persistence than El Niño events. Central Pacific (CP) La Niña events show the highest self-transition probability among all ENSO phases, with a 27.8% chance of recurring in consecutive years, while Eastern Pacific (EP) La Niñas transition to CP El Niño in 40% of cases (Freund et al., 2024). While Eastern Pacific (EP) La Niña has a 40% probability of transitioning to CP El Niño (Freund et al., 2024). La Niña events often bring above-average precipitation to SEA during winter and spring, as well as cooler daytime temperatures (BOM, 2016), heightening the risk of widespread flooding across SEA (Power and Callaghan, 2016).

2.3.2 IOD

While ENSO serves as the primary driver of climate variability in the Pacific Ocean, IOD performs a comparable function within the Indian Ocean basin (Han et al., 2014). IOD represents a coupled ocean-atmosphere mode of climate variability in the tropical Indian Ocean, marked by an east-west dipole pattern of SST anomalies accompanied by corresponding wind and precipitation shifts (Saji et al., 1999; Webster et al., 1999). Unlike ENSO's global reach, the IOD has a more regional impact (Saji et al., 1999), resulting from the Indian Ocean's smaller size and landlocked northern boundary, which limits event duration compared to often longer-lived ENSO events (BOM, 2025c; Han et al., 2014). The IOD demonstrates particular importance during June-October, effecting precipitation distribution across southern Australia and showing significant correlations with SEA climate during winter and spring when drought conditions typically develop (King et al., 2014; Risbey et al., 2009).

IOD is phase-locked to the seasonal cycle (Izumo et al., 2014; Saji et al., 1999), typically initiating during austral autumn with strengthening southeasterly winds near Indonesia (Behera et al., 2006). Events generally span 2-7 months from July to December, reaching peak intensity in September–November (Saji et al., 1999; Yang et al., 2015). Unlike ENSO events that can extend across multiple seasons or years, the IOD demonstrates shorter lifespans attributed to strong monsoon influences on the Indian Ocean's annual climate cycle (BOM, 2025f; Han et al.,

2014; Ummenhofer et al., 2009). Ocean-atmosphere feedback sustains IOD events until the reversal of trade winds around October-November triggers rapid decay as the northwestern monsoon disrupts wind patterns maintaining the temperature gradient (BOM, 2025f; Cai et al., 2013; Feng et al., 2014; Webster et al., 1999)

Neutral IOD phase (Figure 4a) represents conditions when the east-west SST gradient across the equatorial Indian Ocean remains close to the climatological mean state, with no significant anomalies in either basin (Saji et al., 1999). The usual configuration of elevated SST in the eastern Indian Ocean and cooler conditions in the west is maintained, supporting typical westerly surface winds along the equator that accumulate warm water eastward through downwelling Kelvin waves (Saji and Yamagata, 2003; Webster et al., 1999). This balanced state sustains normal Walker circulation with rising motion and precipitation over the eastern basin near the Indonesian maritime continent and relative subsidence over the western Indian Ocean (Webster et al., 1999).

Positive IOD phase (Figure 4b) features anomalously cool SSTs in the eastern equatorial Indian Ocean off Sumatra and warm SSTs in the western basin (Saji and Yamagata, 2003; Saji et al., 1999, Webster et al., 1999). During positive IOD events, the equatorial winds reverse from their normal westerly direction to easterlies, causing a rise in the thermocline in the eastern Indian Ocean (EIO) and a deepening in the western parts of the basin (Yamagata, 2004). This cooling in the east strengthens the equatorial easterlies, further intensifying upwelling while warming the western Indian Ocean (Behera et al., 2006; Webster et al., 1999). The resulting thermocline variations amplify SST anomalies, creating a self-reinforcing zonal temperature gradient and a coupled feedback system where the eastern cooling, western warming, and equatorial easterlies reinforce each other (Behera et al., 2006; Murtugudde et al., 2000; Murtugudde and Busalacchi, 1999; Reverdin et al., 1986). Positive IOD events are typically stronger than negative phases and tend to result in below average precipitation across southern Australia (BOM, 2025g; Ummenhofer et al., 2009).

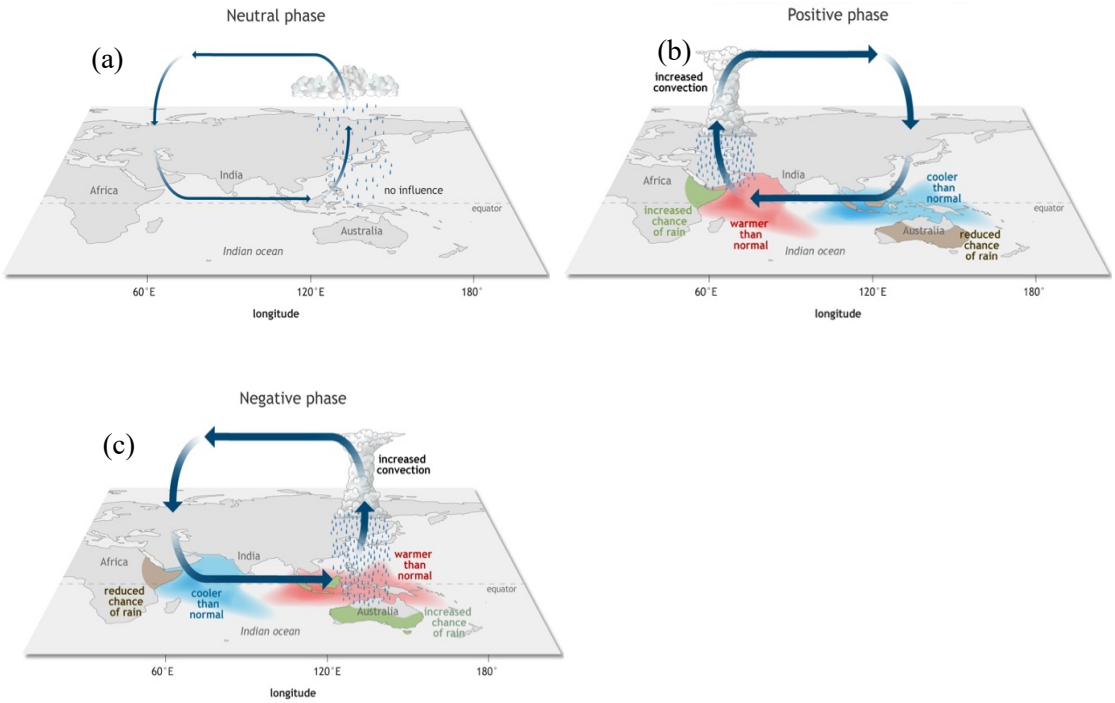

Figure 4. Ocean-atmospheric interactions during neutral (a), positive (b), and negative (c) IOD phases (Derived from (NOAA, 2020)).

During negative IOD phases (Figure 4c), the eastern Indian Ocean (EIO) warms while the western Indian Ocean (WIO) cools, with shifts in atmospheric circulation with westerly wind anomalies developing along the equator and anomalous eastward moisture flux across the eastern Indian Ocean (Abram et al., 2020b; Ummenhofer et al., 2009). Negative IOD events typically bring above-average precipitation to parts of Australia, with enhanced precipitation often observed in SEA (BOM, 2025f; Ummenhofer et al., 2009). Although generally weaker than positive IOD events (Cai et al., 2013), strong negative IODs can still be associated with heavy precipitation across Australia (Lim and Hendon, 2017).

2.3.3 SAM

SAM, also referred as the Antarctic Oscillation (AAO), is the primary driver of atmospheric variability in the Southern Hemisphere's extratropical regions (Gong and Wang, 1999; IPCC, 2007; King et al., 2023). It represents a zonally symmetric oscillation of sea-level pressure between the mid-latitudes (~40°S) and high latitudes around Antarctica (~65–70°S) (IPCC, 2007;

King et al., 2023). This pressure gradient controls the strength and position of the circumpolar westerly winds and associated storm tracks across the Southern Hemisphere (Ho et al., 2012). SAM oscillations typically persist for 1–2 weeks, though longer episodes may occur, with intervals between positive and negative phases ranging from ~1 week to several months (BOM, 2025b; Chung et al., 2025).

SAM has a strong influence on precipitation variability across SEA. It modulates storm track patterns and westerly wind dynamics, accounting for up to 15% of weekly precipitation variance in some regions, which is comparable in magnitude to the impact of ENSO (Hendon et al., 2007). SAM's precipitation impacts on Australia vary significantly by region and season (BOM, 2025h; Risbey et al., 2009) due to the climatological north-south migration of the westerly wind belt. During winter, SAM-induced anomalous easterlies cover most of the continent, whereas in summer they are confined to southern Australia due to the poleward-contracted subtropical ridge and developed monsoon trough over northern Australia (Hendon et al., 2007). Additionally, southeastern Australia's precipitation mechanisms shift from winter midlatitude frontal systems to summer tropical moisture intrusions, causing SAM to produce contrasting seasonal precipitation effects (Hendon et al., 2007). There are considerable disagreement and uncertainty regarding the relationship between SAM and Australian hydroclimatic variability, stemming from both limited reliable observational data in the Southern Ocean region (Ho et al., 2012) and the highly variable precipitation response to positive SAM, where wet and dry conditions occur with roughly equal probability (Holgate et al., 2022). Nevertheless, broad seasonal and regional precipitation patterns associated with different SAM phases are synthesized below.

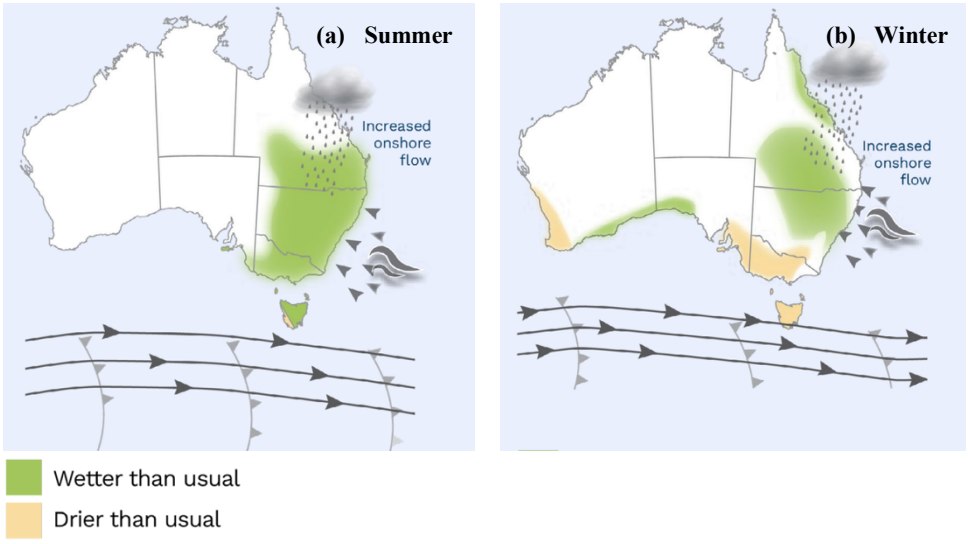

Figure 5. Positive SAM's impact on Australian precipitation in summer (a) and winter (b) (Adapted from (BOM, 2025h)).

Positive SAM phases are characterized by a poleward shift and intensification of the storm track over the Southern Ocean, leading to easterly wind anomalies over southern and central Australia that reduce westerly wind strength (Fyfe, 2003; Hendon et al., 2007; Thompson and Wallace, 2000), typically producing warming across mid-latitude regions of SEA (Gillett et al., 2006). These circulation changes can also prevent rain-bearing La Niña systems from reaching southeastern regions (Ho et al., 2012; Kiem and Verdon-Kidd, 2010).

During summer (Figure 5a), when westerly winds are already positioned south of Australia, positive SAM primarily decreases precipitation in western Tasmania while significantly enhancing moist onshore flow across parts of eastern Australia (BOM, 2025f; Hendon et al., 2007). This effect is especially significant as eastern Australia receives its climatological maximum precipitation during this season (BOM, 2025i).

During winter (Fig. 5b), the poleward shift weakens climatological westerlies, reducing synoptic-scale disturbances and decreasing precipitation in southwestern Australia and southeastern regions west of the Australian Alps (BOM, 2025g; Hendon et al., 2007). However, easterly anomalies enhance the flow of moist air from the Tasman and Coral Seas toward the continent, increasing precipitation in eastern Australia (BOM, 2025j; Warren et al., 2021).

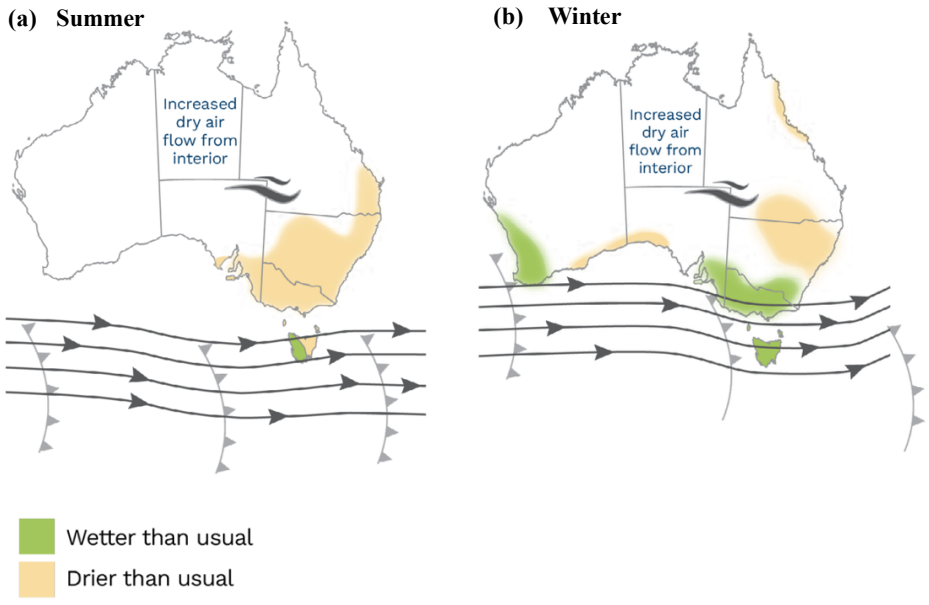

Figure 6. Negative SAM's impact on Australian precipitation in summer (a) and winter (b) (Adapted from (BOM, 2025h)).

A negative SAM is characterized by weaker westerly winds around Antarctica, with higher pressure near the South Pole and lower pressure in the mid-latitudes (around 40°S), causing storm tracks to shift northward and increasing atmospheric flow from dry inland areas rather than moist oceanic sources (Ho et al., 2012; Holgate et al., 2022; Marshall, 2003).

In summer, the northward shift of the westerly winds reduces moist onshore flow from the east, typically decreasing precipitation over eastern Australia, while enhancing westerly flow and precipitation over western Tasmania (BOM, 2025i). During winter, most of eastern Australia experiences decreased precipitation, while southwest and SEA receive increased precipitation due to strengthened westerlies, lower atmospheric pressure, and more frequent cold fronts and storm systems affecting southern regions (BOM, 2025g; Hendon et al., 2007).

2.3.4 Climate Drivers Future Projections

Climate projections indicate ENSO extremes will likely intensify with global warming, implying greater drought risk for SEA (Cai et al., 2021a; Shin et al., 2022). Future changes in the ENSO under global warming remain highly uncertain, as climate models show divergent projections and the strong internal variability of ENSO, making it difficult to distinguish forced changes in both observations and individual simulations (Maher et al., 2023; Wang et al., 2017). Despite these uncertainties, there is broad agreement that global warming will amplify ENSO-related tropical precipitation responses, particularly in the central and eastern equatorial Pacific, consistent with the tendency for greater mean warming in the eastern equatorial Pacific (Power et al., 2013; Santoso et al., 2019), By 2081–2100 compared with the historical baseline, ENSO teleconnections are projected to strengthen across many regions globally, including Australia, with changes scaling proportionally to the level of global warming (McGregor et al., 2022).

Evidence from paleoclimate records, observations, and climate projections indicates that strong positive indicate that strong positive IOD events are occurring more frequently in a warming climate, with their frequency projected to soon surpass the natural variability observed over the past millennium, alongside a shift toward stronger and earlier events and an increase in the amplitude of SST anomalies (Abram et al., 2020a, 2020b; Wang et al., 2024). Millennial-scale climate simulations indicate greenhouse warming will ultimately suppress overall IOD variability over long timescales, though century-scale projections remain uncertain due to large internal variability (Kim et al., 2024). Multi-model ensemble assessments suggest overall weaker IOD

events (Chung et al., 2024), while analyses using models capable of distinguishing between event types project increased strong positive IOD events but decreased moderate events (Cai et al., 2021b), signalling for elevated drought risk in the near future.

SAM projections show divergent seasonal responses due to competing influences of increasing greenhouse gases that enhance autumn/winter SAM, and ongoing ozone recovery (Grose et al., 2020; Thompson et al., 2011), which is curtailing the strengthening of positive summer SAM trends that previously helped mitigate eastern Australian droughts (Banerjee et al., 2020; Holgate et al., 2025). Future positive SAM trends tends to peak in winter, contributing to winter drying in southwestern and southeastern coastal regions while helping to offset drying in eastern Australia (Grose et al., 2020).

Overall, Projected changes in key climate drivers, including intensifying ENSO extremes, more frequent strong positive IOD events, and shift in SAM toward conditions that favour drying, are expected to increase aridity and heighten drought risk across southern Australia.

2.4 Synoptic weather systems

Australian precipitation variability arises from the combined influence of local weather systems and large-scale climate drivers, with their effects varying by region and season (Risbey et al., 2009). While large-scale climate modes set the background conditions for drought by limiting the occurrence of heavy or extreme precipitation, synoptic-scale weather systems can have a stronger influence on drought probability, particularly when the impact of broader climate drivers is weak (Devanand et al., 2024b).

Synoptic precipitation events in SEA are typically generated by extratropical cyclones, frontal systems, thunderstorms, warm conveyor belts and westerly cut-off lows, with the latter being especially important due to their links with blocking high-pressure systems and favourable jet stream configurations (Jin et al., 2024; Pook et al., 2006; Risbey et al., 2009). Past severe droughts in SEA (2017–2019) have coincided with markedly reduced numbers of lows (Pepler and Dowdy, 2022b), whereas exceptionally wet conditions (2020–2022) have been associated with prolonged heavy precipitation from cut-off lows with consecutive La Niña events (Barnes et al., 2023). Recognizing the critical role of regional-scale processes, the second part of this study

will focus on analysing regional synoptic weather systems during drought events to provide a more comprehensive understanding of prolonged drought mechanisms.

2.4.1 Extra-Tropical Cyclones

Amongst low-pressure systems, extratropical cyclones are the primary drivers of both total and extreme precipitation across SEA (Dowdy and Catto, 2017; Utsumi et al., 2017), delivering more than 40% of total precipitation and over 50% of heavy precipitation in southern Australia. In Tasmania and SEA, deep cyclones can contribute more than half of the annual precipitation (Pepler and Dowdy, 2022b).

The influence of extratropical cyclones on SEA appears to be most pronounced during the cool season (Pepler and Dowdy, 2022b), which also coincides with peak drought risk (Parker and Gallant, 2022). Evidence suggests that precipitation is typically enhanced when cyclones follow a southwest–northeast trajectory and interact with adjacent anticyclones that facilitate moisture transport (Pook et al., 2006), whereas drought years are often marked by a reduced frequency and intensity of these systems. This relationship was reflected in past severe prolonged drought events. The Millennium Drought (2001-2009) has been linked to a sustained decline in extratropical cyclone activity, while its termination was associated with the re-emergence of slower-moving, moisture-laden systems, particularly the increased occurrence of intense warm conveyor belts accompanied by persistent anticyclonic circulation over the Tasman Sea, which promoted moisture inflow (Jin et al., 2024; van Dijk et al., 2013). Similarly, the more recent Tinderbox Drought (2017–2019) featured three consecutive cool-season precipitation deficits of around 50% and coincided with historically low extratropical cyclone activity, with 2019 recording the fewest cyclones in southern Australia since at least 1950, approximately 50–60% below long-term averages (Devanand et al., 2024b; Pepler and Dowdy, 2020a).

2.4.2 Anticyclones

While extratropical cyclones are central to precipitation generation in SEA, their impact is strongly modulated by anticyclones. Anticyclones, or high-pressure systems, are dominant midlatitude features characterized by subsiding air and counterclockwise circulation in the Southern Hemisphere, typically producing dry, clear, stable conditions (Marshall, 2003; Pepler et al., 2019). They occur frequently across southern Australia, with the strongest central pressures generally in winter and a spring maximum in the Tasman Sea (Pepler et al., 2019). Despite their

prevalence, anticyclones contribute little direct precipitation, less than 5% across southern Australia (Pepler et al., 2019). The effect of an anticyclone depends on its location.

When positioned over SEA, the anticyclonic system promotes sinking air and clear skies across southeastern Australia, while transporting hot, dry continental air toward the southern coast (Boschat et al., 2015), suppressing precipitation and promoting dry conditions (Pepler et al., 2019; Pook et al., 2013)

In contrast, anticyclones over the Tasman Sea enhance precipitation potential by promoting onshore moisture transport. Their anticlockwise circulation drives northeasterly flows from the Tasman and Coral Seas, which can support cyclone development and heavy precipitation events (Boschat et al., 2015; Holgate et al., 2023; Pook et al., 2013). Slow-moving Tasman Sea anticyclones, in particular, generate persistent easterly flows that increase moisture availability along the east coast (Barnes et al., 2023).

Drought-terminating precipitation in SEA is most strongly associated with deep cyclones over the continent interacting with Tasman Sea anticyclones, which contribute roughly one-third of drought-terminating precipitation (Holgate et al., 2023). These patterns highlight how the location and interactions of cyclones and anticyclones can either promote or terminate droughts, illustrating the dual role of anticyclones in SEA as both drought sustainers and enhancers of precipitation.

2.4.3 Climate modes and synoptic activity

Extratropical cyclone and anticyclone activity in Australia is strongly modulated by large-scale climate modes. Positive IOD phases generally coincide with reduced extratropical cyclone activity and increased drought risk in southeastern Australia, whereas ENSO effects vary seasonally: La Niña can enhance cyclone-driven moisture transport, while El Niño tends to favour anticyclone development over SEA in summer (Gillett et al., 2023; Holgate et al., 2022a; Ummenhofer et al., 2015). SAM also modulates rainfall and synoptic-scale disturbances through storm track shifts and wind anomalies, with high seasonal and regional variations (Hendon et al., 2007). These relationships are illustrated by extreme events such as the 2017-2019 drought in SEA, where a strong positive IOD, negative SAM, and reduced cyclone activity contributed to record-low precipitation and depleted water storages (BOM, 2020b; Pepler, 2020b). Overall, climate modes influence droughts by altering the frequency and positioning of synoptic systems that deliver precipitation from local oceanic sources (Holgate et al., 2025).

2.4.4 Synoptic Weather Systems Future Projections

Climate model future projections suggest a substantial decline in deep subtropical cyclones in southern Australia, reducing the frequency of drought-relieving precipitation despite potential increases in cyclone intensity (Pepler, 2020b; Pepler and Dowdy, 2021). Poleward shifts in storm tracks and a general decrease in midlatitude low-pressure systems are expected to further limit precipitation during the cool season, contributing to more frequent and prolonged droughts (Chemke, 2022; Pepler and Dowdy, 2021; Priestley and Catto, 2022).

Chapter 3: Methodology

3.1 Study region

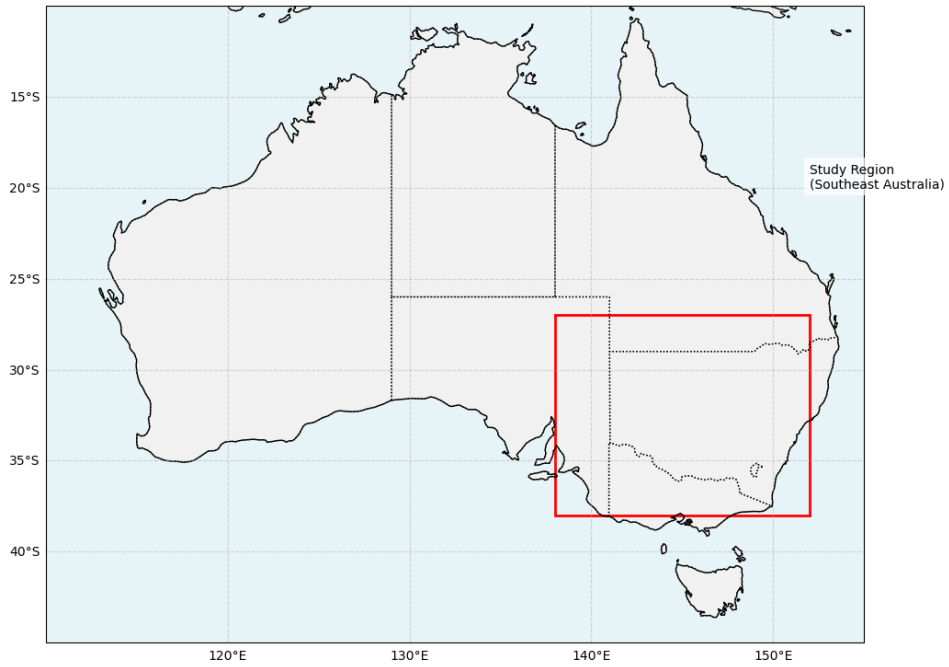

Figure 7. Map of Australia showing the study region in Southeast Australia (red box).

This study focuses on SEA, spanning 138°E–152°E and 28°S–38°S (Figure 7). The domain covers approximately 1.4 million km², encompassing major portions of New South Wales (NSW), Victoria (VIC), and parts of South Australia (SA).

3.2 Model & tool

The GFDL_SPEAR_MED (Seamless System for Prediction and Earth System Research) modelling system is a climate model developed by National Oceanic and Atmospheric Administration (NOAA)'s Geophysical Fluid Dynamics Laboratory (GFDL) to advance predictions and projections across seasonal to multidecadal timescales (Delworth et al., 2020). The system integrates four core components: the AM4 atmosphere model (50–100 km resolution), the MOM6 ocean model (~1° resolution with tropical refinement), the LM4 land model, and the SIS2 sea ice model, enabling simulations of coupled atmosphere-ocean-ice dynamics (Delworth et al., 2020; GFDL, 2020). Its design emphasizes computational efficiency to support large ensemble simulations. The large ensemble models this research used is the 30-member ensemble, spanning 1921-2100 under historical and SSP5-8.5 radiative forcing scenarios, which are critical

for quantifying climate variability and the response to external forcing such as greenhouse gases (Delworth et al., 2020; GFDL, 2020). The SPEAR_MED configuration, featuring a 50 km atmospheric resolution, enhances regional climate fidelity, especially for extreme events such as tropical cyclones, while maintaining a 1° ocean grid to balance local features with ensemble size (GFDL, 2020). The model's hybrid vertical ocean coordinate system and parameterizations for sub grid-scale processes improve representations of ocean heat uptake and circulation patterns, though biases persist in the Southern Ocean ventilation dynamics (GFDL, 2020). The 30-member large ensemble allows for sufficient samples of rare, prolonged drought events to enable robust statistical analysis of drought stage characteristics and driving mechanisms. It is important to note that although this study utilises a long-term climate model simulation spanning both historical and future periods, the analysis does not assess changes in prolonged drought from the past to the future.

Drought and large-scale climate drivers' detection used monthly data from this model for identifying long-term trends and teleconnections, whilst weather system analysis used finer scale daily data, as synoptic-scale features usually have a lifetime counted in days (North et al., 2015).

3.3 Detrending

All variables used for calculating drought indices and identifying climate drivers or weather systems were first detrended by removing the ensemble mean. This step was implemented to eliminate long-term trends, such as those driven by global warming, ensuring that the analysis focuses on interannual and shorter-term variability rather than long-term climatic changes. Detrending is essential to avoid confounding the effects of long-term trends with natural variability, which could otherwise lead to an overestimation of variability in regions experiencing rapid historical climate change (Fallah and Rostami, 2024; Wu et al., 2007). For this study, the ensemble mean was removed from each climate variable across all ensemble members, following established practices for separating forced signals from internal variability in climate model outputs (Maher et al., 2024). This approach ensures that the analysis captures only the variability intrinsic to the system and how this variability itself is influenced by external drivers, improving the reliability of further assessments.

3.4 Drought Metrics

Droughts are commonly monitored using standardized indices, with the Standardized Precipitation Index (SPI) (McKee et al., 1993) and Standardized Precipitation Evapotranspiration

Index (SPEI) (Vicente-Serrano et al., 2010) among the most commonly used tools for assessing meteorological drought (Schneider et al., 2013). The SPI, developed by McKee et al. (1993), provides a probabilistic assessment of accumulated precipitation deficits across various timescales, typically from 1 to 36 months (Devanand et al., 2024b). It is a widely recognized, World Meteorological Organization (WMO) endorsed global standard for drought analysis (Svoboda et al., 2012), offers advantages such as simplicity, spatial consistency, probabilistic nature enabling risk management applications (Svoboda et al., 2012), and the ability to produce multi-scale results that can be directly compared across different regions and climate zones (Lloyd-Hughes and Saunders, 2002). Reliable SPI calculation requires a minimum of 30 years of monthly precipitation data, ideally 50-60 years (Svoboda et al., 2012), which is a criterion met by GFDL-SPEAR simulations (Lu et al., 2020).

Testing revealed that SPEI detected drought events with comparable timing and in similar numbers to the SPI for the study region . Given this similarity, SPI was selected as the drought index for this study due to several methodological concerns with SPEI. Potential evapotranspiration (PET) - based indices like SPEI tend to overestimate future drought severity compared to direct climate model outputs and may double-count surface humidity and temperature effects (Milly and Dunne, 2016; Sheffield et al., 2012; Swann et al., 2016, 2016). Although SPEI theoretically provides more comprehensive drought assessment by incorporating both precipitation and evapotranspiration, these limitations reduce its reliability for climate model-based drought analysis.

SPI-12 was selected for this analysis as it derives from accumulated monthly precipitation values to capture prolonged drought conditions across SEA, with the 12-month accumulation period effectively detecting extended drought episodes that influence groundwater, reservoir storage, and streamflow patterns (McKee et al., 1993; Zargar et al., 2011).

Ocean areas within the study region were masked prior to SPI calculation to ensure the analysis focused exclusively on drought impacts over land areas where human populations and terrestrial ecosystems are directly affected. This approach also avoids possible confounding influences from precipitation processes over the ocean, which could follow different hydrological dynamics than land (Deirdre et al., 2016).

The SPI calculation was performed using the xclim Python package (Bourgault et al., 2023), implementing the established methodology of (McKee et al., 1993). The process involves two stages: (1) fitting a probability distribution to accumulated precipitation data for the specified timescale, and (2) transforming to a standard normal distribution via inverse normal

transformation. The cumulative probability distribution transforms into a standard normal distribution yielding SPI values, where negative values indicate below-median precipitation (drought conditions) and positive values indicate above-median precipitation (McKee et al., 1993). A baseline period of 1921-1980 was established as the climatological reference, representing a pre-warming period for drought assessment (Reid et al., 2016).

Three probability distributions were empirically tested for SPI calculation: Gamma (McKee et al., 1993), Weibull (Sienz et al., 2012), and Fisk (log-logistic) distributions (Vicente-Serrano et al., 2010). Valid SPI calculation requires the resulting time series to be standard normally distributed ($\mu = 0$, $\sigma = 1$) (Pieper et al., 2020). Performance evaluation showed that only the Fisk distribution produced SPI values maintaining the required normality properties with zero-centred results. Both Gamma and Weibull distributions failed to achieve this fundamental requirement when applied to this climate model dataset, whereas the Fisk distribution successfully maintained normality. Given the Fisk distribution's capacity to model skewed precipitation data while preserving normality in transformed SPI values, it was selected as the probability distribution for SPI calculation in this study.

Drought categories of SPI were adopted from WMO's SPI User Guide (Svoboda et al., 2012), classified as mild ($-1 \leq SPI < -1.5$), severe ($-1.5 \leq SPI < -2$), and extreme ($SPI \leq -2$).

Table 2. SPI values (Derived from Svoboda et al., 2012)

2.0+	extremely wet
1.5 to 1.99	very wet
1.0 to 1.49	moderately wet
-.99 to .99	near normal
-1.0 to -1.49	moderately dry
-1.5 to -1.99	severely dry
-2 and less	extremely dry

3.5 Prolonged Droughts Identification

The definition and identification of drought remain highly variable across different studies and regions, with researchers employing diverse indices and methodological approaches to determine drought onset and termination (Mishra and Singh, 2010; Veettil and Mishra, 2023), making it difficult to assess and examine droughts consistently. Given this study's focus on prolonged drought, prolonged drought events were defined as droughts persisting for a minimum duration of 12 months. Drought events, stages, and durations were captured by applying run theory principles (Yevjevich, 1967).

Drought events based on SPI are defined as a period with continuously negative values ≤ -1 (McKee et al., 1993) Drought stages in this study were classified into development, persistence, and termination, and identified using Yevjevich, (1967)'s run theory framework. However, this method inherently detects drought periods only from persistence to termination, as it relies on consecutive sequences of months with drought index values below a chosen threshold to define drought events, with the duration being the length of time values remain continuously below the threshold. Therefore, run theory was applied solely to the persistence-to-termination period, while the development phase was defined separately using a fixed pre-onset period. Drought stages were defined as follows:

- Development Stage: The 12-month period immediately preceding drought persistence. This phase captures the gradual meteorological transition from normal conditions toward the threshold conditions that initiate drought classification.
- Persistence Stage: From the start of 12 consecutive months with SPI-12 ≤ -1.0 until the start of the termination phase. This represents the core drought period when conditions consistently remain at or below the drought threshold.
- Termination Stage: From the last SPI-12 value at or below -1.0 until the end of drought, when SPI-12 reaches +1.0. This phase captures the recovery period as meteorological conditions gradually improve from drought threshold toward normal conditions.

This stage-specific approach provides comprehensive coverage of the complete drought cycle, from the pre-drought developmental conditions through the core drought period to final recovery, enabling detailed analysis of drought evolution patterns and their associated impacts across all temporal stages.

3.6 ENSO Index

The most widely used ENSO index is the Niño 3.4 index, which is calculated by averaging SST anomalies within the Niño 3.4 region in the central-eastern equatorial Pacific (5°S–5°N, 120°–170°W) (Bamston et al., 1997; Trenberth, 2024, 1997). This study adopts the relative Niño 3.4 index as the ENSO metric proposed by (van Oldenborgh et al., 2021). This method accounts for tropical-wide SST variations by subtracting the simultaneous average SST anomaly across the tropics (20°S–20°N) (Johnson and Kosaka, 2016) from the traditional Niño 3.4 index, thereby removing the long-term warming signal. As both the NINO3.4 region and the tropical mean have experienced similar warming rates, relative Niño 3.4 index's subtraction filters out most of the anthropogenic trend while preserving ENSO-driven variability.

$$\text{Relative Niño3.4} = \text{Average SST anomalies Niño 3.4 } (5°\text{S} - 5°\text{N}, 120° - 170°\text{W}) - \text{Tropical mean SST anomaly } (20°\text{S} - 20°\text{N})$$

There are many thresholds to classify ENSO phases across different studies, and threshold selection is somewhat subjective. Some studies define strong events as ±1 standard deviation and weak events between ±0.5 and 1 standard deviation, with neutral conditions within ±0.5 standard deviations (Gillett et al., 2023; Santoso et al., 2017; Trenberth, 1997). Others use fixed temperature thresholds such as ±0.5°C (NOAA, 2025), ±0.8°C approximating one standard deviation (BOM, 2025k), or ±0.5°C (Geng et al., 2023). This study adopts standardized deviation-based thresholds for all climate driver indices to ensure consistency across different variables and maintain comparability with climate model outputs, which typically express anomalies in standardized units. The standard deviation thresholds were converted to equivalent °C anomalies and refined based on empirical analysis of the dataset. The final classification thresholds are presented in Table 3.

After that, the Oceanic Niño Index (ONI) obtained by applying a 3-month running mean to the relative Niño 3.4 anomalies, which smooths short-term, high-frequency variability while preserving the more persistent ENSO signal (Trenberth, 2024).

ENSO events are identified using a persistence-based approach requiring five consecutive months above or below specified thresholds in Table 3. (Trenberth, 2024). Once initiated, events continue as long as monthly values remain above the weak threshold. Event intensity classification is determined by the peak 5-month running average during the entire event duration. Individual months within an event receive the same classification based on this peak intensity

measure, regardless of their individual monthly values. Months not part of any identified ENSO event are classified as neutral.

Table 3. Climate Driver Indexes Thresholds

Intensity	Threshold
Neutral	-0.7σ < value <+0.7σ
Weak	± 0.7σ
Strong	± 1.4σ
Extreme	± 2.0σ

Relative Niño 3.4 index exhibits about 20% less variability due to the removal of much of the ENSO-related signal that overlaps with the tropical mean SST (van Oldenborgh et al., 2021). Consequently, the threshold lines in this plot are naturally smaller. Since no fixed categorical thresholds were used to define events, the relative Niño 3.4 index does not require any adjustment (i.e., re-normalization) in this context, as would be necessary if fixed categorical thresholds had been applied (van Oldenborgh et al., 2021).

3.7 IOD Index

The IOD is most commonly quantified using the Dipole Mode Index (DMI), defined as the difference in SST anomalies between the western equatorial Indian Ocean (50°E–70°E, 10°S–10°N) and the southeastern equatorial Indian Ocean (90°E–110°E, 10°S–0°N) (An et al., 2023; Saji and Yamagata, 2003; Saji et al., 1999)

$$DMI = SST\ Anomoly\ (WIO) - SST\ Anomoly\ (EIO)$$

Although alternative definitions have been proposed, including a revised western boundary of 60°E–80°E (Saji and Yamagata, 2003), the original formulation by Saji et al. (1999) remains the standard metric for IOD intensity. Positive (negative) values of the DMI correspond to positive (negative) IOD phases, with thresholds of ±0.4 °C commonly used to identify events (BOM,

2025c). However, in this study, the same standard deviations threshold in Table X will be used for DMI as well for consistency.

A 3-month running mean was applied to the DMI, and events were classified as IOD events only when the index exceeded the threshold for a minimum duration of three consecutive months. The assessment of event intensity and the identification of monthly IOD phases were conducted following the same methodology applied to ENSO.

3.8 SAM Index

The Marshall SAM index is the most commonly used index to identify SAM events, calculated using the normalized zonal mean sea-level pressure (MSLP) difference between 40°S and 65°S (Cai et al., 2011c; Gong and Wang, 1999; Marshall, 2022, 2003). The index is computed as:

$$SAM = P'_{40\circ S} - P'_{65\circ S}$$

Typically, high and low SAM index days are defined as those when the daily SAM index anomalies exceed certain standard deviation thresholds (Hendon et al., 2007; Marshall et al., 2018; WMO, n.d.). However, Velasquez-Jimenez and Abram (2024) demonstrated that normalization introduces resolution-dependent scaling effects, where SAM values differ artificially depending on temporal resolution. Annual standardized SAM values can be 3.1× larger than monthly derived values and 4.4× larger than daily derived values. Additionally, the standardized index overweighs mid-latitude (40°S) pressure variability relative to Antarctic (65°S) variability, amplifying apparent tropical connections that are not part of SAM's core dynamics while obscuring the asymmetric zonal wave-3 component critical to SAM variability. Though acknowledging this possible limitation, the standardized SAM index is used for threshold consistency with other climate driver indexes while acknowledging that results may reflect resolution-dependent scaling artifacts rather than true atmospheric dynamics.

Due to SAM's high variability, a 12-month centred running mean was applied to reduce high-frequency noise and isolate persistent circulation patterns relevant for prolonged drought analysis. Monthly SAM phases were identified using standardized thresholds based on the temporal variability of this smoothed index. Each month was assigned to exactly one phase category according to standard deviation thresholds in Table 3.

3.9 Cyclone/ Anticyclone Detection

3.9.1 Domains

Cyclone and anticyclone occurrences in SEA and the Tasman Sea were detected using the domains defined by Holgate et al. (2023), and the original two-domain framework was proportionally scaled up to cover the enlarged SEA study area of this study (Figure 8). Both cyclones and anticyclones were detected in the two domains. All systems whose centres were positioned within these domain boundaries and satisfied the identification criteria were captured, regardless of whether the cyclone's boundary extended beyond the domain.

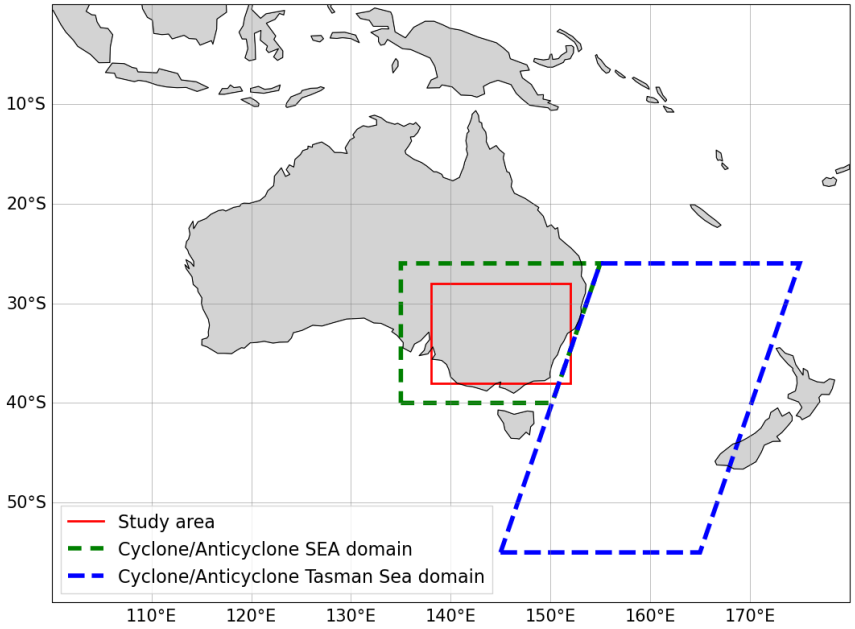

Figure 8. Study domain configuration showing the study area (red line), SEA domain (green dashed box), and Tasman domain (blue dashed box) used for both cyclone and anticyclone detection.

3.9.2 Filtering

Prior to cyclone identification, time-averaged (TAV) filtering (Anderson et al., 2003) was applied to the Sea Level Pressure (PSL) data to isolate synoptic-scale weather systems from large-scale, time-invariant spatial patterns. This filtering procedure removes the long-term temporal mean climatology at each grid point from the daily PSL fields to isolate synoptic-scale weather systems.

Areas above 1000 m elevation were excluded, as orographic influences can affect cyclone dynamics and tracking accuracy (Catto and Raveh-Rubin, 2019; Wernli and Schwierz, 2006). An

elevation mask from ETOPO 2022 global relief model (NOAA NCEI, 2022) was applied to exclude high-altitude grid points.

3.9.3 Cyclone/anticyclone detection

Cyclone and anticyclone detection was performed using the established methodology of Wernli and Schwierz (2006), which has been thoroughly validated and widely used across numerous studies (Catto and Raveh-Rubin, 2019; Dowdy and Catto, 2017; Jin et al., 2025, 2024, 2023) . Following the methodology of Wernli and Schwierz (2006), the cyclone detection algorithm identifies both cyclones and anticyclones through a two-step process within the defined tracking domains. First, it detects pressure extrema: cyclones are local minima in the sea level pressure field, where the centre pressure is lower than all eight surrounding grid points, while anticyclones are local maxima, with the centre pressure higher than all neighbouring points. After identifying these extrema, the algorithm systematically searches for closed pressure contours around each centre by examining successive contour levels outward from the extremum.

Initial testing with the common 2 hPa atmospheric pressure interval yielded unrealistically high system frequencies in the Tasman Sea, likely due to spurious detection of small-scale pressure features arising from the finer grid spacing, as the GFDL-SPEAR dataset (0.5°×0.625°) has higher spatial resolution compared to the typical 1° resolution analyses employed in previous cyclone detection studies (Catto and Raveh-Rubin, 2019; Wernli and Schwierz, 2006). To account for this, a 4 hPa interval was employed instead, ensuring the algorithm remains focused on synoptic-scale atmospheric systems of meteorological significance. Sensitivity testing across different contour intervals (2-6 hPa) indicated that each +1 hPa increase slightly reduced cyclone counts while marginally increasing anticyclone counts, though the overall effect was not so significant. Cyclones/anticyclones contours were generated at center pressure ±4hPa, and so forth, and subsequent decremental levels. The outermost closed contour that encompasses only the pressure extremum under consideration defines the spatial extent of the identified cyclone or anticyclone (Wernli and Schwierz, 2006).

Chapter 4: Results

4.1 Drought Characteristics

The following section presents the results for RQ 1: What are the simulated characteristics of prolonged SPI-12 SEA droughts in their development, persistence, and termination phases?

4.1.1 Types of Drought Development

The 12-month drought development period was selected as a fixed estimate of the drought development period. However, visual inspection of SPI-12 time series for drought events across all ensemble members shows considerable variation in SPI-12 evolution in the 12 months preceding drought events across simulated events and ensemble members, making it difficult to define a precise criterion for drought development. Broadly, drought development could be classified into two categories based on SPI evolution prior to drought events: direct development, and gradual, or pre-conditioned development, though individual events within each category can differ considerably in magnitude and progression.

Type 1: Direct Development

Direct Development (Figure 9) characterizes the development period of approximately 40–60% of all drought samples in the study region. It features a rapid transition from normal or above-normal precipitation to drought conditions. In this pattern, the SPI-12 declines steadily with minimal fluctuations, beginning from values above zero and progressing directly into the persistence phase (SPI12 ≤ -1.0) without significant interruption.

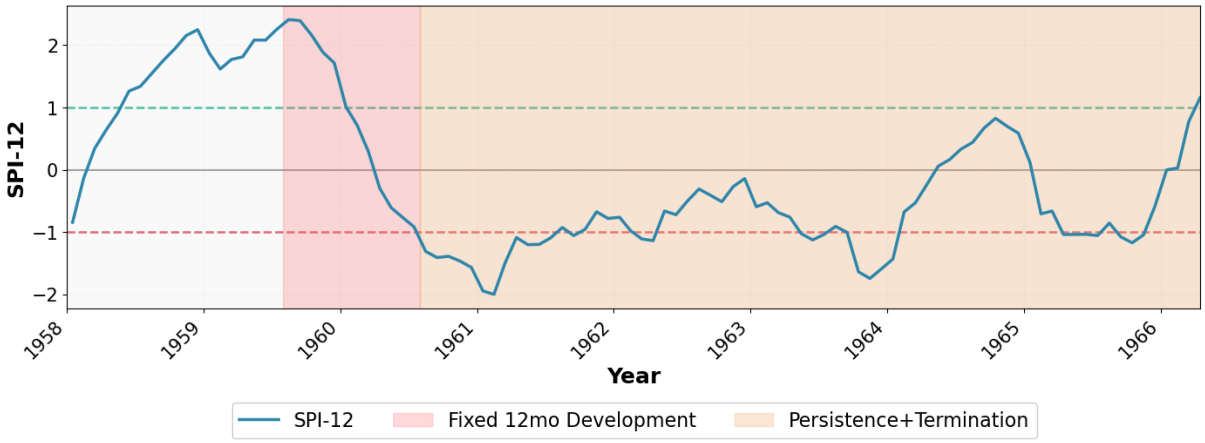

Figure 9. Sample illustration of a direct drought development (drought Sample derived from ensemble 23.). Red shaded area represents the fixed 12-month development period preceding drought persistence applied for all drought samples.

Type 2: Gradual or Pre-conditioned Development

Type 2 involves drought development under pre-existing dry conditions or following incomplete recovery from previous drought episodes. This category includes two scenarios: (a) development from existing slight drought conditions where SPI values are already below normal (Figure 10a), and (b) development following a recent short-duration drought that did not meet the 12-consecutive-month threshold for prolonged drought classification, or during incomplete recovery from a previous drought event (Figure 10b). The latter scenario typically shows periods of precipitation increase followed by renewed decline, with SPI12 values potentially rising above zero but remaining below +1.0, indicating insufficient normalization of meteorological conditions.

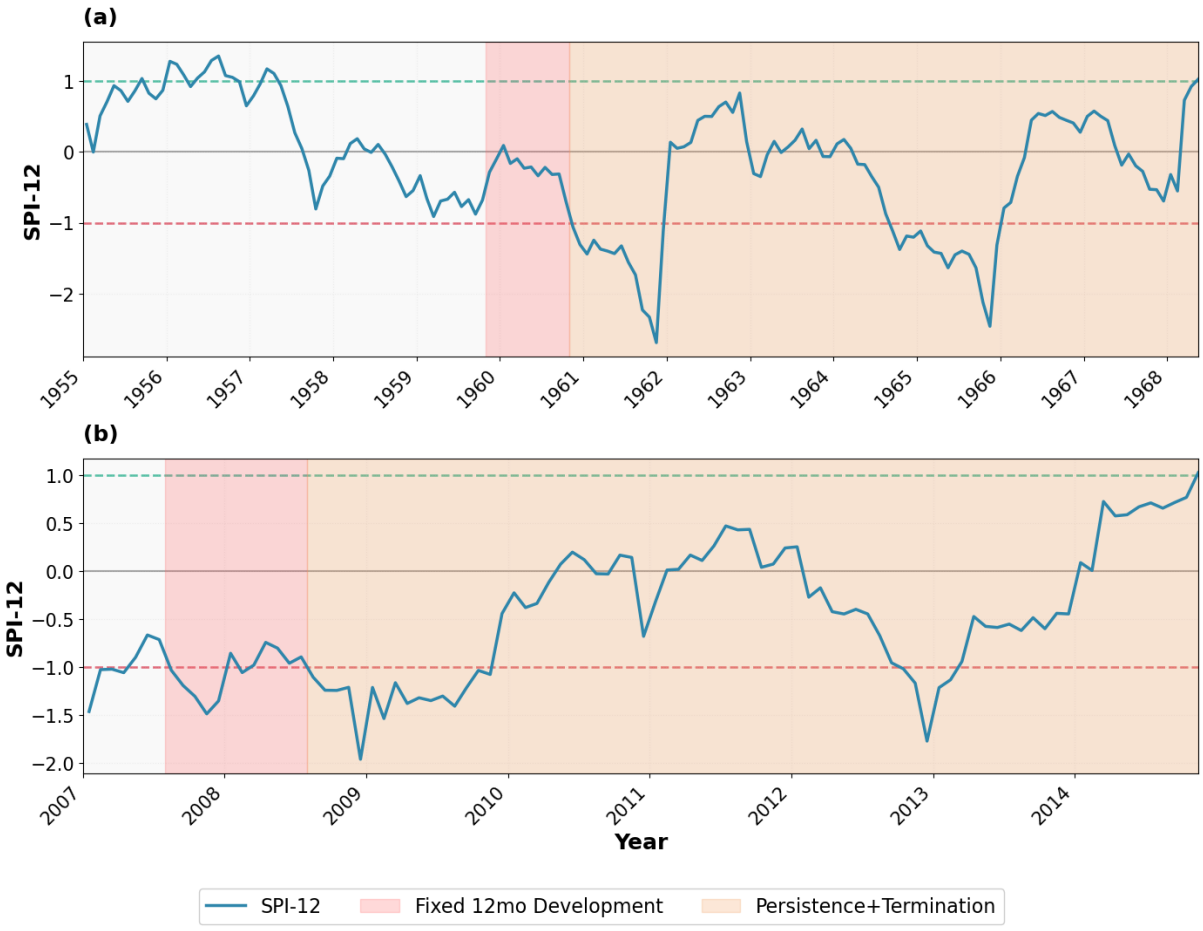

Figure 10. Sam Development **f (a) gradual drought development (drought sample deriv e 29), and (b) pre-conditioned drought onset (drought Sam ensemble 17).**

4.1.2 Drought stages analyses

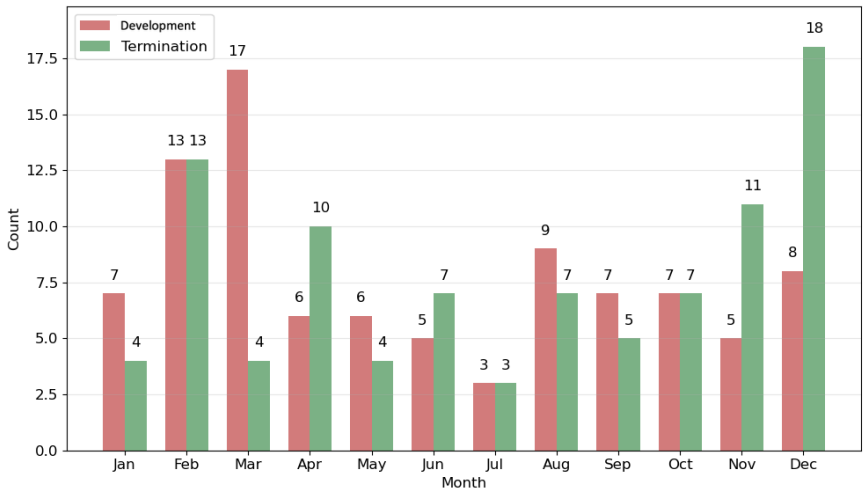

Figure 11. Grouped bar chart showing monthly distribution of drought development (red) and termination (green) for all drought samples (1921-2100).

Drought development month distribution (Figure 11) shows peak frequencies during summer/early autumn months (December-March), with March recording the highest development frequency (17), followed by February (13) and December (8). While mid-autumn to mid-winter months (April-July) demonstrate lower development rates. The prolonged drought termination distribution (Figure 9) is relatively less seasonal compare its onset. Peak frequencies during late spring to summer, with December showing the highest termination frequency (18), followed by February (13) and November (11).

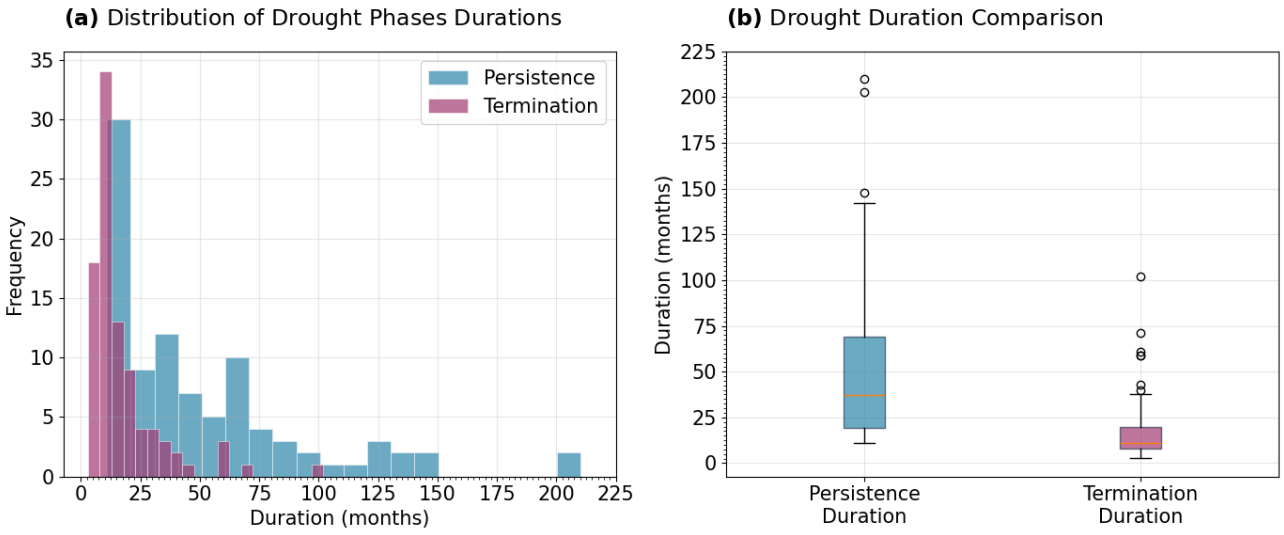

Figure 12. Distribution and comparison of drought stage durations. (a) Overlapping histograms showing the frequency distribution of persistence (blue) and termination (purple) phase durations across all drought events and ensemble members. (b) Box plots comparing statistical distributions of persistence and termination phase durations.

Drought persistence phases substantially exceed termination phases in duration (Figure 12), averaging ~30 vs. ~10 months respectively, making termination approximately one-third the length of persistence (drought development phases were not investigated, as its duration was preset to a fixed 12 months). Persistence phases show high variability, with numerous extreme outliers lasting beyond 200 months (~17 years), while termination phases are more consistent and predictable, rarely exceeding 100 months (~8 years) and generally lasting less than 30 months. Exceptionally long persistence events are rare, and unusually long termination phases are virtually absent relative to their respective typical durations, suggesting that once termination begins, droughts end relatively quickly and consistently.

4.2 Large-scale Conditions

4.2.1 Precipitation, SSTs and atmospheric circulation during drought stages

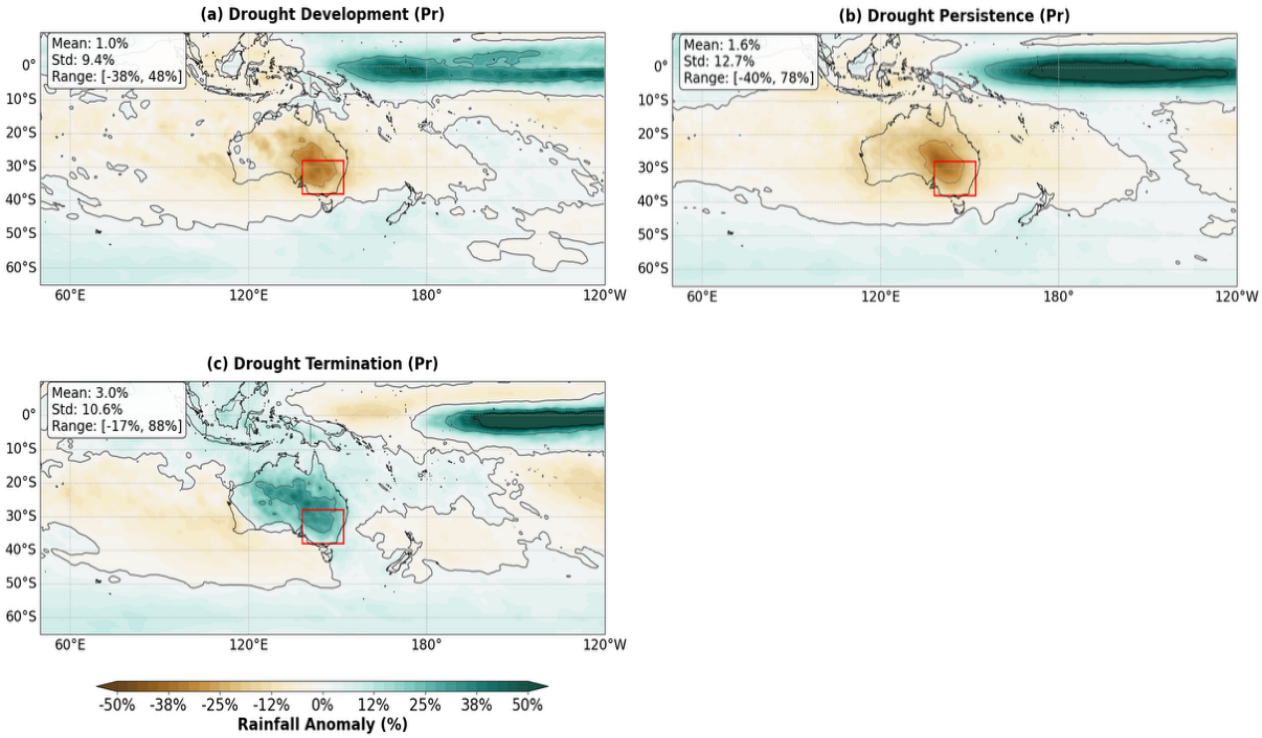

Figure 13. Composite precipitation anomalies during different phases of SEA drought events across the Indo-Pacific region (50°E-240°E, 65°S-10°N). (a) drought development, (b) drought persistence, and (c) drought termination. The red rectangle represents the SEA study region. Black contour lines denote zero anomaly (thick line) and ±1 standard deviation (thin lines). The colour scale was scaled to ±2 standard deviations from the mean of all data points across the three drought stages.

Examining how precipitation evolves through drought stages helps reveal the spatial dynamics of drought across SEA. The composite precipitation patterns indicate an east-to-west progression of impacts throughout Australia's drought lifecycle. During the development phase (Figure 13a), most of the study area experiences dry conditions, except for the coastal and western regions. As drought persists (Figure 13b), dryness intensifies and shifts from eastern to central Australia, reducing the affected area. Across these stages, much of the continent experiences below-average precipitation, with reduced precipitation also extending over the surrounding oceans at similar latitudes. In contrast, higher-than-normal precipitation occurs over parts of the tropical Pacific, reflecting large-scale atmospheric and oceanic influences. During the termination phase (Figure 13c), precipitation gradually increases and spreads westward, marking the onset of recovery.

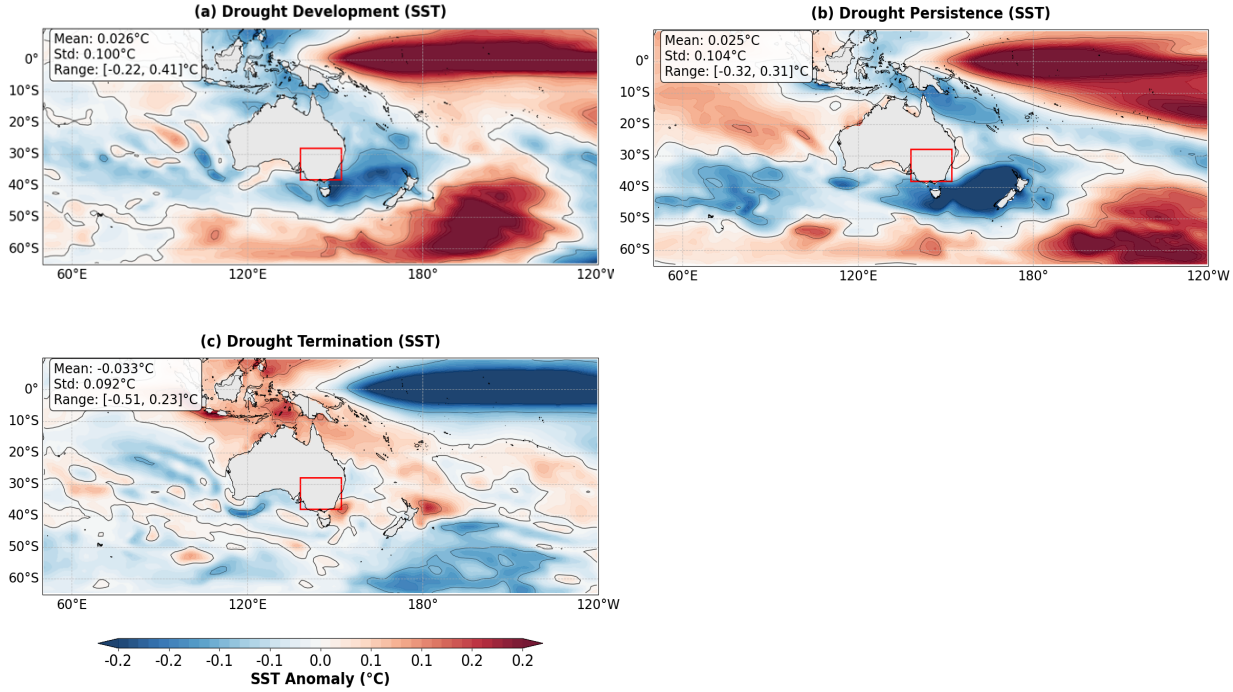

Figure 14. Composite SST anomalies (as for Figure 11).

SST anomaly composites were analysed to identify oceanic influences associated with drought evolution. During drought development (Figure 14a), significant warming anomalies emerge in the central Pacific ENSO region, while pronounced cooling forms around Australia. Weak positive anomalies in the South Pacific connect central Pacific warming to strong anomalies in the southernmost Pacific/Southern Ocean. In the Indian Ocean, weak positive anomalies appear between western and eastern basins.

In the persistence phase (Figure 14b), central Pacific warming becomes more spatially confined with a distinctive eastward extension. Cooling around Australia intensifies, particularly in the Tasman Sea. The continuity of warm SST anomalies across the South Pacific was disrupted as Southern Ocean warming shifts southeast-ward, leaving negative anomalies in the intervening region, which may result from a slight northward Intertropical Convergence Zone (ITCZ) shift. SST anomalies in the Indian Ocean Basin form a meridional gradient, of warmer waters in the north and cooler waters in the south.

SST anomalies pattern over the Pacific Ocean and the seas north of Australia broadly reverse during drought termination (Figure 14c). The Tasman Sea transitions to near-normal conditions with weaker, spatially distributed positive anomalies. In the Indian Ocean, warming shifts eastward/northward, producing strong positives in the western Indian Ocean (WIO) and WIO and

covering the northern Australian coastline, while the eastern Indian Ocean (EIO) develops weak anomalies, representing a complete DMI pattern reversal compared to dry drought stages.

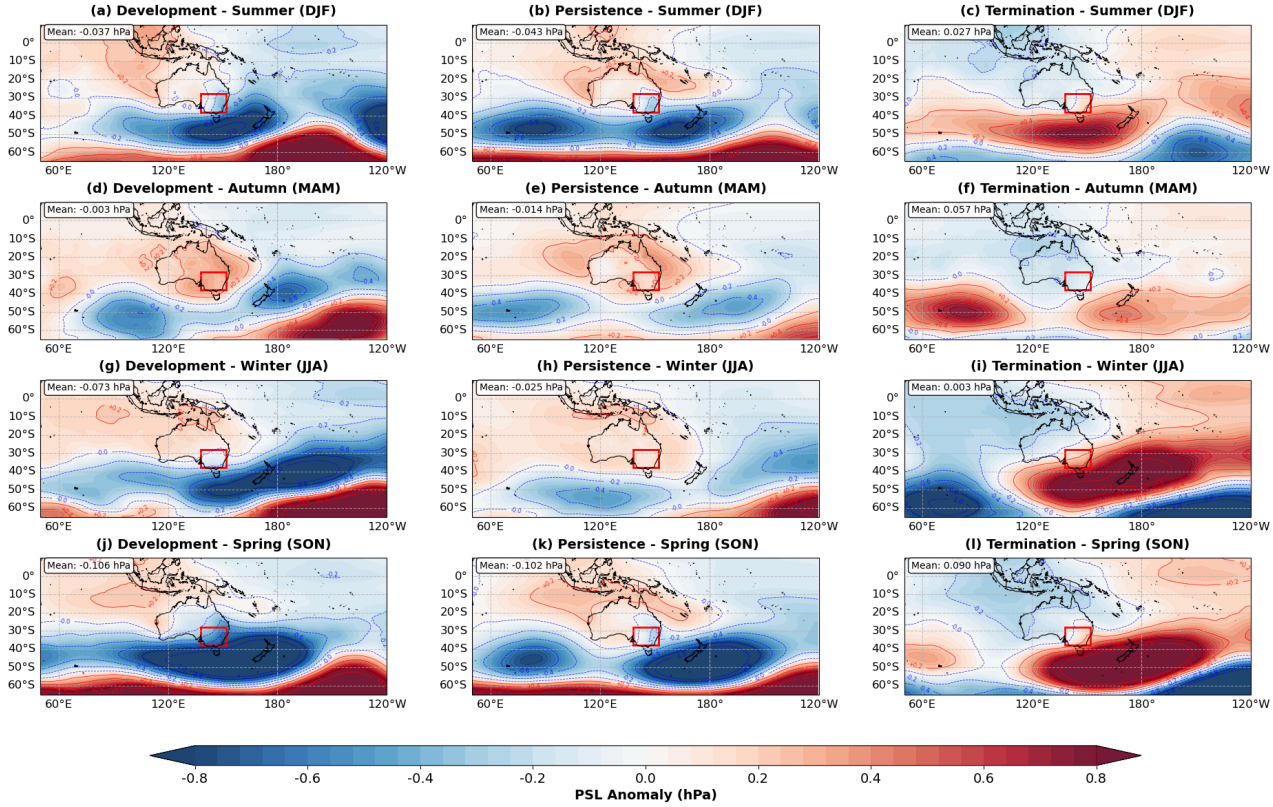

Figure 15. Composite seasonal PSL anomalies during different phases and seasons of SEA during SEA droughts. Seasonal PSL anomalies were derived by calculating seasonal climatological means from detrended monthly data for 1921–1980 (DJF, MAM, JJA, SON) and subtracting these from the corresponding monthly values in each season during drought periods across the time series. This approach removes both the long-term mean and seasonal cycle, isolating anomalous pressure patterns that deviate from typical seasonal conditions.

Composite PSL anomalies describe the lower-atmospheric circulation patterns that influence moisture availability and rainfall distribution during drought stages in SEA. During drought development (Figure 15a, d, g, j) and persistence (Figure 15b, e, h, k), the SEA study area generally experiences higher than normal PSL in most seasons. In some seasons, however, weak negative PSL anomalies are observed over the study region, likely extending from the stronger negative anomalies over the Tasman Sea. Looking at broader regional patterns, during drought development, positive PSL anomalies dominate much of northern Australia and the northern Indian Ocean, except in SON, when the pattern shows slight deviations. At the same time, strong positive PSL anomalies near ~60°S indicate negative SAM conditions. During the persistence stage, the negative anomalies over the Tasman Sea weaken and extend less into SEA, while

positive PSL anomalies continue to cover most of the Australian continent and the northern Indian Ocean, maintaining the broad dry conditions.

A key distinction between the development/persistence and termination stages is the PSL anomaly over the Tasman Sea to the study area's southeast. During the wetter termination stage (Figure 15c, f, i, l), higher PSL over the Tasman Sea is evident and extends slightly into the terrestrial study area during some seasons, a feature absent during the drier development and persistence stages. Broad regions of light negative PSL anomalies are evident across much of Australia and the northern Indian Ocean. Around ~60°S, negative PSL anomalies align with positive SAM conditions, with the SAM signal being weakest in autumn and strengthening through winter and spring.

4.2.2 Large Scale Climate Drivers

The following result section presents results for answering RQ 2: What are the characteristics of individual climate driver phases (ENSO, SAM, IOD) during these drought stages?

It is important to note that instead of analysing climate drivers within their specific temporal positions in individual drought samples (e.g., the occurrence of El Niño during particular drought stages), all months corresponding to each driver's phases across all drought samples were aggregated and analysed together, regardless of their temporal position within individual droughts. Therefore, any temporal patterns observed represents general characteristics of climate driver conditions across prolonged droughts, rather than patterns within individual events.

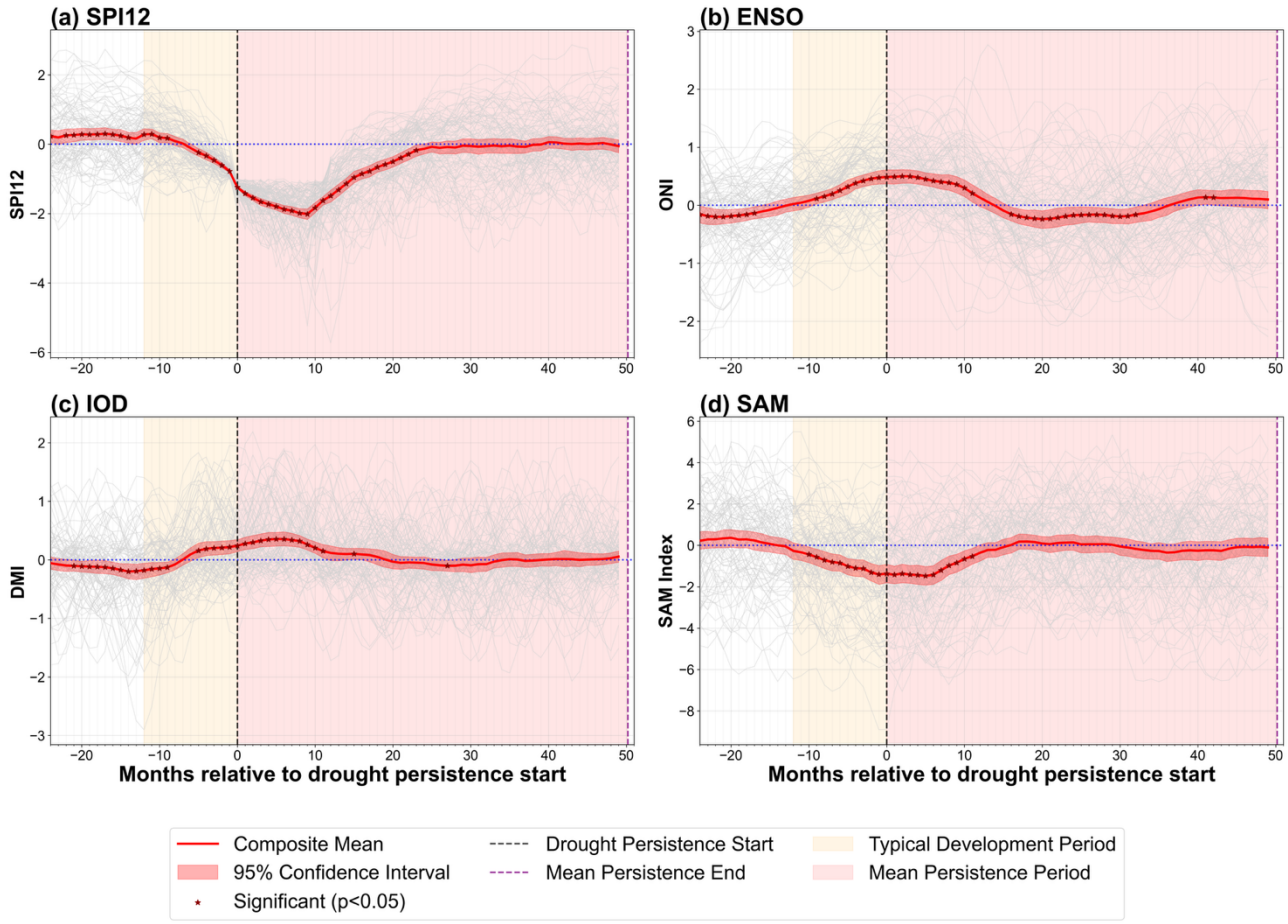

Figure 16. Composite time-series of drought and climate indices during drought stages. Time series showing evolution of (a) SPI-12, (b) ENSO, (c) IOD, and (d) SAM relative to drought persistence start (month 0). Red lines represent ensemble mean composite values with 95% confidence intervals (shaded dark red areas); individual drought events from 30 ensemble members appear as light grey lines. Statistical significance was assessed using one-sample t-tests against a reference mean of zero for all climate indices; red stars indicate months with statistically significant departures ($p < 0.05$). Vertical dashed lines mark drought persistence starts (black) and mean persistence end (purple, ~month 36). Coloured background shading indicates drought stages: development period (yellow, months -12 to 0) and persistence period (red, months 0 to 36). The termination period is excluded as variable drought persistence durations across events result in highly variable termination start times, preventing identification of meaningful or representative composite patterns. Note: y-axis ranges differ between panels.

The SPI time series (Figure 16a)'s temporal evolution matches closely with this study's pre-defined 12-month drought development period, where it first starts to show a declining trend, then recovering toward zero and stabilizing during persistence. ENSO (Figure 16b) and SAM (Figure 16d) show synchronized transitions during drought evolution, with the ENSO index increasing and the SAM index decreasing before development begins. Both converge toward zero at drought

onset, continue to peak around months 14-17, then return to neutral conditions. ENSO displays higher variability, with values sometimes falling well below zero for extended periods without ending drought, followed by rebounds above zero. This indicates that a return to neutral or weak La Niña conditions does not necessarily end droughts in the study region, highlighting the non-linear interactions within the climate system that modulate SEA precipitation, which is further explored in section 4.2.3 by considering combinations of climate drivers. In contrast, the IOD (Figure 16c) demonstrates a delayed response compared to the other climate drivers, beginning around month –7 during the middle of the drought development period. DMI shows the smallest deviation from neutral conditions, making IOD the most stable and persistent among the drivers.

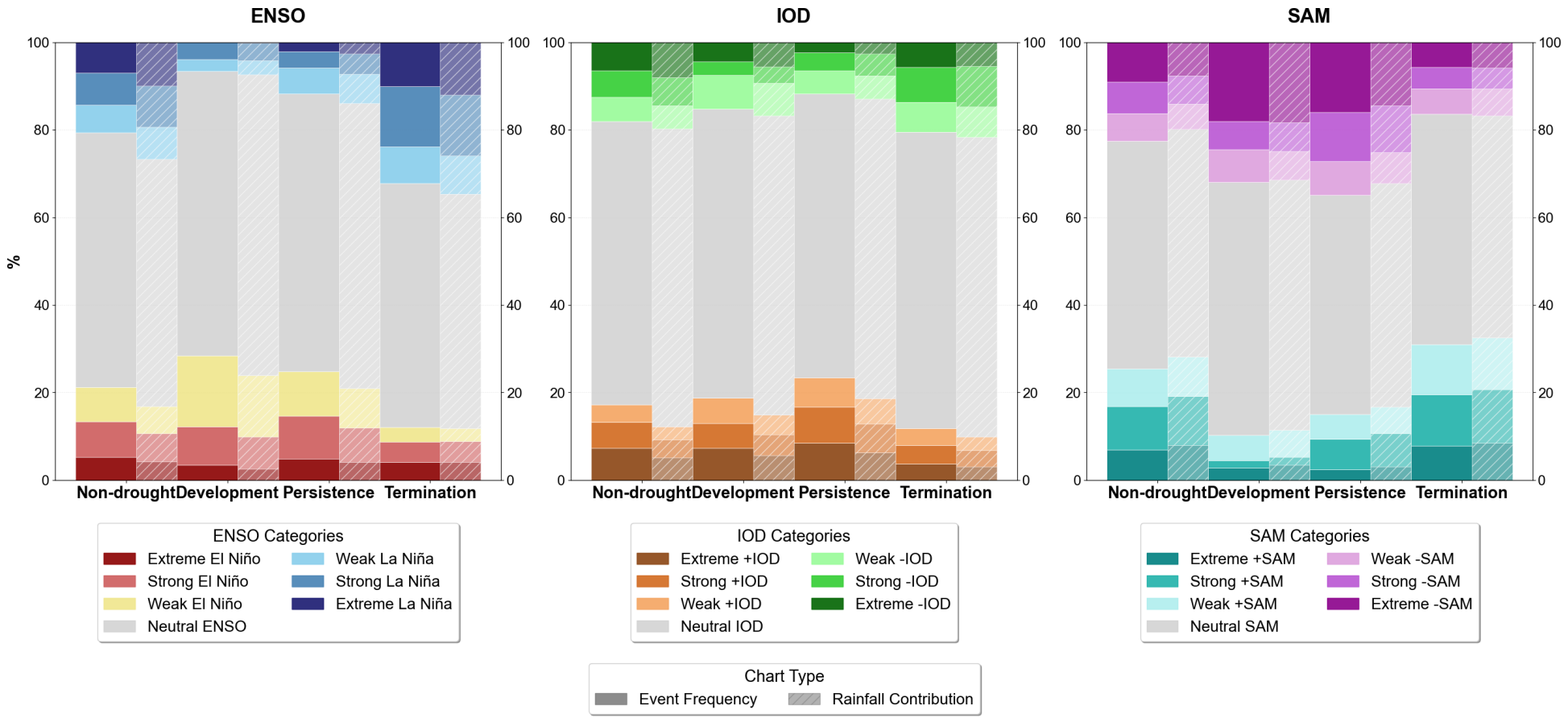

Figure 17. Stacked bar charts showing climate driver event frequency and precipitation contribution across drought stages. Displaying the relative frequency of climate events (solid bars) and their corresponding precipitation contributions (hatched bars) for ENSO, IOD, and SAM during non-drought periods and drought stages across all 30 ensemble members in SEA. Each bar represents 100% of events or precipitation for that phase, with colours indicating different intensity categories. Rainfall contribution is calculated as the cumulative monthly precipitation (mm) during each climate phase category divided by the total precipitation across all categories for that drought stage, expressed as a percentage. Each bar represents 100% of events or precipitation for that phase, with colours indicating different intensity categories.

Building on the patterns identified in Figure 16, where ENSO and SAM exhibited stronger variability compared to the more stable IOD, Figure 17 further highlights that during drought development and persistence, ENSO and SAM display larger deviations from normal conditions compared to the IOD. Specifically, drought development involves a reduced frequency of La Niña events (especially extreme episodes), increased weak El Niño frequency, and weakened -IOD events with more neutral IOD conditions. The most notable changes occur in SAM, showing dramatic decreases in strong/extreme +SAM and substantial increases in extreme -SAM. Persistence shows declining weak El Niño with strengthening strong/extreme El Niño, La Niña recovery across all levels, substantial +IOD increases with continued weak -IOD decline, and -SAM intensification dominated by strong events. Termination shows a reversal, declining El Niño with surging strong/extreme La Niña, +IOD recession with significant -IOD recovery, and diminishing -SAM with substantial +SAM increases across all intensities.

Overall, Drought-inhibiting climate driver phases (strong La Niña, +SAM) systematically weaken during development and persistence while drought-promoting conditions (weak El Niño, -SAM) strengthen, with balanced distributions restored during termination relative to non-drought periods.

La Niña shows the most consistent frequency and precipitation shifts between persistence and termination phases, followed by +SAM, with both showing clear reductions during persistence and pronounced increases during termination that equal or exceed baseline non-drought conditions. Across all drought stages, the magnitude of precipitation responses consistently exceeded the magnitude of climate driver frequency changes.

4.2.3 Climate driver combinations

The following section presents result for answering RQ 3: How do climate driver phase combinations (ENSO-IOD, ENSO-SAM, SAM-IOD) vary during these drought stages?

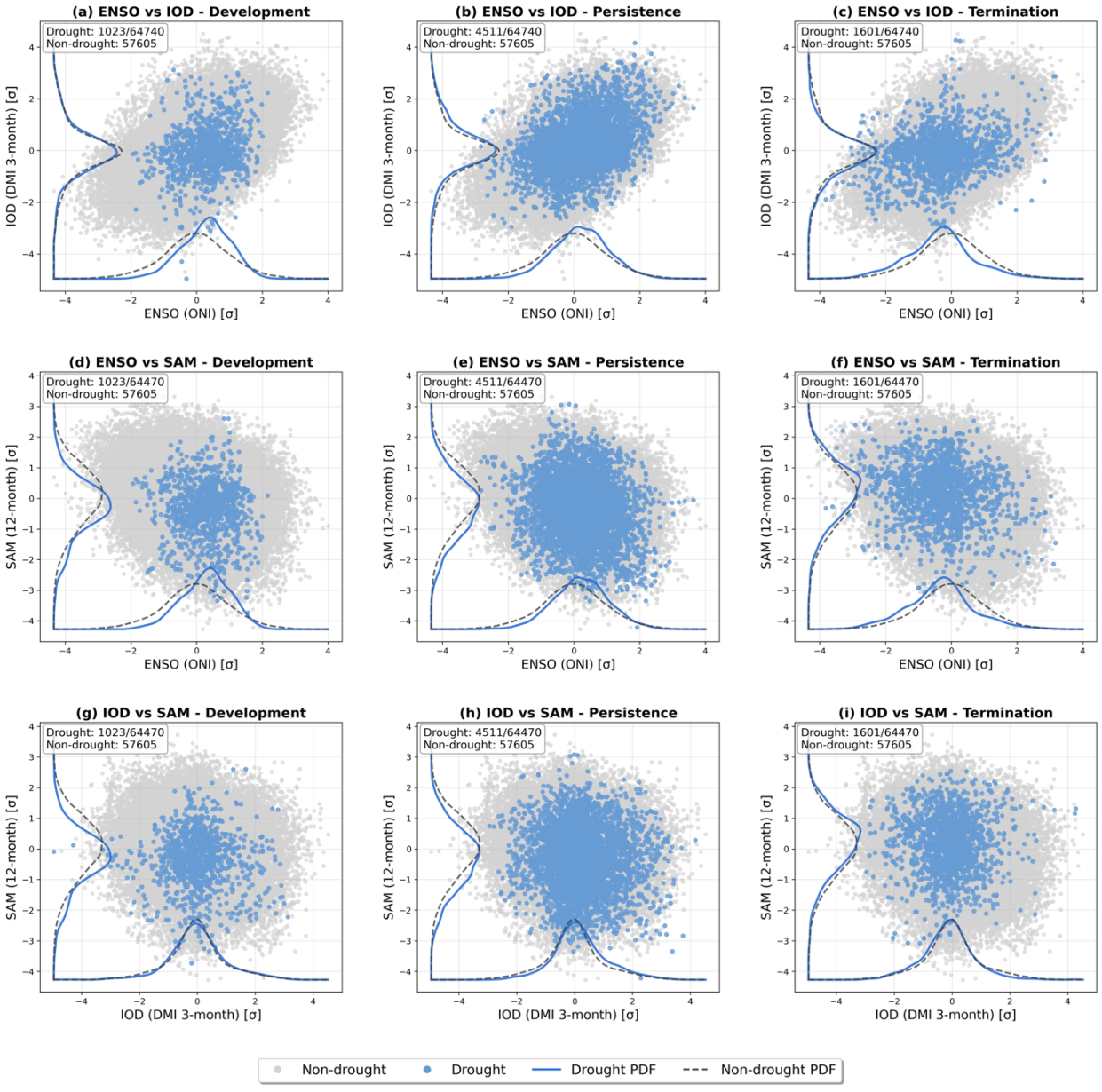

Figure 18. Scatter plots of climate index pairs from all 30 ensemble members during all non-drought months (grey dots) and during drought stages (blue dots): (a-c) ENSO (ONI) vs IOD (DMI 3-month), (d-f) ENSO (ONI) vs SAM (12-month), and (g-i) IOD (DMI 3-month) vs SAM (12-month) across development (left), persistence (middle), and termination (right) phases. Marginal probability density functions show distributions for drought (solid blue) and non-drought (dashed grey) conditions.

Table 4. Kolmogorov-Smirnov test statistics (D) and significance levels (p) comparing climate driver distributions during drought stages against non-drought periods (Figure 16).

	Development	Persistence	Termination
ENSO	D=0.188, p<0.001	D=0.121, p<0.001	D=0.165, p<0.001
IOD	D=0.030, p=0.321	D=0.090, p<0.001	D=0.057, p<0.001
SAM	D=0.187, p<0.001	D=0.150, p<0.001	D=0.085, p<0.001

Climate driver combinations show distinct patterns across drought stages compared to non-drought conditions (Figure 18). Most scatter dots cluster near neutral conditions, shift toward drought-promoting driver combinations during development and persistence and then shifting toward drought-inhibiting combinations during termination. Compared to non-drought periods, scatter points during drought stages show higher variability, more extreme outliers, and sparser distributions, especially during development and termination, indicating greater variability in climate driver conditions during drought.

The Kolmogorov-Smirnov (K-S) test (Table 4) revealed significant differences between the frequency of climate driver combinations between drought and non-drought periods across all climate indices and drought stages ($p < 0.001$ for all climate drivers in all phases, except IOD development: $p = 0.321$). ENSO shows the strongest deviations during development (D=0.188) and termination (D=0.165). El Niño conditions drive drought onset, evidenced by right-shifted probability density functions (PDFs) during development, while La Niña facilitates drought termination, shown by left-shifted PDFs. SAM displays significant distributional shifts across all drought stages, consistently showing the strongest deviations from normal conditions. IOD maintains the smallest overall deviations but shows persistent influence on drought dynamics. During drought development, IOD PDFs shift slightly rightward with reduced peak intensity, signalling weak +IOD conditions. Predominantly +IOD states sustain drought persistence, reflected in the strongest right-skew during this phase, while -IOD conditions support drought termination, evidenced by slight leftward PDF shifts. Overall, drought development is characterized by (El Niño, +IOD, -SAM) conditions as highlighted by rightward PDF shifts, while drought termination is facilitated by (La Niña, -IOD, +SAM) conditions shown by leftward shifts during the termination phase.

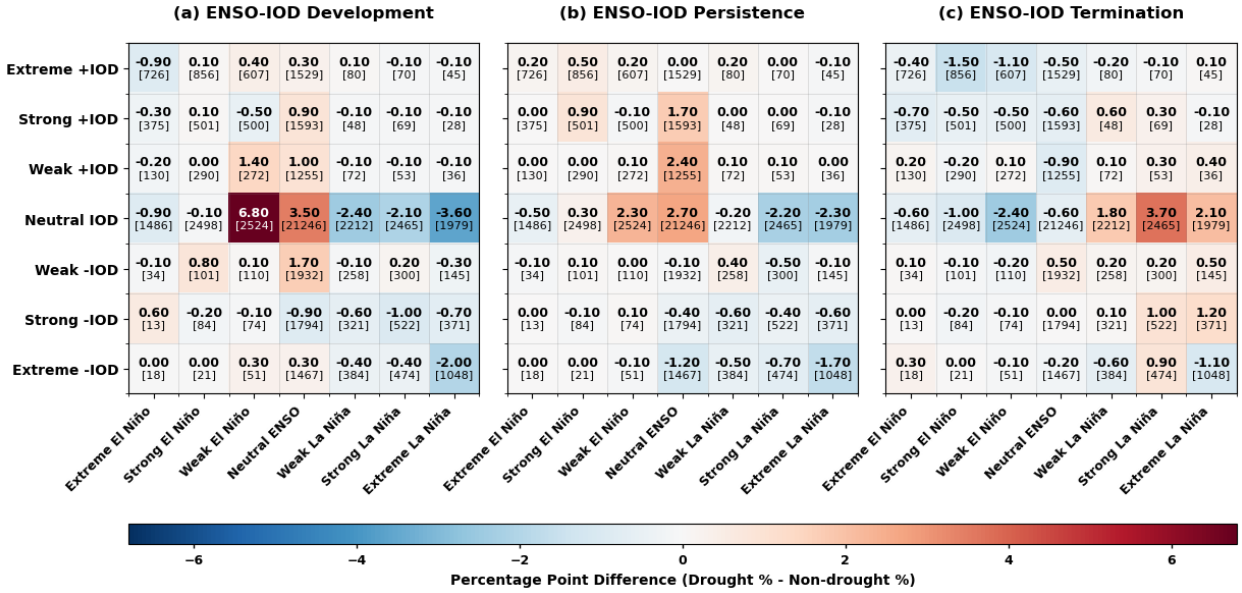

Figure 19. Heatmaps showing ENSO-IOD combinations at different intensity levels across drought stages: (a) development, (b) persistence, and (c) termination. Large bold values in cells represent absolute percentage point differences of each climate driver combination during each phase compared to non-drought baseline. Small values at bottom of cells in [brackets] show raw number of events in each combination during all non-drought months. Blue represents decreases in absolute percentage of combinations, while red represents increases. Darker colours indicate stronger absolute percentage deviations from non-drought periods.

The frequencies of phase combinations differ between drought and non-drought periods (Figure 19). The clearest deviations occur when neutral IOD coincides with climate conditions ranging from weak El Niño to strong La Niña, suggesting a limited influence of the IOD compared to ENSO. During development and persistence, La Niña/-IOD combinations (lower right quadrant of heatmaps) show larger frequency increases relative to non-drought periods, whereas during termination, El Niño/+IOD combinations (upper left quadrant of heatmaps) exhibit larger frequency decreases, with more intense combinations showing the greatest magnitude of change.

Drought development (Figure 19a) shows the largest ENSO-IOD frequency deviations across all drought stages. The largest ENSO-IOD frequency deviations occur primarily in neutral IOD combinations. Neutral IOD/weak El Niño shows the most substantial increase (+6.8%), while neutral IOD/ extreme La Niña exhibits the largest decrease (-3.6%). Additionally, neutral-neutral ENSO-IOD combinations, representing months without influence from either climate driver, also increases substantially (+3.5%). El Niño/+IOD combinations generally show increases, although decreases occur in extreme El Niño/+IOD, while weak El Niño/weak +IOD combinations show the largest increase (+1.4%). In contrast, La Niña/+IOD combinations show consistent decreasing trends, led by reductions in extreme La Niña/extreme +IOD.

The overall pattern during persistence resembles that of development (Figure 19b). The prevalence of neutral IOD across ENSO-IOD combinations maintains its dominance, even though the corresponding trends are relatively weak. Frequencies are more consistent than in development, with increases in +IOD/El Niño and decreases in -IOD/La Niña, although these deviations are smaller in magnitude. Neutral ENSO/+IOD combinations increase at both weak (+2.4%) and strong (+1.7%) intensity levels.

At termination (Figure 19c), the pattern reverses, with El Niño/-IOD combinations decreasing overall, while La Niña paired with any IOD state (La Niña/ all IOD) shows overall increase. However, the largest shifts still occur when El Niño or La Niña events pair with neutral IOD conditions.

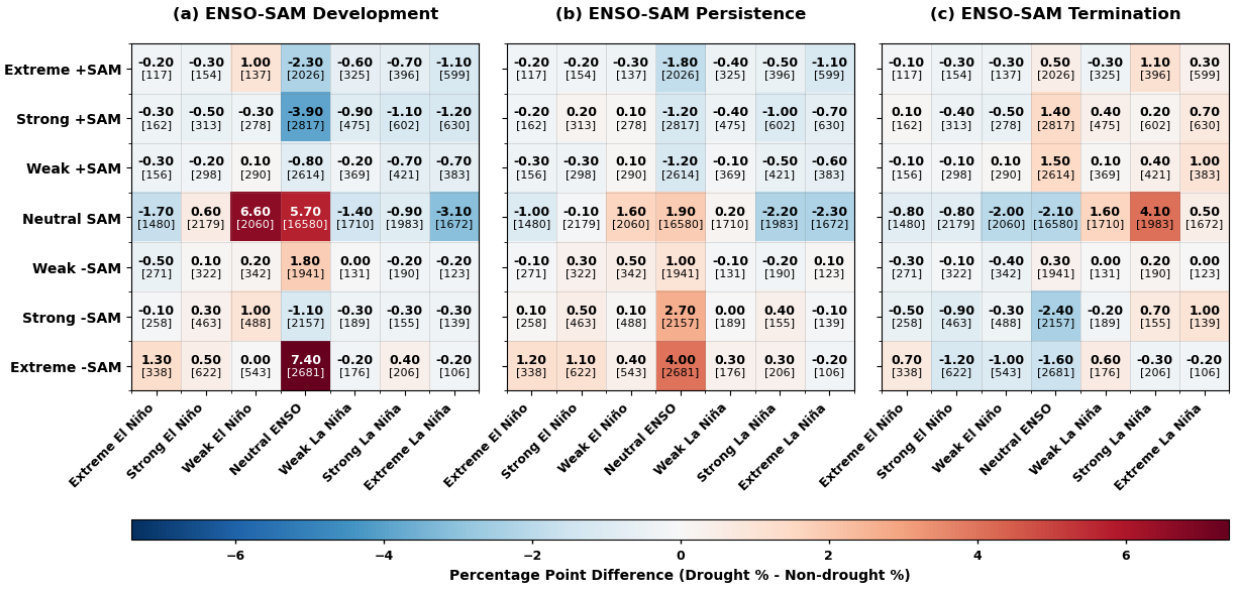

Figure 20. As for Figure 19., but for ENSO-SAM combinations.

The most evident deviation in ENSO-SAM combinations relative to normal conditions occur when neutral ENSO aligns with all SAM events during development and persistence, and when neutral SAM aligns with all ENSO events across all stages (Figure 20). Stronger pairings are observed in the dry (El Niño/-SAM) and wet (La Niña/+SAM) quadrants, producing larger magnitude shifts, particularly during drought development and persistence.

Development (Figure 20a) shows the clearest shift in ENSO-SAM combinations, particularly in neutral SAM/all ENSO and neutral ENSO/all SAM combinations. Neutral-neutral ENSO/SAM combinations also increase considerably (+5.7%). There are strong shifts in neutral SAM/all ENSO and neutral ENSO/all SAM combinations. Beyond these, the shifting trends at

most intensity levels are quite disordered, showing no clear pattern or sometimes opposite shifts; the only consistent trend is the decrease in all La Niña/+SAM events.

During persistence (Figure 20b), the dominant pattern of neutral SAM/all ENSO and neutral ENSO/all SAM combinations remain but is less pronounced. There is also clearer overall ENSO-SAM frequency shifting pattern compared with development, marked by a general increase in El Niño/-SAM and a decrease in La Niña/+SAM combinations.

During termination (Figure 20c), shifts in ENSO-SAM pattern is relatively subdued, with most shifts still occurring in neutral SAM/all ENSO and neutral ENSO/all SAM combinations. El Niño/all SAM frequencies decrease slightly overall, while La Niña/SAM frequencies show an overall increase.

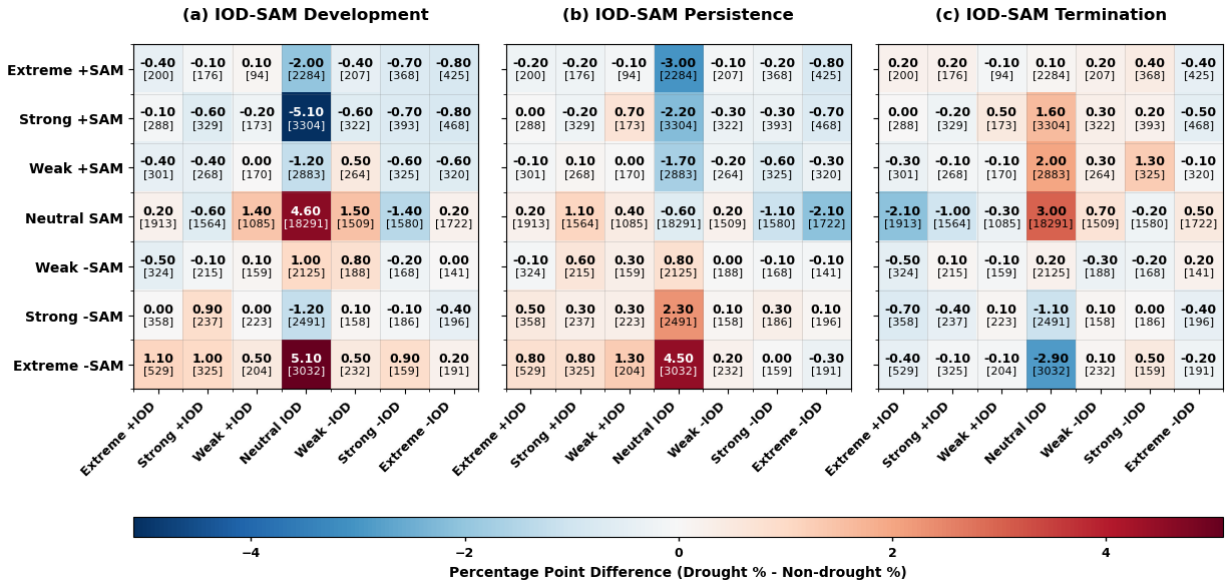

Figure 21. As for Figure 19, but for IOD-SAM combinations

The clearest shift for IOD-SAM occurs when neutral IOD aligns with all SAM events across all stages (Figure 21). Generally, more intense pairings in the dry (+IOD/-SAM)/ wet (-IOD/+SAM) quadrant produces greater magnitude shifts.

During development (Figure 21a), neutral-neutral combinations increase (+4.6%), accompanied by decreases in more extreme +SAM/-IOD combinations and increases in more extreme +IOD/-SAM combinations.

A similar but weaker trend continues into persistence (Figure 21b), where shifts across quadrants are more consistent, with notable changes in neutral SAM/all IOD combinations.

During termination (Figure 21c), neutral-neutral combinations again increase (+3.0%), alongside a general decrease in +IOD/–SAM combinations and an increase in weak-to-strong -IOD/+SAM combinations.

4.3 Synoptic Weather Systems

4.3.1 Cyclone Frequency and Intensity anomalies

The following section presents result for answering RQ 4: How do extratropical cyclone and anticyclone frequency and intensity anomalies evolve across drought development, persistence, and termination phases in SEA and the Tasman Sea regions?

SEA Domain

Extratropical cyclone and anticyclone frequency anomalies display distinct patterns during drought stages (Figure 22a). During development, anticyclone frequency increases substantially across most seasons, with the strongest positive anomalies occurring in MAM (+35%) and SON (+30%). Cyclone frequency shows consistently negative anomalies, with the largest reductions in MAM (-25%) and JJA (-17%).

The persistence phase maintains positive anticyclone anomalies but with reduced magnitude compared to development, with MAM (+25%) and SON (+33%) showing the largest values, while JJA shifts to negative values (-10%). Cyclone frequency anomalies remain negative but are weaker than during development, with MAM showing the largest reduction (-10%) while SON approaches near-neutral values.

During termination, the pattern reverses. Anticyclone frequency anomalies decline sharply, especially in JJA and SON (-20%), while DJF (+8%) and MAM (+19%) retain positive but diminished values compared to persistence. Cyclone anomalies rebound overall, turning positive in most seasons.

Cyclone and anticyclone intensity anomalies for the SEA domain (Figure 22c) show predominantly negative values across all phases and seasons. The strongest intensity reductions occur during development and termination compared to persistence. Notably, positive cyclone intensity anomalies only emerge during termination, with MAM displaying the strongest increase.

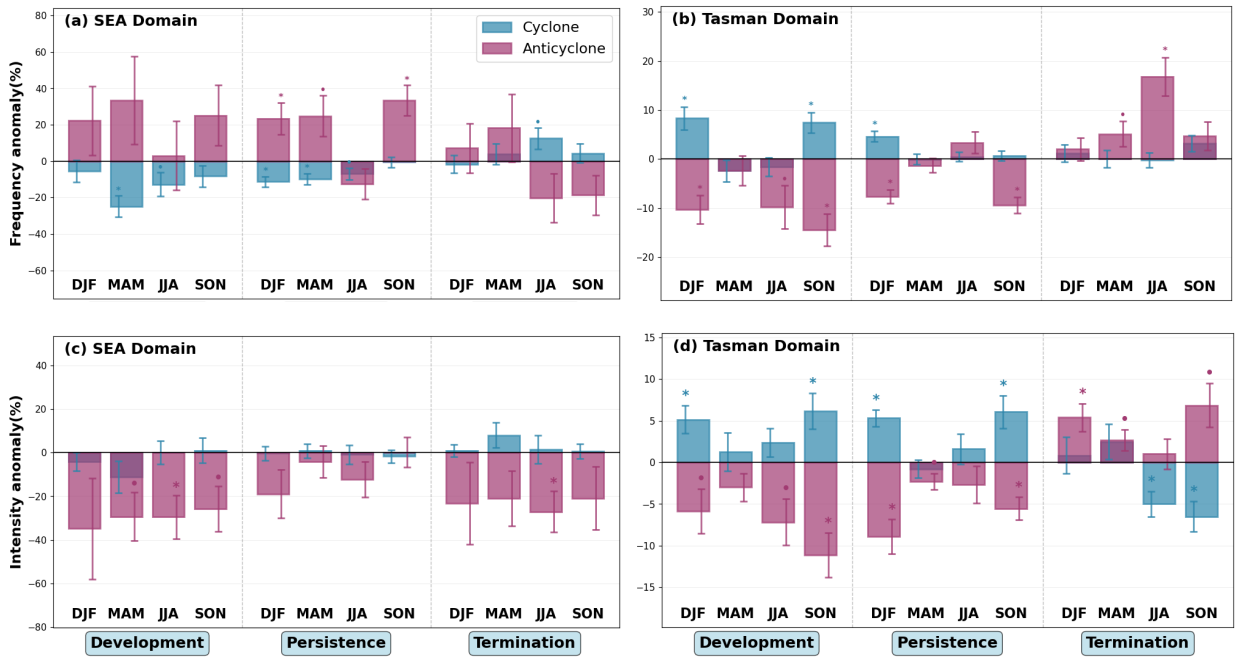

Figure 22. Bar charts show frequency and pressure intensity anomalies of cyclone (blue) and anticyclone (purple) occurrence percentage (a-b) and intensity (c-d) anomalies during different seasonal and drought stages, relative to non-drought conditions, for the SEA domain (a, c) and Tasman domain (b, d). Anomalies are calculated relative to the mean non-drought frequency for each ensemble and season, averaged across 30 ensemble members. Error bars show standard error, with significance indicated (• p < 0.05, * p < 0.01).

Tasman Domain

Patterns in the Tasman domain contrast with those in the SEA domain (Fig. 22b). During development, cyclone frequency shows modest increases in DJF (+8%) and SON (+5%), with minimal changes in JJA (-2%) and MAM (-3%). Anticyclone frequency and intensity tend to be lower than normal, especially in SON (-15%), DJF and JJA (-10%). Intensity patterns reveal positive cyclone anomalies (<7%) contrasting with strongly negative anticyclone anomalies (>-12%). The persistence phase maintains generally positive cyclone frequency anomalies across most seasons, with DJF showing the most notable increase (+5%). Anticyclone frequency remains negative in all seasons except JJA, with the strongest negative anomalies in DJF and SON. During persistence, anomaly magnitudes weaken overall, though seasonal variability increases. MAM represents an exception, with cyclone intensity shifting to negative anomalies.

By termination, anticyclone frequency anomalies increase across all seasons, with JJA displaying the largest increase (+17%), whilst cyclone frequency anomalies showing overall slight increase DJF (+2%) and SON (+4%), in MAM and JJA remain near-neutral.

Tasman domain intensity patterns (Fig. 22d) for development and persistence show similar shifts, with overall positive cyclone and negative anticyclone intensity anomalies, most pronounced in DJF and SON, while anomaly magnitudes weaken slightly during persistence. By termination, patterns largely reverse, with anticyclone intensity anomalies becoming strongly positive, particularly in DJF (+6%) and SON (+8%), while cyclone intensity anomalies decrease, and turns negative JJA (-5%) and SON (-7%). These changes aligns with Figure 15, which shows an increase in high-pressure systems in the Tasman during termination compared to development and persistence.

Domain Comparison

Overall, across both domains and for both frequency and intensity metrics, anticyclones consistently show larger magnitude anomalies than cyclones. Between domains, cyclone and anticyclone anomalies exhibit distinct regional differences in both magnitude and seasonality. In the Tasman domain, anomalies are generally weaker, with frequency changes largely confined to -20% to +20% and intensity anomalies restricted to -15% to +10%. In contrast, the SEA domain displays a much broader range of variability, with frequency anomalies spanning -30% to +40% and intensity anomalies extending from -40% to +10%. Seasonally, Tasman anomalies tend to peak during DJF and SON and weaken in MAM, whereas in SEA the seasonal signal is less systematic, although JJA consistently produces the lowest anticyclone frequency anomalies. Taken together, these results suggest that Tasman variability is more moderate and seasonally structured, while SEA variability is larger in magnitude but less uniform across seasons.

4.3.2 Spatial Distribution

The following section presents results for answering RQ 5: What are the spatial patterns of cyclone and anticyclone distribution during different drought stages?

Frequency

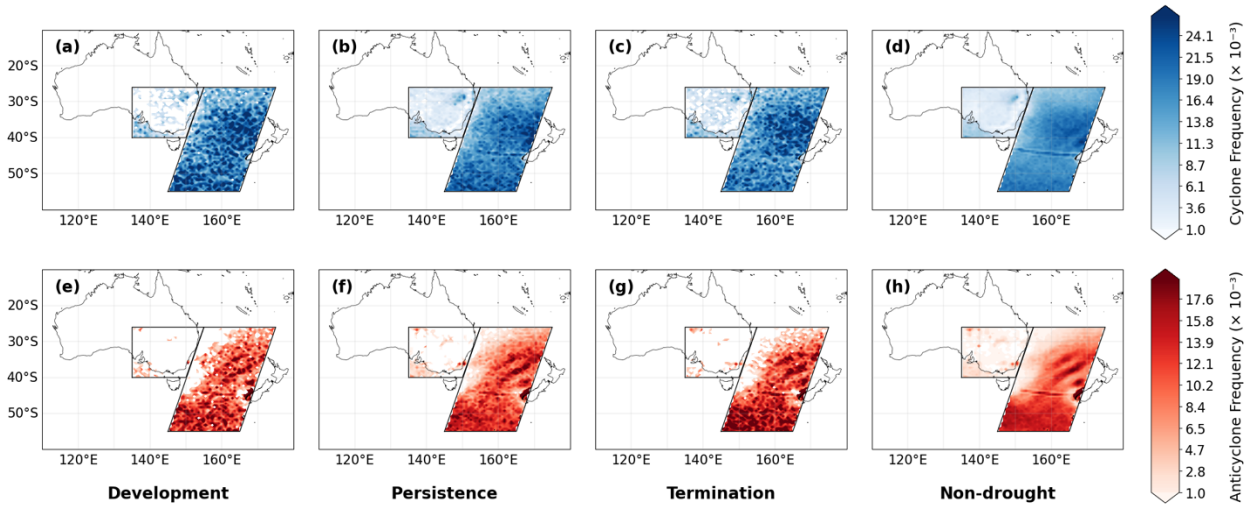

Figure 23. Frequency of cyclones (a–d) and anticyclones (e–h) centres during different drought stages across the SEA and Tasman Sea domains. Maps show the percentage of ensemble-days with system centres cell from all 30-member simulations in each drought stages. Panels represent Development (a,e), Persistence (b,f), Termination (c,g), and Non-drought (d,h) phases. Colour bars are scaled to the 95th percentile of non-zero frequency values for each system.

The spatial distribution of cyclone and anticyclone centres across the SEA and Tasman domains during different drought stages (Figure 23) shows that cyclone centres occur more frequently overall and exhibit a more spatially uniform distribution compared to anticyclones. Cyclone centres show relatively high concentrations over the middle and southern portions of the Tasman domain, especially during drought development. Anticyclones show a much stronger spatial clustering, forming two distinct NW-SE-oriented corridors across the Tasman domain, with the highest frequencies along its southern boundary.

A clear contrast emerges between terrestrial and oceanic regions, with cyclone and anticyclones occurring more often over the ocean regardless of drought stages. Within the SEA domain, anticyclones preferentially occur near the western and southwestern edges, which also represent the only oceanic portion of this domain. While shorter drought stages (e.g., development and termination) naturally yield fewer samples and thus lower frequencies, the preferred regions of cyclone and anticyclone occurrence remain spatially consistent across drought stages. This

persistence indicates that, despite the removal of ensemble-mean background signals through TAV filtering, the underlying climatological preferences for cyclone and anticyclone tracks remain robust, reflecting the ensemble-wide consistency of the underlying dynamical processes.

Intensity

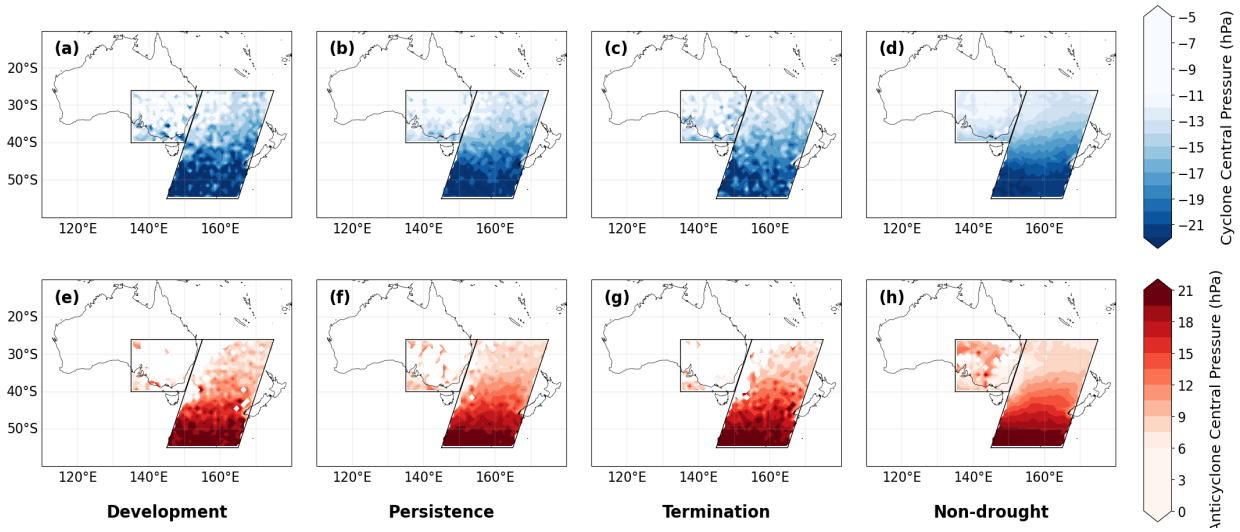

Figure 24. Average central pressure of cyclones (a–d) and anticyclones (e–h) during different drought stages across the SEA and Tasman Sea domains

Similarly, the intensity maps (Figure 24) show fairly consistent spatial patterns for both cyclones and anticyclones, with systems generally intensifying at higher latitudes. Cyclones deepen noticeably as they move south across the Tasman Sea, while those in the SEA region are generally weaker. Anticyclones follow a similar pattern, with the strongest high-pressure systems in the southern Tasman Sea. Over the ocean, systems overall have higher central pressures than over continental areas.

Overall, the Tasman Sea domain supports both more frequent and intense cyclones and anticyclones than SEA domain, with southern oceanic regions emerging as preferred zones for their development and intensification.

Chapter 5: Discussion

5.1 Simulated Characteristics of Prolonged SEA Droughts

This section discusses the simulated characteristics of prolonged droughts during their lifecycle.

Prolonged droughts spanning multiple years have different development patterns that could broadly be classified into two categories of direct development (rapid transition from normal/above-normal conditions representing 40-60% of events) and gradual/pre-conditioned development (development under pre-existing dry conditions or following incomplete recovery from previous drought episodes). Previous research has conducted similar investigations, such as Yevjevich (1967), who identified six types of drought temporal evolution patterns. However, these classifications focused only on the stage equivalent to persistence in the present study, rather than using the three-stage approach applied here, which highlights considerable variability in patterns during the development stage. More recent studies have distinguished drought types based on onset and development duration (Goswami and Gallant, 2025; NIDIS, n.d.). Nonetheless, long-term droughts, (prolonged/ multiyear/ mega-droughts), lack a standardized onset duration due to their highly variable temporal extent (Cook et al., 2022; Falster et al., 2024a; NIDIS, n.d.), which also makes it difficult to define a clear onset period for these events.

Apart from the highly variable development period, there are notable asymmetries in the durations of dry and wet stages, with drought persistence substantially exceeding termination length. This observation is consistent with both observational records and paleoclimate studies, which show considerable variability in prolonged drought duration across Australia (Falster et al., 2024a; Ho et al., 2015; Vance et al., 2015). In contrast, once termination begins, droughts end relatively quickly and consistently, with rare extreme outliers compared to persistence phases. This is possibly because termination is driven by intense precipitation events, as evidenced by studies showing that Australian droughts are often terminated by short-lived, high-intensity rainfall episodes (Holgate et al., 2025; Parker and Gallant, 2022).

Whilst no clear seasonal preference pattern for drought onset and termination indicates that these events can occur at any time of the year, this limits predictability and necessitates continuous monitoring rather than season-based management approaches.

5.2 Large-Scale Climate Drivers

This section discusses the characteristics of ENSO, IOD, and SAM conditions, both individually and in combination, throughout prolonged droughts stages.

5.2.1 Climate Drivers' changes in drought

This research found that prolonged droughts in SEA are characterized by distinct climate driver patterns, with dry phases associated with El Niño, +IOD and -SAM conditions, while wet phases exhibit the opposite configuration (La Niña, -IOD, +SAM). These findings align with well-established understanding of usual "wet" and "dry" phases of each climate driver, as extensively documented in observational records of past drought events (Cai et al., 2011d, 2011a; Chung et al., 2025a; Devanand et al., 2024a; Hendon et al., ; Holgate et al., 2022a, 2025; King et al., 2020; Ummenhofer et al., 2009; van Dijk et al., 2013; Verdon-Kidd and Kiem, 2009).

The following sub sections discusses how climate driver conditions (including phases, frequency and intensity) vary systematically across different drought stages.

ENSO

This study shows that drought development is marked by a sharp reduction in La Niña occurrence, with extreme La Niña episodes almost disappearing and a concurrent increase in weak El Niño events. The stronger changes in La Niña phases compared to El Niño suggest that shifts in La Niña behaviour are more critical for shaping regional drought and precipitation variability. This is consistent with earlier work, showing SEA precipitation during La Niña events exhibits stronger and more consistent impacts than during El Niño events (King et al., 2013; McGregor et al., 2024). In support of this, Gillett et al. (2023) showed that Australian mean and extreme precipitation are more strongly influenced by the intensity of La Niña than by that of El Niño. The absence of extreme La Niña events reduces the chance of heavy to extreme precipitation events (Holgate et al., 2025), thereby facilitating the development of prolonged drought. On the other hand, more frequent weak El Niño events promote greater precipitation deficits across SEA (Ummenhofer et al., 2009), amplifying the effect of La Niña absence and, together, contributing to prolonged dry conditions.

During drought persistence, weak El Niño events decline, while stronger and more extreme El Niño events become more frequent. At the same time, there is a slight recovery in extreme La Niña events, indicating a shift toward the more intense end of the El Niño spectrum. The increase in stronger El Niño events during drought persistence likely contributes to greater precipitation

deficits by intensifying atmospheric subsidence and reducing regional moisture availability (Holgate et al., 2022). On the other hand, some extreme La Niña events occur during the persistence stage, which might alleviate the precipitation deficit somewhat without terminating the drought altogether, highlighting the high degree of variability in SEA precipitation. This variability is expected given that the persistence stage is inherently longer than the development or termination stages, naturally encompassing more diverse climatic conditions.

The termination stage exhibits contrasting patterns to the dry stages (development and persistence). El Niño frequency decreases substantially, while La Niña events show a marked increase in strong and extreme episodes, which would enhance atmospheric moisture availability for more precipitation (Holgate et al., 2022). This drought terminating pattern is consistent with past exceptionally high precipitation across Australia, namely the 2010-11 Queensland floods and eastern Australia's two wettest years (2010-2012) that coincided with consecutive La Niña events (Nicholls, 2011; BOM, 2012).

ENSO shows the largest shifts in phase frequency during prolonged droughts amongst all climate drivers, particularly at onset and termination, reflecting its role as the dominant climate driver of interannual drought variability (Risbey et al., 2009). El Niño phases, in particular, have historically driven major droughts such as Australia’s Millennium Drought (2001–2009) and are closely linked to precipitation deficits across Southeast Australia (van Dijk et al., 2013; Holgate et al., 2025).

IOD

The IOD demonstrates a temporally lagged influence on drought dynamics, with no statistically significant effect during early stage of drought development, but notable contributions during the middle of development and throughout persistence. During this period, IOD intensity increases, peaking in persistence (Figure 18c), with a marked rise in +IOD events and a decline in weak -IOD occurrences.

The IOD demonstrates a temporally lagged influence on drought dynamics, showing no statistically significant effect during the early stage of drought development, but notable contributions during the middle stage of development and the entire persistence stage. During the middle stage of development, IOD intensity increases, peaking in the persistence stage (Figure 18c), accompanied by a marked rise in +IOD events and a decline in weak -IOD occurrences.

This direction of IOD phase shift is supported by historical analysis of Australia's major 20th-century multi-year droughts, notably the Federation Drought (1895-1902) and the WWII drought (1937-1945), which consistently coincided with positive or neutral IOD phases and absence of negative phases (Ummenhofer et al., 2009). However, the delayed influence of IOD suggests it may function more as a drought amplifier during persistence phases of prolonged droughts compared to ENSO and SAM, rather than as a leading mechanism. This temporal lag and peak timing may be explained by IOD's seasonal phase locking to Asian-Australian monsoons (Cai et al., 2013; Abram et al., 2020). IOD development requires specific monsoon wind conditions to initiate, creating inherent temporal constraints. Since positive IOD events typically start forming around May-June, coinciding with the establishment of southeasterly trade winds in the tropical eastern Indian Ocean (Abram et al., 2020), its influence is limited to droughts aligning with these seasonal conditions. Consequently, for droughts that onset outside this period, early stages are more likely governed by other modes such as ENSO and SAM. This delayed IOD timing may also result from El Niño events in boreal spring/summer that force positive IOD events in fall (SON) through atmospheric C-mode circulation (Stuecker et al., 2017), demonstrating how ENSO can shift IOD development to later periods. Tong and Zhou (2023) further support this, finding that IOD events peak later when ENSO is present compared to when ENSO is absent. This indicates that ENSO-IOD interactions can delay IOD development, constraining IOD to later seasonal windows during drought conditions when specific ENSO states interfere with typical IOD timing.

During drought termination, results show a decrease of +IOD conditions with -IOD events becoming more frequent, consistent with studies demonstrating that -IOD events are associated with above-average/drought breaking rainfall and wet periods in SEA (Ummenhofer et al., 2009; Risbey et al., 2009; King et al., 2020).

Overall, IOD displays the smallest changes across all drought stages, with minimal shifts in phase frequency compared to ENSO and SAM. This relative stability is noteworthy given that previous studies have identified IOD, rather than ENSO, as primary driver of major droughts in SEA (Ummenhofer et al., 2009). The constrained variability observed in this study may reflect IOD's mixed origins and forcing mechanisms. IOD events can be classified as either internal IOD (developing independently in June with monsoon onset) or ENSO-forced IOD (emerging under ENSO influence with broader meridional patterns) (Behera et al., 2006; Yang et al., 2015). The interaction between ENSO forcing and internal variability modulates IOD strength, with constructive interference amplifying events and destructive interference suppressing them (Yang et al., 2015). IOD's smaller phase shifts may therefore reflect its dependence on multiple,

sometimes competing factors rather than a single dominant driver, making it the least variable among the three climate modes during drought evolution.

SAM

This study shows that during drought development, there were more frequent -SAM extremes and fewer strong and extreme +SAM events. While existing literature has not documented exceptional effects of more extreme SAM phases on drought development, SAM's impact on Australian precipitation is widely recognized to vary significantly across both space and time (Chung et al., 2025). -SAM typically suppresses precipitation by strengthening westerly winds that block easterly moisture flow and reduce atmospheric moisture content to eastern Australia (Holgate et al., 2022). The observed increase in -SAM extremes during drought development periods in this study confirms -SAM's drought-promoting role, as also demonstrated during the Tinderbox Drought (2017-2019), where -SAM conditions exacerbated the drought condition (Devnand et al., 2024). In contrast, +SAM shows more complex and seasonally dependent effects on eastern Australian precipitation. It is often linked to a shift of the midlatitude storm track toward the poles and enhanced easterly winds from the Tasman Sea, increasing precipitation along eastern Australia in spring and summer but reducing precipitation in southeastern regions during winter (Hendon et al., 2007). Without a consistent directional effect, the precipitation outcomes of +SAM are nearly balanced between above-average (53% of months) and below-average (47% of months) conditions (Holgate et al., 2022). However, this study's finding of fewer +SAM during drought development periods suggests that +SAM in prolonged drought may promote wetter conditions.

SAM conditions during drought persistence show a similar pattern to drought development, with the shift toward extreme negative values continuing but with reduced intensity, suggesting a sustained atmospheric configuration that maintains reduced moisture transport and suppressed precipitation conditions throughout drought persistence.

SAM patterns during termination show more balanced distribution across intensity levels compared to dry phases, with declining -SAM frequency and substantial increases in +SAM events. Though +SAM's effect on precipitation is highly variable, this shift toward more +SAM conditions align with documented patterns of exceptional wet periods in SEA, which have been associated with weak +SAM phases (BOM, 2022).

Since SAM events typically fluctuate on weekly to monthly timescales (Chung et al., 2025), the 12-month smoothing applied to the SAM index in this study emphasizes sustained SAM patterns by filtering out short-term variability. This means that the observed shifts toward more frequent -SAM extremes/fewer +SAM extremes during drought development, along with increased +SAM and decreased -SAM during termination reflect sustained, long-term SAM conditions that are relevant to prolonged drought development and persistence, rather than transient fluctuations that might have limited influence on specific drought cases. However, the specific precipitation contribution of SAM events at different intensities during prolonged drought would require further investigation.

Compared to other climate drivers, SAM ranks second only to ENSO in overall phase shifts during drought evolution, with its greatest impact during the development and persistence phases. This substantial influence stems from SAM's role as a dominant mode of variability in the Southern Hemisphere extra-tropics, accounting for approximately 30% of regional climate variability (Marshall, 2022). The expression of this influence varies seasonally, as evidenced by composite maps (Figure 15) showing weaker SAM values in autumn and stronger values during winter and spring. This seasonal difference likely arises as SAM actively contributes to drought evolution. As +SAM phases reduce winter precipitation in southern Australia while enhancing summer precipitation along the eastern coastline (Risbey et al., 2009; Hendon et al., 2007). Conversely, -SAM during the warm season increase the likelihood of reduced precipitation and extreme heat events across eastern regions (Lim et al., 2019; Meneghini et al., 2007).

5.2.2 Climate driver combinations

When climate modes synchronize, their combined influence can produce more severe shifts in precipitation across Australia than any single mode alone, with prolonged dry conditions often arising when multiple drivers persist in drought-promoting phases (Agriculture Victoria, 2025; Cleverly et al., 2016). This is particularly evident in SEA, where several drivers frequently act simultaneously (Risbey et al., 2009). Overall climate driver combination patterns (ENSO-IOD; ENSO-SAM; IOD-SAM) mirror individual driver tendencies as discussed in Section 5.2.1 across drought stages, with expected increases in drought-promoting combinations during persistence and drought-inhibiting combinations during termination, alongside a notable increase in standalone climate driver occurrences (i.e., El Niño-only or +IOD-only conditions).

This study found that climate driver combinations influence drought through three concurrent processes:

5.2.2.1.1 Drought promoting/inhibiting combinations

The first pattern is an increase in drought promoting combinations (El Niño/+IOD; El Niño/-SAM; +IOD/-SAM) during dry drought stages (development and persistence) where persistence generally shows an overall weaker tendency, accompanied by a significant decline in wet-phase combinations. Conversely, there is a shift toward drought inhibiting combinations (La Niña/-IOD; La Niña/+SAM; -IOD/+SAM) during the wet drought stage (termination) (Fogt et al., 2011) with decrease in drought promoting combinations. This pattern shows an overall shift of climate driver combinations toward drought-promoting phases during dry periods and toward drought-inhibiting phases during wet periods of prolonged drought. In general, higher-intensity combinations (e.g., extreme -SAM or extreme El Niño) tends show greater shifts.

ENSO-IOD

This study shows that for ENSO-IOD, La Niña/-IOD combinations show greater decreases during drier phases than the increases seen in the El Niño/+IOD combinations, while El Niño/+IOD combinations show more decreases during termination than La Niña/-IOD combinations show increases, although these differences are not strong. This might suggest an asymmetric response, where the suppression of drought-inhibiting combinations may have a greater influence than the enhancement of drought-promoting combinations during lifecycle of prolonged droughts. While the general shift in distribution of ENSO-IOD combinations align with established understanding of these coupled modes' regional impacts. With El Niño/+IOD combinations produce the most severe drought conditions (ARC Centre of Excellence for Climate Extremes, 2022; Risbey et al., 2009; Ummenhofer et al., 2009). In contrast, La Niña/–IOD combinations generate the strongest enhancement of moisture transport from the Tasman and Coral Seas, leading to well above-average precipitation (Holgate et al., 2022). These combinations were found to co-occur frequently, showing amplifying impacts on Australian precipitation (Holgate et al., 2022; Ummenhofer et al., 2011).

ENSO-SAM

Among all climate mode pairings, ENSO-SAM combinations show the clearest shifting patterns with temporal evolution of drought, and with stronger intensity pairings showing larger frequency magnitude shifts across all drought stages compared to weaker pairings. The results

reveal increased El Niño/-SAM combinations alongside decreased La Niña/+SAM pairings during dry drought stages (development and persistence), with termination phases showing the reverse trend. This observed pattern aligns with the established millennial-scale negative correlation between ENSO and SAM indices (Dätwyler et al., 2020) and reflects the underlying physical mechanisms whereby ENSO modulates SAM through stratospheric-tropospheric coupling. Studies have shown that El Niño weakens the polar vortex promoting -SAM conditions, while La Niña strengthens the vortex favouring +SAM phases (Baldwin et al., 2021; Fogt et al., 2011). These physical mechanisms translate into contrasting precipitation impacts, with strong La Niña/+SAM combinations producing exceptional precipitation and flooding events (Hendon et al., 2014; van Dijk et al., 2013), while El Niño/-SAM combinations intensify drought conditions in southeastern Australia (ARC Centre of Excellence for Climate Extremes, 2023), explaining the observed distribution shift of ENSO-SAM combinations across the different drought stages identified in this study.

IOD-SAM

IOD-SAM combinations show the smallest co-occurrence shifts during drought stages and diverge from the general trend that more intense climate driver combinations produce larger shifts at termination, where no clear pattern emerges. Studies have shown that SAM, similar to IOD, is strongly influenced by ENSO-forced signals, primarily through the Pacific-South America (PSA) pattern (Cai et al., 2012; Hoskins and Karoly, 1981; Karoly, 1989). Also, SAM does not control IOD; rather, the large IOD-SAM correlation emerges as both respond to ENSO forcing, when ENSO influence is statistically removed, this correlation weakens considerably (Cai et al., 2011c). Historical major droughts were rarely considered to have been driven primarily by SAM-IOD; most involve multiple climate drivers, especially the concurrent presence of ENSO (Parker and Gallant, 2022; Ummenhofer et al., 2009). However, SAM could act as a critical amplifier for IOD-driven droughts (Devanand et al., 2024b). These factors together may explain the smallest co-occurrence shifts and unclear termination patterns of IOD-SAM combinations in the present results.

5.2.2.1.2 Standalone active phases

Second and the most significant pattern observed involves a single climate mode being active while other modes remain neutral. These configurations show substantial deviation from non-drought to drought conditions across all drought stages during most climate driver combinations. This indicates that, although climate driver combinations shift during drought

stages, the largest changes occur in standalone events. This implies that the impact of standalone events on drought may be proportionally greater than that of any climate driver combination.

5.2.2.1.3 Neutral-neutral conditions

Thirdly, an increase in neutral-neutral conditions, where neither climate mode is active, which appears most prominently during drought development and typically weakens during persistence. This tendency toward simultaneous neutrality is apparent across all climate driver combinations and throughout different drought stages, including ENSO-IOD during both development and persistence, ENSO-SAM during development, and IOD-SAM during development and termination. This indicates that drought results not solely from increases in drought-promoting combinations or decreases in drought-inhibiting combinations, but from a broader shift toward neutrality in precipitation-driving climate modes combinations, reflecting the absence of climate processes that would otherwise bring heavy, drought-breaking rainfall(King et al., 2020; Parker and Gallant, 2022).

Interestingly, for all driver combinations, the specific combination type showing the clearest differences between drought and non-drought periods generally remain evident across all drought stages. This suggests that the physical interactions among ENSO, IOD, and SAM remain consistent across drought stages, even if their frequencies vary.

5.3 Synoptic Weather Systems

5.3.1 Dynamics During Drought stages

This section examines how extratropical cyclone and anticyclone frequency and spatial distribution change across drought stages in SEA and the Tasman Sea.

SEA Domain

During prolonged drought development and persistence, the SEA region experiences higher-than-normal PSL with increased anticyclone frequency and decreased cyclone frequency, consistent with the expectation that anticyclones bring dry, clear conditions through descending air and subsidence (Boschat et al., 2015; Pepler et al., 2019). These high-pressure systems reduce cloud cover and increase incoming radiation, altering land-atmosphere feedbacks that further reduce precipitation and worsen drought conditions (Evans et al., 2017; Holgate et al., 2020a). Such persistent anticyclonic systems have become more common and intense during multi-year droughts across Australia and globally (Faranda et al., 2023; Holgate et al., 2022b; Kautz et al., 2022; Larsen and Nicholls, 2009; Pepler et al., 2019; Swain et al., 2016). Interestingly, although anticyclone frequency increases during dry stages, the intensity of individual systems tends to be lower than normal. This may reflect that drought periods represent a smaller temporal subset in which sampling of extreme-intensity events is reduced, or alternatively, that prolonged droughts tend to associate with persistent but weaker-intensity blocking rather than by anomalously strong individual systems. The sustained positive anticyclone anomalies coupled with neutral cyclone anomalies suggest anticyclonic blocking remains the dominant mechanism maintaining drought during persistence, though with diminishing intensity compared to development. The important role of anticyclones sustaining drought is also noted by Pepler et al. (2019), who highlight their contribution to long-term SEA precipitation decline, particularly in the cool season when increased anticyclone frequency accounts for about one-third of the reduction.

During drought termination anticyclone frequency anomalies in SEA decline sharply and cyclone anomalies rebound to near neutral or positive values. This transition enables the breakdown of anticyclonic blocking patterns, allowing easterlies carrying marine moisture to strengthen and return (Holgate et al., 2020a). The concurrent cyclone recovery restores precipitation-generating systems, with both processes facilitating drought breakdown through the reestablishment of normal moisture transport and precipitation patterns.

Tasman Domain

Tasman Sea anticyclones play a central role in the evolution of prolonged droughts in SEA. During drought development, persistent negative Tasman anticyclone anomalies occur alongside only modest positive cyclone anomalies. Reduced anticyclonic circulation in the Tasman Sea disrupts moisture transport, reducing inflow from the Coral and Tasman Seas during drought onset and intensification (Devanand et al., 2024b; Holgate et al., 2020a). As precipitation in SEA is primarily sustained by moisture from these oceanic sources (Holgate et al., 2022b; McIntosh, et al., 2012), this suppression reinforces drought conditions. During the persistence phase, Tasman anticyclones continue to exhibit negative anomalies, while cyclones remain generally neutral or slightly positive.

Drought termination is characterized by higher PSL over the Tasman Sea. With strong positive Tasman anticyclone anomalies across all seasons, especially in the cool season, while cyclone anomalies remain weaker. This presence of higher pressure in the Tasman during the wetter stage, and its absence during the drier stage, aligns with current understanding of SEA rainfall variability (Gillett et al., 2023). Strengthened Tasman Sea anticyclones could enhance onshore moisture transport via moist easterly and northeasterly flows, driving anomalously high precipitation and supporting drought recovery (Boschat et al., 2015; Gillett et al., 2023; Holgate et al., 2023, 2020a; Jin et al., 2023). Overall, these results confirm the critical role of Tasman Sea anticyclones in shaping prolonged drought evolution, with their negative anomalies suppressing moisture supply during development and persistence, and their positive anomalies enhancing inflow and precipitation during termination.

5.3.2 Spatial Patterns

The Tasman Sea was identified as a general hotspot of both extratropical cyclone activity, consistent with Pepler and Dowdy (2020a), and anticyclone activities (Figure 23,24), with both system frequency and intensity exceeding those over SEA. While the underlying causes of these intensity differences have not been explicitly addressed, Marshall et al. (2013) suggested that anticyclones tend to be larger and more persistent over oceans, such as the Tasman Sea, and smaller along the coastal areas, likely due to topographic constraints. Similar mechanisms may explain their greater frequency and intensity over oceans than over terrestrial areas. For the Tasman domain specifically, both cyclone and anticyclone intensity, as well as anticyclone frequency, tends to increase toward higher southern latitudes. Ulbrich et al. (2009) similarly showed that cyclonic activity forms a Southern Hemisphere belt, peaking in the southern Indian Ocean and south of the Tasman Sea.

Comparative analysis of drought-phase anomalies shows that SEA experiences stronger variability in cyclone frequency and intensity, whereas the Tasman Sea exhibits more moderate, seasonally structured shifts that peak during warm phases. There has been limited research directly comparing extratropical cyclone frequencies or intensity anomaly patterns across SEA and the Tasman Sea or terrestrial versus oceanic regions with respect to drought stages. These patterns may suggest differences in how land-ocean contrasts influence extratropical cyclone variability during drought conditions. The higher frequency in the southern part of the Tasman domain corresponds to the Southern Hemisphere storm track, where storm activity peaks between approximately 40° and 60°S (Campbell and Renwick, 2023).

5.4 Limitations

The extended duration of prolonged droughts allows for greater cumulative impacts and interactions with variable external factors compared to shorter events such as seasonal droughts (van Dijk et al., 2013). Although the drought stage definition used in this study is suitable for identifying prolonged meteorological droughts, it may not capture the finer-scale variability of drought evolution. Such events often include intervals of above-average precipitation, meaning that the "prolonged meteorological droughts" examined here reflect a sustained cumulative precipitation deficit rather than the consistently dry conditions typical of shorter-term droughts. Such distinctions also affect the identification of drought development, as a fixed 12-month period was applied to all drought events despite the potential for considerable variability in the actual periods that might more accurately represent each drought. As observed in Section 4.1.1, drought onset patterns were visually classified into two main types: direct onset and gradual or pre-conditioned onset. However, this classification is very general, and in fact, there is much greater variability across different drought samples. Additionally, as noted by Holgate et al. (2025), drought characteristics can vary greatly depending on the threshold used, which means results presented in this study may not be entirely applicable if alternative drought definitions were employed.

Climate driver phases may not consistently produce their expected precipitation responses, particularly given the large spatial extent of the study region & the inherent variability in how climate drivers affect local precipitation patterns. Widespread drought does not occur with every climate driver event, and the strength of climate driver events is not directly proportional to the precipitation impacts (e.g., El Niño 1997-98, 2002-03, 2018-19) (BOM, 2021; CSIRO, 2023). Also, effects of climate drivers on Australian precipitation varies between seasons, showing stronger effect on precipitation for eastern Australia during winter and spring (Risbey et al., 2009). This seasonal dependency and spatial variation in impact is particularly significant for SAM, which may not consistently produce expected precipitation patterns according to its specific phase throughout the year (Gallant et al., 2012). Given that seasonal investigation of climate drivers is beyond the scope of this study, when interpreting results, it is important to note that the analytical method used for climate driver analyses (by pooling all months of driver phases during each drought stage together) naturally obscures seasonal patterns and spatial heterogeneity across the temporal scale of each drought stage and throughout the study region. Overall, this research investigates prolonged periods of sustained dry conditions where insufficient precipitation fails to break cumulative precipitation deficits, allowing precipitation stress to accumulate over time.

The modes of variability patterns observed serve as broad-scale probabilistic indicators that increase the likelihood of drought conditions rather than providing definitive predictions of precipitation or drought occurrence over SEA drought (Devanand et al., 2024b; Hobeichi et al., 2024; Holgate et al., 2025).

For synoptic system detection, several methodological aspects may have influenced the results. First is the 4 hPa contour interval adopted for cyclone/anticyclone detection that influences absolute system frequencies and should be accounted for when making direct numerical comparisons with studies employing different intervals. Second is the TAV filtering procedure, which was chosen to remove the background field for its simplicity and computational efficiency. However, Anderson et al. (2003) noted that this filtering approach may alter storm characteristics by potentially redistributing weather systems and creating artificial symmetry between positive and negative pressure anomalies. Future studies could consider more advanced methods such as spatial harmonic filtering (SPC filter with wavenumber cutoff $n \leq 5\text{-}7$), that was found to better preserve the natural characteristics of weather systems while maintaining effective background field removal (Anderson et al., 2003). Overall, the entire synoptic system detection algorithm consistently identified more cyclones than anticyclones, which could reflect either true atmospheric asymmetry or methodological bias.

Lastly, it is important to acknowledge that this study uses climate models, which are not direct representations of real-world observations and may reflect various sources of bias and uncertainty. Quantitative climate projections from Global Climate Models (GCMs) such as the GFDL_SPEAR_MED model employed in this study, are subject to biases stemming from incomplete understanding of climate system physics and the imperfect representation of this knowledge within the models (Wilby et al., 1998; Zhuan et al., 2019), as well as coarse spatial resolution, which prevents adequate representation of fine-scale physical and dynamical processes (Chen et al., 2021). Such bias can be substantial at regional scales and represent an inherent source of uncertainty in the drought dynamics, climate drivers and synoptic patterns observed in this study.

5.5 Future research

Future research could explore more advanced drought detection techniques to improve the accurate identification of drought stages, with particular emphasis on the development stage. Results of this study shows that onset pathways can vary considerably, yet there is currently no robust method for identifying an appropriate development period for each drought event, rather than applying a fixed duration across all events. This aligns with the recent National Environmental Science Program report, which emphasized the need for improved metrics to more reliably capture the onset of Australian droughts (Chung et al., 2025). Addressing this gap is critical, as the development period represents the earliest stage of prolonged droughts, which is also when signals of drought are the strongest and most consistent. Improving detection at this stage would enable more accurate early warning systems, strengthen drought risk assessments, and ultimately support more effective preparedness and management strategies. Investigation of the underlying dynamical reasons for the shorter termination periods also remains limited in the literature and represents a further avenue for research.

Higher-resolution climate models could also be explored to better represent drought dynamics, although given the computational resources needed to run such models, would be difficult to obtain the sample size needed to study drought. Downscaling climate models has been shown to improve precipitation simulation at spatial scales relevant for local impacts and reduce biases (Chapman et al., 2023), thereby potentially enhancing drought projections. Beyond model resolution, future research could also apply the analytical framework developed in this study to other climate models to evaluate the robustness of the results.

The present analysis examined pairwise co-occurrences of climate drivers during drought stages, yet the simultaneous influence of all three mechanisms (ENSO-IOD-SAM) remains unexplored. Given that the combined effects of these drivers amplify individual impacts on Australian precipitation (Cleverly et al., 2016; Holgate et al., 2025), comprehensive multi-driver analyses would advance understanding of drought dynamics. Moreover, additional large-scale mechanisms including the Interdecadal Pacific Oscillation (IPO), Madden-Julian Oscillation (MJO), atmospheric blocking, and subtropical ridge could also substantially alter SEA precipitation and drought characteristics (Holgate et al., 2025; King et al., 2014; Devanand et al., 2024). Incorporating these mechanisms would provide a more complete understanding of how combined climate modes shape regional prolonged drought risk in SEA.

Separating the independent influence of each climate driver would also enhance insights into drought dynamics. For example, isolating the effect of IOD from ENSO using approaches such as partial correlation (Cai et al., 2011a; Risbey et al., 2009), POGA experiments (Yang et al.,

2015), or Empirical Orthogonal Function (EOF) decomposition with ENSO removed (Behera et al., 2006) could clarify how ENSO-forced and internal IOD variations individually contribute differently to drought periods. Similarly, examining seasonal variations could reveal finer-scale patterns and provide more nuanced insights into how climate drivers like SAM exert varying effects on regional precipitation throughout the year.

Future work could strengthen findings from this study by applying alternative cyclone detection methods and validating results against observational datasets (Simmonds et al., 1999; Ullrich et al., 2021) for more robust results and providing a stronger connection between model simulations and real-world dynamics. System speed and structure may also be investigated, as fast-moving cyclones disrupt inland moisture transport, while slower systems promote easterly inflows that increase precipitation (Barnes et al., 2023). This study used surface-based cyclone tracking with sea level pressure, which is generally more effective than upper-level identification when restricted to a single level, given the stronger association of surface cyclones with winds and precipitation (Pepler and Dowdy, 2020a). However, only about half of surface systems extend vertically through the troposphere, with deeper systems exerting stronger impacts and frequently associated with drought-breaking precipitation in SEA (Holgate et al., 2023; Pepler and Dowdy, 2022b). Expanding this work to include three-dimensional tracking or explicit assessment of vertical structure could improve the identification of severe events and clarify their role during drought periods (Pepler and Dowdy, 2020a). Additionally, further investigation could probe specific cyclone–anticyclone configurations in the SEA and Tasman Sea, such as cases where deep lows coincide with Tasman highs, which have been shown to substantially enhance extreme precipitation and serve as key drought-breaking mechanisms. (Holgate et al., 2023). Quantifying precipitation contributions from individual systems across different drought stages would also be valuable, as studies have shown that historical drought precipitation variability was driven mainly by system intensity rather than frequency (Jin et al., 2024).

Chapter 6: Conclusion

This research aimed to enhance understanding of prolonged drought mechanisms in SEA through comprehensive analysis of climate drivers and synoptic weather systems using GFDL_SPEAR_MED large-ensemble climate model simulations.

This study demonstrates the value of large-ensemble climate models in detecting and characterizing prolonged droughts that extend beyond the temporal limits of observational records. The 30-member GFDL-SPEAR ensemble provides 93 samples of prolonged drought events enabling robust statistical analysis of this rare, but consequential climate hazard beyond the limits of observational records. The effectiveness of stage-specific approaches in analysing prolonged drought mechanisms was demonstrated, as temporal differentiation across drought stages (development, persistence, and termination) reveals critical insights often obscured when treating the drought period as a single entity.

This research strengthens understanding of prolonged droughts in SEA by demonstrating that drought development patterns are highly variable and lack consistent initiating conditions. The climate model simulations reveal persistence phases potentially exceeding 200 months with systematic precipitation deficits, indicating sustained stress on water resources, agriculture, and ecosystems. These substantial variations in drought development underscore the need for advanced detection techniques that accurately identify critical early stages when the overall drying signals are strongest. In contrast, termination phases are markedly shorter and more consistent in duration, suggesting that droughts end relatively quickly once the recovery process starts. This rapid transition to wet conditions following prolonged dry periods necessitates adaptive water management strategies in SEA. For example, dam operators needs to balance the competing demands of retaining water to meet downstream needs and maintain water security during drought, while also releasing water in advance of flooding to preserve capacity for flood mitigation (MDBA, 2025). In addition, drought-induced weakening of infrastructure, such as cracking in dikes and levees, increases the likelihood of failure during subsequent wet periods (Barendrecht et al., 2024). Although extreme precipitation following major droughts is initially beneficial, as the first rains help restore ecosystems and replenish water supplies, if heavy precipitation persists, it can quickly become disastrous depending on atmospheric, hydrological, and socio-economic conditions (Barendrecht et al., 2024).

Large-scale climate driver analysis confirmed systematic ENSO, IOD, and SAM phase shifts across prolonged drought stages in SEA, with dry stages dominated by drought-promoting combinations (El Niño, +IOD, -SAM) and wet stages by opposite configurations (La Niña, -IOD, +SAM). ENSO demonstrates the largest changes in phase frequency during drought development and termination, with suppression of La Niña conditions proving more critical than enhancement of El Niño conditions. Critically, the return to neutral or weak La Niña conditions does not necessarily end droughts; breakdown requires strong to extreme La Niña events combined with favourable IOD and SAM configurations. IOD exhibits a temporally lagged influence, functioning primarily as a drought amplifier during mid-development and persistence rather than an initiating mechanism, while SAM shows substantial influence during development and persistence, ranking second to ENSO. Analysis of climate driver combinations reveals increased drought-promoting /drought inhibiting combinations during dry phases/wet, with more extreme pairings producing greater shifts. Notably, standalone events, where only one mode is active, produced the most anomalous conditions relative to non-drought periods, while neutral-neutral conditions increase substantially during drought development. These findings indicate that prolonged droughts result not solely from amplified extreme combinations but from both the absence of wet-phase driver combinations and a broader shift toward neutrality in precipitation-driving mechanisms.

At the synoptic scale, SEA experiences increased anticyclone and decreased cyclone frequency during drought development and persistence, with patterns reversing during termination. The Tasman Sea emerges as a hotspot for both cyclone and anticyclone activity compared to SEA, with anticyclones showing reduced frequency during dry stages and strengthened intensity during termination.

Given that meteorological drought represents the foundational process in the drought cascade, understanding its mechanisms has direct implications for water resource management, particularly as extended periods of below-average precipitation are critical for water security (Chung et al., 2025). By identifying key mechanisms underlying sustained precipitation deficits across different drought stages, this study provides essential building blocks that enhance predictive capabilities for long-term water security planning across SEA.

This study establishes both a methodological framework and empirical foundation that enables future research to investigate additional drivers of prolonged droughts, advancing

toward a more complete understanding of these impactful events. By identifying key climate drivers and synoptic patterns across drought stages, this study enables future research to integrate these stage-specific patterns with projected changes in climate drivers under various SSP scenarios, thereby improving drought prediction accuracy and informing adaptation strategies as prolonged droughts are projected to increase in duration in coming decades.

References

Abram, N.J., Hargreaves, J.A., Wright, N.M., Thirumalai, K., Ummenhofer, C.C., England, M.H., 2020b. Palaeoclimate perspectives on the Indian Ocean Dipole. Quat. Sci. Rev. 237, 106302. https://doi.org/10.1016/j.quascirev.2020.106302

Abram, N.J., Henley, B.J., Gupta, A.S., Lippmann, T.J.R., Clarke, H., Dowdy, A.J., Sharples, J.J., Nolan, R.H., Zhang, T., Wooster, M.J., Wurtzel, J.B., Meissner, K.J., Pitman, A.J., Ukkola, A.M., Murphy, B.P., Tapper, N.J., Boer, M.M., 2021. Connections of climate change and variability to large and extreme forest fires in southeast Australia. Commun. Earth Environ. 2. https://doi.org/10.1038/s43247-020-00065-8

Abram, N.J., Wright, N.M., Ellis, B., Dixon, B.C., Wurtzel, J.B., England, M.H., Ummenhofer, C.C., Philibosian, B., Cahyarini, S.Y., Yu, T.-L., Shen, C.-C., Cheng, H., Edwards, R.L., Heslop, D., 2020a. Coupling of Indo-Pacific climate variability over the last millennium. Nature 579, 385–392. https://doi.org/10.1038/s41586-020-2084-4

Agriculture Victoria, 2025. Climate drivers that affect South Eastern Australia - Agriculture [WWW Document]. Agric. Vic. URL https://agriculture.vic.gov.au/climate-and-weather/understanding-weather-climate-and-forecasting/using-seasonal-forecasts-in-south-eastern-australia/climate-drivers-that-affect-south-eastern-australia (accessed 9.19.25).

An, S.-I., Park, H.-J., Kim, S.-K., Cai, W., Santoso, A., Kim, D., Kug, J.-S., 2023. Main drivers of Indian Ocean Dipole asymmetry revealed by a simple IOD model. Npj Clim. Atmospheric Sci. 6, 1–7. https://doi.org/10.1038/s41612-023-00422-2

Anderson, D., Hodges, K.I., Hoskins, B.J., 2003. Sensitivity of Feature-Based Analysis Methods of Storm Tracks to the Form of Background Field Removal.

ARC Centre of Excellence for Climate Extremes, 2023. El Niño's Impact on Australia's Weather and Climate. The ARC Centre of Excellence for Climate Extremes.

ARC Centre of Excellence for Climate Extremes, 2022. Briefing Note 20: Multi-year La Niña events. The ARC Centre of Excellence for Climate Extremes.

Ashcroft, L., Karoly, D.J., Gergis, J., 2014. Southeastern Australian climate variability 1860–2009: a multivariate analysis. Int. J. Climatol. 34, 1928–1944. https://doi.org/10.1002/joc.3812

Ashok, K., Guan, Z., Yamagata, T., 2003. Influence of the Indian Ocean Dipole on the Australian winter rainfall. Geophys. Res. Lett. 30. https://doi.org/10.1029/2003GL017926

Baldwin, M.P., Ayarzagüena, B., Birner, T., Butchart, N., Butler, A.H., Charlton-Perez, A.J., Domeisen, D.I.V., Garfinkel, C.I., Garny, H., Gerber, E.P., Hegglin, M.I., Langematz, U., Pedatella, N.M., 2021. Sudden Stratospheric Warmings. Rev. Geophys. 59, e2020RG000708. https://doi.org/10.1029/2020RG000708

Bamston, A.G., Chelliah, M., Goldenberg, S.B., 1997. Documentation of a highly ENSO-related sst region in the equatorial pacific: Research note. Atmosphere-Ocean 35, 367–383. https://doi.org/10.1080/07055900.1997.9649597

Banerjee, A., Fyfe, J.C., Polvani, L.M., Waugh, D., Chang, K.-L., 2020. A pause in Southern Hemisphere circulation trends due to the Montreal Protocol. Nature 579, 544–548. https://doi.org/10.1038/s41586-020-2120-4

Barendrecht, M.H., Matanó, A., Mendoza, H., Weesie, R., Rohse, M., Koehler, J., de Ruiter, M., Garcia, M., Mazzoleni, M., Aerts, J.C.J.H., Ward, P.J., Di Baldassarre, G., Day, R., Van Loon, A.F., 2024. Exploring drought-to-flood interactions and dynamics: A global case review. WIREs Water 11, e1726. https://doi.org/10.1002/wat2.1726

Barnes, M.A., King, M., Reeder, M., Jakob, C., 2023. The dynamics of slow-moving coherent cyclonic potential vorticity anomalies and their links to heavy rainfall over the eastern seaboard of Australia. Q. J. R. Meteorol. Soc. 149, 2233–2251. https://doi.org/10.1002/qj.4503

Behera, S.K., Luo, J.J., Masson, S., Rao, S.A., Sakuma, H., Yamagata, T., 2006. A CGCM Study on the Interaction between IOD and ENSO. https://doi.org/10.1175/JCLI3797.1

Bjerknes, J., 1966. A possible response of the atmospheric Hadley circulation to equatorial anomalies of ocean temperature. Tellus 18, 820–829. https://doi.org/10.1111/j.2153-3490.1966.tb00303.x

BOM, 2021. What is El Niño and what might it mean for Australia? [WWW Document]. URL https://www.bom.gov.au/climate/updates/articles/a008-el-nino-and-australia.shtml (accessed 9.23.25).

BOM, 2016. What is La Niña and how does it impact Australia? [WWW Document]. URL https://www.bom.gov.au/climate/updates/articles/a020.shtml (accessed 10.1.25).

BOM, 2011. Rainfall data information [WWW Document]. URL http://www.bom.gov.au/climate/cdo/about/cdo-rainfall-feature.shtml (accessed 3.10.25).

BOM, 2020a. Previous droughts [WWW Document]. URL http://www.bom.gov.au/climate/drought/knowledge-centre/previous-droughts.shtml (accessed 3.30.25a).

BOM, 2020a. Special Climate Statement 70 update—drought conditions in Australia and impact on water resources in the Murray–Darling Basin.

BOM, 2025c. Australian rainfall during El Niño and La Niña events [WWW Document]. URL https://www.bom.gov.au/climate/history/enso/ (accessed 9.17.25).

BOM, 2025d. About Australian Climate [WWW Document]. URL http://www.bom.gov.au/climate/about/?bookmark=enso (accessed 5.5.25).

BOM, 2025e. Southern hemisphere monitoring [WWW Document]. URL http://www.bom.gov.au/climate/enso/?ninoIndex=nino3.4&index=nino34&period=weekly#tabs=Overview (accessed 3.3.25).

BOM, 2025f. Indian Ocean and Australian climate [WWW Document]. URL http://www.bom.gov.au/climate/iod/ (accessed 4.13.25).

BOM, 2025g. Indian Ocean climate influences [WWW Document]. URL http://www.bom.gov.au/climate/iod/#tabs=Positive-IOD-impacts (accessed 5.16.25).

BOM, 2025h. Southern Annular Mode [WWW Document]. URL http://www.bom.gov.au/climate/sam/ (accessed 4.30.25).

BOM, 2025i. Southern Annular Mode (SAM in Summer) [WWW Document]. URL https://www.bom.gov.au/climate/sam/#tabs=SAM-in-summer

BOM, 2025j. Southern Annular Mode (SAM in Winter) [WWW Document]. URL https://www.bom.gov.au/climate/sam/#tabs=SAM-in-winter (accessed 10.2.25).

BOM, 2020b. Annual Australian Climate Statement 2019 [WWW Document]. URL http://www.bom.gov.au/climate/current/annual/aus/2019/ (accessed 8.20.25).

BOM, 2025k. About ENSO Outlooks [WWW Document]. Aust. Gov. Bur. Meteorol. URL http://www.bom.gov.au/climate/ahead/about-ENSO-outlooks.shtml (accessed 5.1.25).

Boschat, G., Pezza, A., Simmonds, I., Perkins, S., Cowan, T., Purich, A., 2015. Large scale and sub-regional connections in the lead up to summer heat wave and extreme rainfall events in eastern Australia. Clim. Dyn. 44, 1823–1840. https://doi.org/10.1007/s00382-014-2214-5

Bourgault, P., Huard, D., Smith, T.J., Logan, T., Aoun, A., Lavoie, J., Dupuis, É., Rondeau-Genesse, G., Alegre, R., Barnes, C., Laperrière, A.B., Biner, S., Caron, D., Ehbrecht, C., Fyke, J., Keel, T., Labonté, M.-P., Lierhammer, L., Low, J.-F., Quinn, J., Roy, P., Squire, D., Stephens, A., Tanguy, M., Whelan, C., 2023. xclim: xarray-based climate data analytics. J. Open Source Softw. 8, 5415. https://doi.org/10.21105/joss.05415

Cai, W., Rensch, P. van, Cowan, T., Hendon, H.H., 2012. An Asymmetry in the IOD and ENSO Teleconnection Pathway and Its Impact on Australian Climate. https://doi.org/10.1175/JCLI-D-11-00501.1

Cai, W., Rensch, P. van, Cowan, T., Hendon, H.H., 2011a. Teleconnection Pathways of ENSO and the IOD and the Mechanisms for Impacts on Australian Rainfall. https://doi.org/10.1175/2011JCLI4129.1

Cai, W., Santoso, A., Collins, M., Dewitte, B., Karamperidou, C., Kug, J.-S., Lengaigne, M., McPhaden, M.J., Stuecker, M.F., Taschetto, A.S., Timmermann, A., Wu, L., Yeh, S.-W., Wang, G., Ng, B., Jia, F., Yang, Y., Ying, J., Zheng, X.-T., Bayr, T., Brown, J.R., Capotondi, A., Cobb, K.M., Gan, B., Geng, T., Ham, Y.-G., Jin, F.-F., Jo, H.-S., Li, X., Lin, X., McGregor, S., Park, J.-H., Stein, K., Yang, K., Zhang, L., Zhong, W., 2021a. Changing El Niño–Southern Oscillation in a warming climate. Nat. Rev. Earth Environ. 2, 628–644. https://doi.org/10.1038/s43017-021-00199-z

Cai, W., Sullivan, A., Cowan, T., 2011c. Interactions of ENSO, the IOD, and the SAM in CMIP3 Models. https://doi.org/10.1175/2010JCLI3744.1

Cai, W., van Rensch, P., Borlace, S., Cowan, T., 2011d. Does the Southern Annular Mode contribute to the persistence of the multidecade-long drought over southwest Western Australia? Geophys. Res. Lett. 38. https://doi.org/10.1029/2011GL047943

Cai, W., Yang, K., Wu, L., Huang, G., Santoso, A., Ng, B., Wang, G., Yamagata, T., 2021b. Opposite response of strong and moderate positive Indian Ocean Dipole to global warming. Nat. Clim. Change 11, 27–32. https://doi.org/10.1038/s41558-020-00943-1

Cai, W., Zheng, X.-T., Weller, E., Collins, M., Cowan, T., Lengaigne, M., Yu, W., Yamagata, T., 2013. Projected response of the Indian Ocean Dipole to greenhouse warming. Nat. Geosci. 6, 999–1007. https://doi.org/10.1038/ngeo2009

Campbell, I., Renwick, J.A., 2023. Southern Hemisphere Storm Tracks and Large-Scale Variability: What Do the Latest Reanalyses Say? https://doi.org/10.1175/JCLI-D-22-0726.1

Cane, M.A., 2005. The evolution of El Niño, past and future. Earth Planet. Sci. Lett. 230, 227–240. https://doi.org/10.1016/j.epsl.2004.12.003

Catto, J.L., Raveh-Rubin, S., 2019. Climatology and dynamics of the link between dry intrusions and cold fronts during winter. Part I: global climatology. Clim. Dyn. 53, 1873–1892. https://doi.org/10.1007/s00382-019-04745-w

Chemke, R., 2022. The future poleward shift of Southern Hemisphere summer mid-latitude storm tracks stems from ocean coupling. Nat. Commun. 13, 1730. https://doi.org/10.1038/s41467-022-29392-4

Chen, J., Arsenault, R., Brissette, F.P., Zhang, S., 2021. Climate Change Impact Studies: Should We Bias Correct Climate Model Outputs or Post-Process Impact Model Outputs? Water Resour. Res. 57, e2020WR028638. https://doi.org/10.1029/2020WR028638

Chung, C.T.Y., Kirono, D., Gallant, A., Bloustein, H., Taschetto, A., Goswami, P., Round, V., Boschat, J., Risbey, J., Monselesan, D., McGregor, s, Li, H., Planton, Y., Gillett, Z., 2025b. Deluge and drought: Insights into swings between dry, wet, and hot-and-dry conditions, National Environmental Science Program. Climate Systems Hub, Australia.

Chung, C.T.Y., Power, S.B., Boschat, G., Gillett, Z., Taschetto, A., Narsey, S., Pepler, A., 2025a. Springtime rainfall changes in Australia related to projected changes in large-scale modes of variability. J. South. Hemisphere Earth Syst. Sci. 75, NULL-NULL. https://doi.org/10.1071/ES25030

Chung, C.T.Y., Power, S.B., Boschat, G., Gillett, Z.E., Narsey, S., 2024. Projected Changes to Characteristics of El Niño-Southern Oscillation, Indian Ocean Dipole, and Southern Annular Mode Events in the CMIP6 Models. Earths Future 12, e2024EF005166. https://doi.org/10.1029/2024EF005166

Cleverly, J., Eamus, D., Luo, Q., Restrepo Coupe, N., Kljun, N., Ma, X., Ewenz, C., Li, L., Yu, Q., Huete, A., 2016. The importance of interacting climate modes on Australia's contribution to global carbon cycle extremes. Sci. Rep. 6, 23113. https://doi.org/10.1038/srep23113

CoastAdapt, 2018. Australia's climate - drivers, variability and extremes [WWW Document]. URL https://coastadapt.com.au/australias-climate-drivers-variability-and-extremes#:~:text=Climates%20are%20variable%20and%20prone,and%20the%20Southern%20Annular%20Mode. (accessed 3.7.25).

Cook, B.I., Smerdon, J.E., Cook, E.R., Williams, A.P., Anchukaitis, K.J., Mankin, J.S., Allen, K., Andreu-Hayles, L., Ault, T.R., Belmecheri, S., Coats, S., Coulthard, B., Fosu, B., Grierson, P., Griffin, D., Herrera, D.A., Ionita, M., Lehner, F., Leland, C., Marvel, K., Morales, M.S., Mishra, V., Ngoma, J., Nguyen, H.T.T., O'Donnell, A., Palmer, J., Rao, M.P., Rodriguez-Caton, M., Seager, R., Stahle, D.W., Stevenson, S., Thapa, U.K., Varuolo-Clarke, A.M., Wise, E.K., 2022. Megadroughts in the Common Era and the Anthropocene. Nat. Rev. Earth Environ. 3, 741–757. https://doi.org/10.1038/s43017-022-00329-1

CSIRO, 2023. Expert Commentary: 2023/24 El Niño for Australia [WWW Document]. URL https://www.csiro.au/en/news/All/News/2023/September/Expert-commentary-El-Nino (accessed 9.23.25).

CSIRO, 2021. Drought in south-east Australia [WWW Document]. URL https://www.csiro.au/en/research/disasters/drought/Forecasting-and-monitoring/South-east-Australia (accessed 3.10.25).

Dätwyler, C., Grosjean, M., Steiger, N.J., Neukom, R., 2020. Teleconnections and relationship between the El Niño–Southern Oscillation (ENSO) and the Southern Annular Mode (SAM) in reconstructions and models over the past millennium. Clim. Past 16, 743–756. https://doi.org/10.5194/cp-16-743-2020

Deirdre, B., Garcia-Soto, C., Hamilton, H., Leuliette, E., Yu, L., Campos, E., Durack, P.J., 2016. Chapter 4. The Ocean's Role in the Hydrological Cycle. Camb. Univ. Press Camb. UK N. Y. NY USA 582 pp.

Delworth, T.L., Cooke, W.F., Adcroft, A., Bushuk, M., Chen, J.-H., Dunne, K.A., Ginoux, P., Gudgel, R., Hallberg, R.W., Harris, L., Harrison, M.J., Johnson, N., Kapnick, S.B., Lin, S.-J., Lu, F., Malyshev, S., Milly, P.C., Murakami, H., Naik, V., Pascale, S., Paynter, D., Rosati, A., Schwarzkopf, M. d., Shevliakova, E., Underwood, S., Wittenberg, A.T., Xiang, B., Yang, X., Zeng, F., Zhang, H., Zhang, L., Zhao, M., 2020. SPEAR: The Next Generation GFDL Modeling System for Seasonal to Multidecadal Prediction and Projection. J. Adv. Model. Earth Syst. 12, e2019MS001895. https://doi.org/10.1029/2019MS001895

Deser, C., Phillips, A., Bourdette, V., Teng, H., 2012. Uncertainty in climate change projections: the role of internal variability. Clim. Dyn. 38, 527–546. https://doi.org/10.1007/s00382-010-0977-x

Devanand, A., Abram, N., Evans, J., Ukkola, A., Aillie, G., Pitman, A., 2024a. Australia's Tinderbox Drought (2017 – 2019) [WWW Document]. ARC Cent. Excell. Clim. Extrem. URL https://climateextremes.org.au/australias-tinderbox-drought-2017-2019/ (accessed 3.10.25).

Devanand, A., Falster, G.M., Gillett, Z.E., Hobeichi, S., Holgate, C.M., Jin, C., Mu, M., Parker, T., Rifai, S.W., Rome, K.S., Stojanovic, M., Vogel, E., Abram, N.J., Abramowitz, G., Coats, S., Evans, J.P., Gallant, A.J.E., Pitman, A.J., Power, S.B., Rauniyar, S.P., Taschetto, A.S., Ukkola, A.M., 2024b. Australia's Tinderbox Drought: An extreme natural event likely worsened by human-caused climate change. Sci. Adv.

Devanand, A., Pitman, A., Abram, N., Gallant, A., King, A., 2022. IPCC AR6 Working Group 1 report: conclusions on the evolving risk of drought. Briefing notes: Expert briefings from climate science experts. ARC Cent. Excell. Clim. Extrem.

Dikshit, A., Pradhan, B., Assiri, M.E., Almazroui, M., Park, H.-J., 2022. Solving transparency in drought forecasting using attention models. Sci. Total Environ. 837, 155856. https://doi.org/10.1016/j.scitotenv.2022.155856

Dowdy, A.J., Catto, J.L., 2017. Extreme weather caused by concurrent cyclone, front and thunderstorm occurrences. Sci. Rep. 7, 40359. https://doi.org/10.1038/srep40359

Evans, J.P., Argueso, D., Olson, R., Di Luca, A., 2017. Bias-corrected regional climate projections of extreme rainfall in south-east Australia. Theor. Appl. Climatol. 130, 1085–1098. https://doi.org/10.1007/s00704-016-1949-9

Fallah, B., Rostami, M., 2024. Exploring the impact of the recent global warming on extreme weather events in Central Asia using the counterfactual climate data ATTRICI v1.1. Clim. Change 177, 80. https://doi.org/10.1007/s10584-024-03743-0

Falster, G., Coats, S., Abram, N., 12/2024b. How unusual was Australia's 2017–2019 Tinderbox Drought? Weather Clim. Extrem. 46, 100734. https://doi.org/10.1016/j.wace.2024.100734

Falster, G.M., Wright, N.M., Abram, N.J., Ukkola, A.M., Henley, B.J., 2024a. Potential for historically unprecedented Australian droughts from natural variability and climate change. Hydrol. Earth Syst. Sci. 28, 1383–1401. https://doi.org/10.5194/hess-28-1383-2024

Faranda, D., Pascale, S., Bulut, B., 2023. Persistent anticyclonic conditions and climate change exacerbated the exceptional 2022 European-Mediterranean drought. Environ. Res. Lett. 18, 034030. https://doi.org/10.1088/1748-9326/acbc37

Feng, J., Hu, D., Yu, L., 2014. How does the Indian Ocean subtropical dipole trigger the tropical Indian Ocean dipole via the Mascarene high? Acta Oceanol. Sin. 33, 64–76. https://doi.org/10.1007/s13131-014-0425-6

Fogt, R.L., Bromwich, D.H., Hines, K.M., 2011. Understanding the SAM influence on the South Pacific ENSO teleconnection. Clim. Dyn. 36, 1555–1576. https://doi.org/10.1007/s00382-010-0905-0

Freund, M., Henley, B.J., Karoly, D.J., Allen, K.J., Baker, P.J., 2017. Multi-century cool- and warm-season rainfall reconstructions for Australia's major climatic regions. Clim. Past 13, 1751–1770. https://doi.org/10.5194/cp-13-1751-2017

Freund, M.B., Brown, J.R., Marshall, A.G., Tozer, C.R., Henley, B.J., Risbey, J.S., Ramesh, N., Lieber, R., Sharmila, S., 2024. Interannual ENSO diversity, transitions, and projected changes in observations and climate models. Environ. Res. Lett. 19, 114005. https://doi.org/10.1088/1748-9326/ad78db

Fyfe, J.C., 2003. Separating Extratropical Zonal Wind Variability and Mean Change.

Gallant, A.J.E., Kiem, A.S., Verdon-Kidd, D.C., Stone, R.C., Karoly, D.J., 2012. Understanding hydroclimate processes in the Murray-Darling Basin for natural resources management. Hydrol. Earth Syst. Sci. 16, 2049–2068. https://doi.org/10.5194/hess-16-2049-2012

Geng, T., Jia, F., Cai, W., Wu, L., Gan, B., Jing, Z., Li, S., McPhaden, M.J., 2023. Increased occurrences of consecutive La Niña events under global warming. Nature 619, 774–781. https://doi.org/10.1038/s41586-023-06236-9

Gillett, N.P., Kell, T.D., Jones, P.D., 2006. Regional climate impacts of the Southern Annular Mode. Geophys. Res. Lett. 33. https://doi.org/10.1029/2006GL027721

Gillett, Z.E., Taschetto, A.S., Holgate, C.M., Santoso, A., 2023. Linking ENSO to Synoptic Weather Systems in Eastern Australia. Geophys. Res. Lett. 50, e2023GL104814. https://doi.org/10.1029/2023GL104814

Gong, D., Wang, S., 1999. Definition of Antarctic Oscillation index. Geophys. Res. Lett. 26, 459–462. https://doi.org/10.1029/1999GL900003

Goswami, P., Gallant, A.J.E., 2025. Understanding drought onset: What makes flash droughts different from conventional droughts? Weather Clim. Extrem. 49, 100782. https://doi.org/10.1016/j.wace.2025.100782

Grose, M.R., Narsey, S., Delage, F.P., Dowdy, A.J., Bador, M., Boschat, G., Chung, C., Kajtar, J.B., Rauniyar, S., Freund, M.B., Lyu, K., Rashid, H., Zhang, X., Wales, S., Trenham, C., Holbrook, N.J., Cowan, T., Alexander, L., Arblaster, J.M., Power, S., 2020. Insights From CMIP6 for Australia's Future Climate. Earths Future 8, e2019EF001469. https://doi.org/10.1029/2019EF001469

Han, W., Vialard, J., McPhaden, M.J., Lee, T., Masumoto, Y., Feng, M., Ruijter, W.P.M. de, 2014. Indian Ocean Decadal Variability: A Review. https://doi.org/10.1175/BAMS-D-13-00028.1

Hendon, H.H., Lim, E.-P., Arblaster, J.M., Anderson, D.L.T., 2014. Causes and predictability of the record wet east Australian spring 2010. Clim. Dyn. 42, 1155–1174. https://doi.org/10.1007/s00382-013-1700-5

Hendon, H.H., Thompson, D.W.J., Wheeler, M.C., 2007a. Australian Rainfall and Surface Temperature Variations Associated with the Southern Hemisphere Annular Mode. https://doi.org/10.1175/JCLI4134.1

Hendon, H.H., Thompson, D.W.J., Wheeler, M.C., 2007b. Australian Rainfall and Surface Temperature Variations Associated with the Southern Hemisphere Annular Mode. https://doi.org/10.1175/JCLI4134.1

Ho, M., Kiem, A.S., Verdon-Kidd, D.C., 2015. A paleoclimate rainfall reconstruction in the Murray-Darling Basin (MDB), Australia: 2. Assessing hydroclimatic risk using paleoclimate records of wet and dry epochs. https://doi.org/10.1002/2015WR017059

Ho, M., Kiem, A.S., Verdon-Kidd, D.C., 2012. The Southern Annular Mode: a comparison of indices. Hydrol. Earth Syst. Sci. 16, 967–982. https://doi.org/10.5194/hess-16-967-2012

Hobeichi, S., Abramowitz, G., Sen Gupta, A., Taschetto, A.S., Richardson, D., Rampal, N., Ayat, H., Alexander, L.V., Pitman, A.J., 2024. How well do climate modes explain precipitation variability? Npj Clim. Atmospheric Sci. 7, 295. https://doi.org/10.1038/s41612-024-00853-5

Holgate, C., Evans, J.P., Taschetto, A.S., Gupta, A.S., Santoso, A., 2022a. The Impact of Interacting Climate Modes on East Australian Precipitation Moisture Sources. https://doi.org/10.1175/JCLI-D-21-0750.1

Holgate, C., Evans, J.P., Taschetto, A.S., Gupta, A.S., Santoso, A., 2022b. The Impact of Interacting Climate Modes on East Australian Precipitation Moisture Sources. https://doi.org/10.1175/JCLI-D-21-0750.1

Holgate, C.M., Falster, G.M., Gillett, Z.E., Goswami, P., Grant, M.O., Hobeichi, S., Hoffmann, D., Jiang, X., Jin, C., Lu, X., Mu, M., Page, J.C., Parker, T.J., Vogel, E., Abram, N.J., Evans, J.P., Gallant, A.J.E., Henley, B.J., Kala, J., King, A.D., Maher, N., Nguyen, H., Pitman, A.J., Power, S.B., Rauniyar, S.P., Taschetto, A.S., Ukkola, A.M., 2025. Physical mechanisms of meteorological drought development, intensification and termination: an Australian review. Commun. Earth Environ. 6, 1–14. https://doi.org/10.1038/s43247-025-02179-3

Holgate, C.M., Pepler, A.S., Rudeva, I., Abram, N.J., 2023. Anthropogenic warming reduces the likelihood of drought-breaking extreme rainfall events in southeast Australia. Weather Clim. Extrem. 42, 100607. https://doi.org/10.1016/j.wace.2023.100607

Holgate, C.M., Van Dijk, A.I.J.M., Evans, J.P., Pitman, A.J., 2020a. Local and Remote Drivers of Southeast Australian Drought. Geophys. Res. Lett. 47, e2020GL090238. https://doi.org/10.1029/2020GL090238

Hoskins, B.J., Karoly, D.J., 1981. The Steady Linear Response of a Spherical Atmosphere to Thermal and Orographic Forcing.

IPCC, 2007. 3.6.5 The Southern Hemisphere and Southern Annular Mode - AR4 WGI Chapter 3: Observations: Surface and Atmospheric Climate Change [WWW Document]. URL https://archive.ipcc.ch/publications_and_data/ar4/wg1/en/ch3s3-6-5.html (accessed 4.28.25).

Jain, S., Scaife, A.A., Shepherd, T.G., Deser, C., Dunstone, N., Schmidt, G.A., Trenberth, K.E., Turkington, T., 2023. Importance of internal variability for climate model assessment. Npj Clim. Atmospheric Sci. 6, 1–7. https://doi.org/10.1038/s41612-023-00389-0

Jin, C., Gallant, A.J.E., Parker, T., Reeder, M.J., 2025. Weather systems and their contribution to seasonal rainfall in Australia. Q. J. R. Meteorol. Soc. n/a, e5013. https://doi.org/10.1002/qj.5013

Jin, C., Reeder, M.J., Gallant, A.J.E., Parker, T., Sprenger, M., 2024. A Synoptic-Dynamic View of the Millennium Drought (2001–2009) in Southeastern Australia. J. Geophys. Res. Atmospheres 129, e2024JD041657. https://doi.org/10.1029/2024JD041657

Jin, C., Reeder, M.J., Gallant, A.J.E., Parker, T., Sprenger, M., 2023. Changes in Weather Systems during Anomalously Wet and Dry Years in Southeastern Australia. https://doi.org/10.1175/JCLI-D-23-0305.1

Johnson, N.C., Kosaka, Y., 2016. The impact of eastern equatorial Pacific convection on the diversity of boreal winter El Niño teleconnection patterns. Clim. Dyn. 47, 3737–3765. https://doi.org/10.1007/s00382-016-3039-1

Karoly, D.J., 1989. Southern Hemisphere Circulation Features Associated with El Niño-Southern Oscillation Events.

Kautz, L.-A., Martius, O., Pfahl, S., Pinto, J.G., Ramos, A.M., Sousa, P.M., Woollings, T., 2022. Atmospheric blocking and weather extremes over the Euro-Atlantic sector – a review. Weather Clim. Dyn. 3, 305–336. https://doi.org/10.5194/wcd-3-305-2022

Kiem, A.S., Verdon-Kidd, D.C., 2010. Towards understanding hydroclimatic change in Victoria, Australia – preliminary insights into the "Big Dry." Hydrol. Earth Syst. Sci. 14, 433–445. https://doi.org/10.5194/hess-14-433-2010

Kim, S.-K., Park, H.-J., An, S.-I., Liu, C., Cai, W., Santoso, A., Kug, J.-S., 2024. Decreased Indian Ocean Dipole variability under prolonged greenhouse warming. Nat. Commun. 15, 2811. https://doi.org/10.1038/s41467-024-47276-7

King, A.D., Klingaman, N.P., Alexander, L.V., Donat, M.G., Jourdain, N.C., Maher, P., 2014. Extreme Rainfall Variability in Australia: Patterns, Drivers, and Predictability. https://doi.org/10.1175/JCLI-D-13-00715.1

King, A.D., Pitman, A.J., Henley, B.J., Ukkola, A.M., Brown, J.R., 2020. The role of climate variability in Australian drought. Nat. Clim. Change 10, 177–179. https://doi.org/10.1038/s41558-020-0718-z

King, Andrew.D., LewiS, S.C., Perkins, S.E., Alexander, L.V., Donat, M.G., Karoly, D.J., Black, M.T., 2013. Limited evidence of anthropogenic influence on the 2011–12 extreme rainfall over southeast Australia. [in '"Explaining Extreme Events of 2012 from a Climate Perspective"'].

King, J., Anchukaitis, K.J., Allen, K., Vance, T., Hessl, A., 2023. Trends and variability in the Southern Annular Mode over the Common Era. Nat. Commun. 14, 2324. https://doi.org/10.1038/s41467-023-37643-1

Kirono, D.G.C., Round, V., Heady, C., Chiew, F.H.S., Osbrough, S., 2020. Drought projections for Australia: Updated results and analysis of model simulations. Weather Clim. Extrem. 30, 100280. https://doi.org/10.1016/j.wace.2020.100280

Lafaysse, M., Hingray, B., Mezghani, A., Gailhard, J., Terray, L., 2014. Internal variability and model uncertainty components in future hydrometeorological projections: The Alpine Durance basin. Water Resour. Res. 50, 3317–3341. https://doi.org/10.1002/2013WR014897

Larsen, S.H., Nicholls, N., 2009. Southern Australian rainfall and the subtropical ridge: Variations, interrelationships, and trends. Geophys. Res. Lett. 36, L08708. https://doi.org/10.1029/2009GL037786

Leblanc, M., Tweed, S., Van Dijk, A., Timbal, B., 2012. A review of historic and future hydrological changes in the Murray-Darling Basin. Glob. Planet. Change 80–81, 226–246. https://doi.org/10.1016/j.gloplacha.2011.10.012

Lim, E.-P., Hendon, H.H., 2017. Causes and Predictability of the Negative Indian Ocean Dipole and Its Impact on La Niña During 2016. Sci. Rep. 7, 12619. https://doi.org/10.1038/s41598-017-12674-z

Lim, E.-P., Hendon, H.H., Boschat, G., Hudson, D., Thompson, D.W.J., Dowdy, A.J., Arblaster, J.M., 2019. Australian hot and dry extremes induced by weakenings of the stratospheric polar vortex. Nat. Geosci. 12, 896–901. https://doi.org/10.1038/s41561-019-0456-x

Lloyd-Hughes, B., Saunders, M.A., 2002. A drought climatology for Europe. https://doi.org/10.1002/joc.846

Lu, F., Harrison, M.J., Rosati, A., Delworth, T.L., Yang, X., Cooke, W.F., Jia, L., McHugh, C., Johnson, N.C., Bushuk, M., Zhang, Y., Adcroft, A., 2020. GFDL's SPEAR Seasonal Prediction System: Initialization and Ocean Tendency Adjustment (OTA) for Coupled Model Predictions. J. Adv. Model. Earth Syst. 12, e2020MS002149. https://doi.org/10.1029/2020MS002149

Maher, N., Matei, D., Milinski, S., Marotzke, J., 2018. ENSO Change in Climate Projections: Forced Response or Internal Variability? Geophys. Res. Lett. 45, 11,390-11,398. https://doi.org/10.1029/2018GL079764

Maher, N., Phillips, A.S., Deser, C., Wills, R.C.J., Lehner, F., Fasullo, J., Caron, J.M., Brunner, L., Beyerle, U., 2024. The updated Multi-Model Large Ensemble Archive and the Climate Variability Diagnostics Package: New tools for the study of climate variability and change. https://doi.org/10.5194/egusphere-2024-3684

Maher, N., Wills, R.C.J., DiNezio, P., Klavans, J., Milinski, S., Sanchez, S.C., Stevenson, S., Stuecker, M.F., Wu, X., 2023. The future of the El Niño–Southern Oscillation: using

large ensembles to illuminate time-varying responses and inter-model differences. Earth Syst. Dyn. 14, 413–431. https://doi.org/10.5194/esd-14-413-2023

Marshall, A.G., Hemer, M.A., Hendon, H.H., McInnes, K.L., 2018. Southern annular mode impacts on global ocean surface waves. Ocean Model. 129, 58–74. https://doi.org/10.1016/j.ocemod.2018.07.007

Marshall, A.G., Hudson, D., Wheeler, M.C., Alves, O., Hendon, H.H., Pook, M.J., Risbey, J.S., 2013. Intra-seasonal drivers of extreme heat over Australia in observations and POAMA-2. Clim. Dyn. 43, 1915–1937. https://doi.org/10.1007/s00382-013-2016-1

Marshall, G., 2022. The Climate Data Guide: Marshall Southern Annular Mode (SAM) Index (Station-based).

Marshall, G.J., 2003. Trends in the Southern Annular Mode from Observations and Reanalyses.

McGregor, S., Cassou, C., Kosaka, Y., Phillips, A.S., 2022. Projected ENSO Teleconnection Changes in CMIP6. Geophys. Res. Lett. 49, e2021GL097511. https://doi.org/10.1029/2021GL097511

McGregor, S., Gallant, A., van Rensch, P., 2024. Quantifying ENSOs Impact on Australia's Regional Monthly Rainfall Risk. Geophys. Res. Lett. 51, e2023GL106298. https://doi.org/10.1029/2023GL106298

McIntosh, P.C., Risbey, J.S., Brown, J.N., Pook, M.J., 2012. Apparent and real sources of rainfall associated with a cutoff low in southeast Australia. CAWCR Res. Lett., 8, 4–9.

McKay, R.C., Boschat, G., Rudeva, I., Pepler, A., Purich, A., Dowdy, A., Hope, P., Gillett, Z.E., Rauniyar, S., 2023. Can southern Australian rainfall decline be explained? A review of possible drivers. WIREs Clim. Change 14, e820. https://doi.org/10.1002/wcc.820

McKee, T.B., Doesken, N.J., Kleist, J., 1993. The Relationship of Drought Freqeuncy and Duration to Time Scales.

McPhaden, M.J., Zebiak, S.E., Glantz, M.H., 2006. ENSO as an Integrating Concept in Earth Science. Science 314, 1740–1745. https://doi.org/10.1126/science.1132588

MDBA, 2025. Dam management to reduce the impact of flooding | Murray–Darling Basin Authority [WWW Document]. URL https://www.mdba.gov.au/water-management/managing-water-quality/water-quality-threats/flooding/dam-management-reduce-impact-flooding (accessed 10.19.25).

Meneghini, B., Simmonds, I., Smith, I.N., 2007. Association between Australian rainfall and the Southern Annular Mode. Int. J. Climatol. 27, 109–121. https://doi.org/10.1002/joc.1370

Milly, P.C.D., Dunne, K.A., 2016. Potential evapotranspiration and continental drying. Nat. Clim. Change 6, 946–949. https://doi.org/10.1038/nclimate3046

Mishra, A.K., Singh, V.P., 2010. A review of drought concepts. J. Hydrol. 391, 202–216. https://doi.org/10.1016/j.jhydrol.2010.07.012

Murphy, B.F., Timbal, B., 2008. A review of recent climate variability and climate change in southeastern Australia. Int. J. Climatol. 28, 859–879. https://doi.org/10.1002/joc.1627

Murray-Darling Basin Authority, 2010. Murray–Darling Basin Authority Annual Report 2010–11.

Murtugudde, R., Busalacchi, A.J., 1999. Interannual Variability of the Dynamics and Thermodynamics of the Tropical Indian Ocean.

Murtugudde, R., McCreary Jr., J.P., Busalacchi, A.J., 2000. Oceanic processes associated with anomalous events in the Indian Ocean with relevance to 1997–1998. J. Geophys. Res. Oceans 105, 3295–3306. https://doi.org/10.1029/1999JC900294

Nicholls, N., Drosdowsky, W., Lavery, B., 1997. Australian rainfall variability and change. Weather 52, 66–72. https://doi.org/10.1002/j.1477-8696.1997.tb06274.x

NIDIS, n.d. Drought Timescales: Short- vs. Long-Term Drought [WWW Document]. URL https://www.drought.gov/what-is-drought/drought-timescales-short-vs-long-term-drought (accessed 3.7.25).

NOAA, 2025. El Niño / Southern Oscillation (ENSO) | Equatorial Pacific Sea Surface Temperatures (SST) [WWW Document]. NOAA Clim. URL https://www.ncei.noaa.gov/access/monitoring/enso/sst (accessed 5.1.25).

NOAA, 2024. What are El Nino and La Nina? [WWW Document]. URL https://oceanservice.noaa.gov/facts/ninonina.html (accessed 5.4.25).

North, G.R., Pyle, J., Zhang, F., 2015. Synoptic Meterolofy | Weather Maps, in: Encyclopedia of Atmospheric Sciences (Second Edition). Elsevier, pp. 289–298. https://doi.org/10.1016/B978-0-12-382225-3.00397-2

NSW DPI, 2019. NSW State Seasonal Update - December 2019 [WWW Document]. URL https://www.dpi.nsw.gov.au/climate-landing/ssu/december-2019 (accessed 9.29.25).

Okumura, Y.M., Deser, C., 2010. Asymmetry in the Duration of El Niño and La Niña. https://doi.org/10.1175/2010JCLI3592.1

Parker, T., Gallant, A.J.E., 2022. The role of heavy rainfall in drought in Australia. Weather Clim. Extrem. 38, 100528. https://doi.org/10.1016/j.wace.2022.100528

Pepler, A., 2020b. Record Lack of Cyclones in Southern Australia During 2019. Geophys. Res. Lett. 47, e2020GL088488. https://doi.org/10.1029/2020GL088488

Pepler, A., Dowdy, A., 2021. Fewer deep cyclones projected for the midlatitudes in a warming climate, but with more intense rainfall. Environ. Res. Lett. 16, 054044. https://doi.org/10.1088/1748-9326/abf528

Pepler, A., Dowdy, A., 2020a. A Three-Dimensional Perspective on Extratropical Cyclone Impacts. https://doi.org/10.1175/JCLI-D-19-0445.1

Pepler, A., Hope, P., Dowdy, A., 2019. Long-term changes in southern Australian anticyclones and their impacts. Clim. Dyn. 53, 4701–4714. https://doi.org/10.1007/s00382-019-04819-9

Pepler, A.S., Dowdy, A.J., 2022b. Australia's Future Extratropical Cyclones. https://doi.org/10.1175/JCLI-D-22-0312.1

Pieper, P., Düsterhus, A., Baehr, J., 2020. A universal Standardized Precipitation Index candidate distribution function for observations and simulations. Hydrol. Earth Syst. Sci. 24, 4541–4565. https://doi.org/10.5194/hess-24-4541-2020

Pook, M.J., McIntosh, P.C., Meyers, G.A., 2006. The Synoptic Decomposition of Cool-Season Rainfall in the Southeastern Australian Cropping Region. https://doi.org/10.1175/JAM2394.1

Pook, M.J., Risbey, J.S., McIntosh, P.C., 2012. The Synoptic Climatology of Cool-Season Rainfall in the Central Wheatbelt of Western Australia. https://doi.org/10.1175/MWR-D-11-00048.1

Pook, M.J., Risbey, J.S., McIntosh, P.C., Ummenhofer, C.C., Marshall, A.G., Meyers, G.A., 2013. The Seasonal Cycle of Blocking and Associated Physical Mechanisms in the Australian Region and Relationship with Rainfall. https://doi.org/10.1175/MWR-D-13-00040.1

Power, S., Delage, F., Chung, C., Kociuba, G., Keay, K., 2013. Robust twenty-first-century projections of El Niño and related precipitation variability. Nature 502, 541–545. https://doi.org/10.1038/nature12580

Power, S.B., Callaghan, J., 2016. The frequency of major flooding in coastal southeast Australia has significantly increased since the late 19th century. J. South. Hemisphere Earth Syst. Sci. 66, 2–11. https://doi.org/10.1071/es16002

Priestley, M.D.K., Catto, J.L., 2022. Future changes in the extratropical storm tracks and cyclone intensity, wind speed, and structure. Weather Clim. Dyn. 3, 337–360. https://doi.org/10.5194/wcd-3-337-2022

Reid, P.C., Hari, R.E., Beaugrand, G., Livingstone, D.M., Marty, C., Straile, D., Barichivich, J., Goberville, E., Adrian, R., Aono, Y., Brown, R., Foster, J., Groisman, P., Hélaouët, P., Hsu, H.-H., Kirby, R., Knight, J., Kraberg, A., Li, J., Lo, T.-T., Myneni, R.B., North, R.P., Pounds, J.A., Sparks, T., Stübi, R., Tian, Y., Wiltshire, K.H., Xiao, D., Zhu, Z., 2016. Global impacts of the 1980s regime shift. Glob. Change Biol. 22, 682–703. https://doi.org/10.1111/gcb.13106

Reverdin, G., Cadet, D.L., Gutzler, D., 1986. Interannual displacements of convection and surface circulation over the equatorial Indian Ocean. Q. J. R. Meteorol. Soc. 112, 43–67. https://doi.org/10.1002/qj.49711247104

Risbey, J.S., McIntosh, P.C., Pook, M.J., 2012. Synoptic components of rainfall variability and trends in southeast Australia. https://doi.org/10.1002/joc.3597

Risbey, J.S., Pook, M.J., McIntosh, P.C., Wheeler, M.C., Hendon, H.H., 2009. On the Remote Drivers of Rainfall Variability in Australia. https://doi.org/10.1175/2009MWR2861.1

Rudeva, I., Boschat, G., McKay, R., Pepler, A., Dowdy, A., 2021. Weather systems related to wet and dry extremes.

Saji, N., Yamagata, T., 2003. Possible impacts of Indian Ocean Dipole mode events on global climate. Clim. Res. 25, 151–169. https://doi.org/10.3354/cr025151

Saji, N.H., Goswami, B.N., Vinayachandran, P.N., Yamagata, T., 1999. A dipole mode in the tropical Indian Ocean. Nature 401, 360–363. https://doi.org/10.1038/43854

Santoso, A., Hendon, H., Watkins, A., Power, S., Dommenget, D., England, M.H., Frankcombe, L., Holbrook, N.J., Holmes, R., Hope, P., Lim, E.-P., Luo, J.-J., McGregor, S., Neske, S., Nguyen, H., Pepler, A., Rashid, H., Gupta, A.S., Taschetto, A.S., Wang, G., Abellán, E., Sullivan, A., Huguenin, M.F., Gamble, F., Delage, F., 2019. Dynamics and Predictability of El Niño–Southern Oscillation: An Australian Perspective on Progress and Challenges. https://doi.org/10.1175/BAMS-D-18-0057.1

Santoso, A., Mcphaden, M.J., Cai, W., 2017. The Defining Characteristics of ENSO Extremes and the Strong 2015/2016 El Niño. Rev. Geophys. 55, 1079–1129. https://doi.org/10.1002/2017RG000560

Schneider, D.P., Deser, C., Fasullo, J., Trenberth, K.E., 2013. Climate Data Guide Spurs Discovery and Understanding. Eos Trans. Am. Geophys. Union 94, 121–122. https://doi.org/10.1002/2013EO130001

Sen, A., Deb, P., Matthews, A.J., Joshi, M.M., 2024. Teleconnection and the Antarctic response to the Indian Ocean Dipole in CMIP5 and CMIP6 models. Q. J. R. Meteorol. Soc. 150, 5020–5036. https://doi.org/10.1002/qj.4854

Sheffield, J., Wood, E.F., Roderick, M.L., 2012. Little change in global drought over the past 60 years. Nature 491, 435–438. https://doi.org/10.1038/nature11575

Shin, N.-Y., Kug, J.-S., Stuecker, M.F., Jin, F.-F., Timmermann, A., Kim, G.-I., 2022. More frequent central Pacific El Niño and stronger eastern pacific El Niño in a warmer climate. Npj Clim. Atmospheric Sci. 5, 1–8. https://doi.org/10.1038/s41612-022-00324-9

Sienz, F., Bothe, O., Fraedrich, K., 2012. Monitoring and quantifying future climate projections of dryness and wetness extremes: SPI bias. Hydrol. Earth Syst. Sci. 16, 2143–2157. https://doi.org/10.5194/hess-16-2143-2012

Simmonds, I., Murray, R.J., Leighton, R.M., 1999. A refinement of cyclone tracking methods with data from FROST. Aust. Meteorol. Mag. 48.

Stevenson, S., Coats, S., Touma, D., Cole, J., Lehner, F., Fasullo, J., Otto-Bliesner, B., 2022. Twenty-first century hydroclimate: A continually changing baseline, with more frequent extremes. Proc. Natl. Acad. Sci. 119, e2108124119. https://doi.org/10.1073/pnas.2108124119

Stuecker, M.F., Timmermann, A., Jin, F.-F., Chikamoto, Y., Zhang, W., Wittenberg, A.T., Widiasih, E., Zhao, S., 2017. Revisiting ENSO/Indian Ocean Dipole phase relationships. Geophys. Res. Lett. 44, 2481–2492. https://doi.org/10.1002/2016GL072308

Svoboda, M., Hayes, M., Wood, D., 2012. Standardized Precipitation Index: User Guide. Natl. Drought Mitig. Cent. Fac. Publ.

Swain, D.L., Horton, D.E., Singh, D., Diffenbaugh, N.S., 2016. Trends in atmospheric patterns conducive to seasonal precipitation and temperature extremes in California. Sci. Adv. 2, e1501344. https://doi.org/10.1126/sciadv.1501344

Swann, A.L.S., Hoffman, F.M., Koven, C.D., Randerson, J.T., 2016. Plant responses to increasing CO_2 reduce estimates of climate impacts on drought severity. Proc. Natl. Acad. Sci. 113, 10019–10024. https://doi.org/10.1073/pnas.1604581113

Thompson, D.W.J., Solomon, S., Kushner, P.J., England, M.H., Grise, K.M., Karoly, D.J., 2011. Signatures of the Antarctic ozone hole in Southern Hemisphere surface climate change. Nat. Geosci. 4, 741–749. https://doi.org/10.1038/ngeo1296

Thompson, D.W.J., Wallace, J.M., 2000. Annular Modes in the Extratropical Circulation. Part I: Month-to-Month Variability.

Thompson, D.W.J., Wallace, J.M., Hegerl, G.C., 2000. Annular Modes in the Extratropical Circulation. Part II: Trends.

Trenberth, K., 2024. The Climate Data Guide: Nino SST Indices (Nino 1+2, 3, 3.4, 4; ONI and TNI).

Trenberth, K.E., 1997. The Definition of El Niño. Bull. Am. Meteorol. Soc. 78, 2771–2777. https://doi.org/10.1175/1520-0477(1997)078%253C2771:TDOENO%253E2.0.CO;2

Ukkola, A.M., De Kauwe, M.G., Pitman, A.J., Best, M.J., Abramowitz, G., Haverd, V., Decker, M., Haughton, N., 2016. Land surface models systematically overestimate the intensity, duration and magnitude of seasonal-scale evaporative droughts. Environ. Res. Lett. 11, 104012. https://doi.org/10.1088/1748-9326/11/10/104012

Ukkola, A.M., De Kauwe, M.G., Roderick, M.L., Abramowitz, G., Pitman, A.J., 2020. Robust Future Changes in Meteorological Drought in CMIP6 Projections Despite Uncertainty in Precipitation. Geophys. Res. Lett. 47, e2020GL087820. https://doi.org/10.1029/2020GL087820

Ukkola, A.M., Pitman, A.J., Donat, M.G., De Kauwe, M.G., Angélil, O., 2018. Evaluating the Contribution of Land-Atmosphere Coupling to Heat Extremes in CMIP5 Models. Geophys. Res. Lett. 45, 9003–9012. https://doi.org/10.1029/2018GL079102

Ulbrich, U., Leckebusch, G.C., Pinto, J.G., 2009. Extra-tropical cyclones in the present and future climate: a review. Theor. Appl. Climatol. 96, 117–131. https://doi.org/10.1007/s00704-008-0083-8

Ullrich, P.A., Zarzycki, C.M., McClenny, E.E., Pinheiro, M.C., Stansfield, A.M., Reed, K.A., 2021. TempestExtremes v2.1: a community framework for feature detection, tracking, and analysis in large datasets. Geosci. Model Dev. 14, 5023–5048. https://doi.org/10.5194/gmd-14-5023-2021

Ummenhofer, C.C., England, M.H., McIntosh, P.C., Meyers, G.A., Pook, M.J., Risbey, J.S., Gupta, A.S., Taschetto, A.S., 2009. What causes southeast Australia's worst droughts? Geophys. Res. Lett. 36. https://doi.org/10.1029/2008GL036801

Ummenhofer, C.C., Gupta, A.S., Briggs, P.R., England, M.H., McIntosh, P.C., Meyers, G.A., Pook, M.J., Raupach, M.R., Risbey, J.S., 2011. Indian and Pacific Ocean Influences on Southeast Australian Drought and Soil Moisture. https://doi.org/10.1175/2010JCLI3475.1

Ummenhofer, C.C., Sen Gupta, A., England, M.H., Taschetto, A.S., Briggs, P.R., Raupach, M.R., 2015. How did ocean warming affect Australian rainfall extremes during the 2010/2011 La Niña event? Geophys. Res. Lett. 42, 9942–9951. https://doi.org/10.1002/2015GL065948

UNDRR, 2021. UNDRR Annual report [WWW Document]. URL https://www.undrr.org/publication/undrr-annual-report-2021 (accessed 3.7.25).

Utsumi, N., Kim, H., Kanae, S., Oki, T., 2017. Relative contributions of weather systems to mean and extreme global precipitation. J. Geophys. Res. Atmospheres 122, 152–167. https://doi.org/10.1002/2016JD025222

van Dijk, A.I.J.M., Beck, H.E., Crosbie, R.S., de Jeu, R.A.M., Liu, Y.Y., Podger, G.M., Timbal, B., Viney, N.R., 2013. The Millennium Drought in southeast Australia (2001–2009): Natural and human causes and implications for water resources, ecosystems, economy, and society. Water Resour. Res. 49, 1040–1057. https://doi.org/10.1002/wrcr.20123

Van Lanen, H. a. J., Wanders, N., Tallaksen, L.M., Van Loon, A.F., 2013. Hydrological drought across the world: impact of climate and physical catchment structure. Hydrol. Earth Syst. Sci. 17, 1715–1732. https://doi.org/10.5194/hess-17-1715-2013

Van Loon, A.F., 2015. Hydrological drought explained. WIREs Water 2, 359–392. https://doi.org/10.1002/wat2.1085

Van Loon, A.F., 2013. On the Propagation of Drought .: How Climate and Catchment Characteristics Influence Hydrological Drought Development and Recovery (Ph.D.). Wageningen University and Research, Netherlands.

van Oldenborgh, G.J., Hendon, H., Stockdale, T., L'Heureux, M., Coughlan de Perez, E., Singh, R., van Aalst, M., 2021. Defining El Niño indices in a warming climate. Environ. Res. Lett. 16, 044003. https://doi.org/10.1088/1748-9326/abe9ed

Vance, T.R., Roberts, J.L., Plummer, C.T., Kiem, A.S., van Ommen, T.D., 2015. Interdecadal Pacific variability and eastern Australian megadroughts over the last millennium. Geophys. Res. Lett. 42, 129–137. https://doi.org/10.1002/2014GL062447

Veettil, A.V., Mishra, A.K., 2023. Quantifying thresholds for advancing impact-based drought assessment using classification and regression tree (CART) models. J. Hydrol. 625, 129966. https://doi.org/10.1016/j.jhydrol.2023.129966

Velasquez-Jimenez, L., Abram, N.J., 2024. Technical note: An improved methodology for calculating the Southern Annular Mode index to aid consistency between climate studies. Clim. Past 20, 1125–1139. https://doi.org/10.5194/cp-20-1125-2024

Verdon-Kidd, D.C., Kiem, A.S., 2009. Nature and causes of protracted droughts in southeast Australia: Comparison between the Federation, WWII, and Big Dry droughts. Geophys. Res. Lett. 36. https://doi.org/10.1029/2009GL041067

Vicente-Serrano, S.M., Beguería, S., López-Moreno, J.I., 2010. A Multiscalar Drought Index Sensitive to Global Warming: The Standardized Precipitation Evapotranspiration Index. https://doi.org/10.1175/2009JCLI2909.1

Wang, C., 2001. On the ENSO Mechanisms. Adv. Atmospheric Sci. 18, 674–691. https://doi.org/10.1007/BF03403493

Wang, C., Deser, C., Yu, J.-Y., DiNezio, P., Clement, A., 2017. El Niño and Southern Oscillation (ENSO): A Review, in: Glynn, P.W., Manzello, D.P., Enochs, I.C. (Eds.), Coral Reefs of the Eastern Tropical Pacific: Persistence and Loss in a Dynamic Environment. Springer Netherlands, Dordrecht, pp. 85–106. https://doi.org/10.1007/978-94-017-7499-4_4

Wang, C., Picaut, J., 2004. Understanding Enso Physics—A Review, in: Earth's Climate. American Geophysical Union (AGU), pp. 21–48. https://doi.org/10.1029/147GM02

Wang, G., Cai, W., Santoso, A., Abram, N., Ng, B., Yang, K., Geng, T., Doi, T., Du, Y., Izumo, T., Ashok, K., Li, J., Li, T., McKenna, S., Sun, S., Tozuka, T., Zheng, X., Liu, Y., Wu, L., Jia, F., Hu, S., Li, X., 2024. The Indian Ocean Dipole in a warming world. Nat. Rev. Earth Environ. 5, 588–604. https://doi.org/10.1038/s43017-024-00573-7

Warren, R.A., Jakob, C., Hitchcock, S.M., White, B.A., 2021. Heavy versus extreme rainfall events in southeast Australia. Q. J. R. Meteorol. Soc. 147, 3201–3226. https://doi.org/10.1002/qj.4124

Webster, P.J., Moore, A.M., Loschnigg, J.P., Leben, R.R., 1999. Coupled ocean–atmosphere dynamics in the Indian Ocean during 1997–98. Nature 401, 356–360. https://doi.org/10.1038/43848

Wernli, H., Schwierz, C., 2006. Surface Cyclones in the ERA-40 Dataset (1958–2001). Part I: Novel Identification Method and Global Climatology. https://doi.org/10.1175/JAS3766.1

Wilby, R.L., Hassan, H., Hanaki, K., 1998. Statistical downscaling of hydrometeorological variables using general circulation model output. J. Hydrol. 205, 1–19. https://doi.org/10.1016/S0022-1694(97)00130-3

WMO, n.d. Climatological Normals [WWW Document]. World Meterological Organistion. URL https://community.wmo.int/en/activity-areas/climate-services/climate-products-and-initiatives/wmo-climatological-normals (accessed 3.17.25).

Wu, Z., Huang, N.E., Long, S.R., Chung-Kang, P., 2007. On the trend, detrending, and variability of nonlinear and nonstationary time series. https://doi.org/10.1073/pnas.0701020104

Wyrtki, K., 1975. El Niño—The Dynamic Response of the Equatorial Pacific Oceanto Atmospheric Forcing.

Yang, Y., Xie, S.-P., Wu, L., Kosaka, Y., Lau, N.-C., Vecchi, G.A., 2015. Seasonality and Predictability of the Indian Ocean Dipole Mode: ENSO Forcing and Internal Variability. https://doi.org/10.1175/JCLI-D-15-0078.1

Yevjevich, V., 1967. An objective approach to definitions and investigations of continental hydrologic droughts. J. Hydrol. 7, 353. https://doi.org/10.1016/0022-1694(69)90110-3

Zargar, A., Sadiq, R., Naser, B., Khan, F.I., 2011. A review of drought indices. Environ. Rev. 19, 333–349. https://doi.org/10.1139/a11-013

Zhuan, M., Chen, J., Xu, C.-Y., Zhao, C., Xiong, L., Liu, P., 2019. A method for investigating the relative importance of three components in overall uncertainty of climate projections. Int. J. Climatol. 39, 1853–1871. https://doi.org/10.1002/joc.5920